COMPUTER SIMULATION OF WHITE PINE BLISTER RUST EPIDEMICS

I. MODEL FORMULATION

Geral I. McDonald, Raymond J. Hoff, and William R. Wykoff

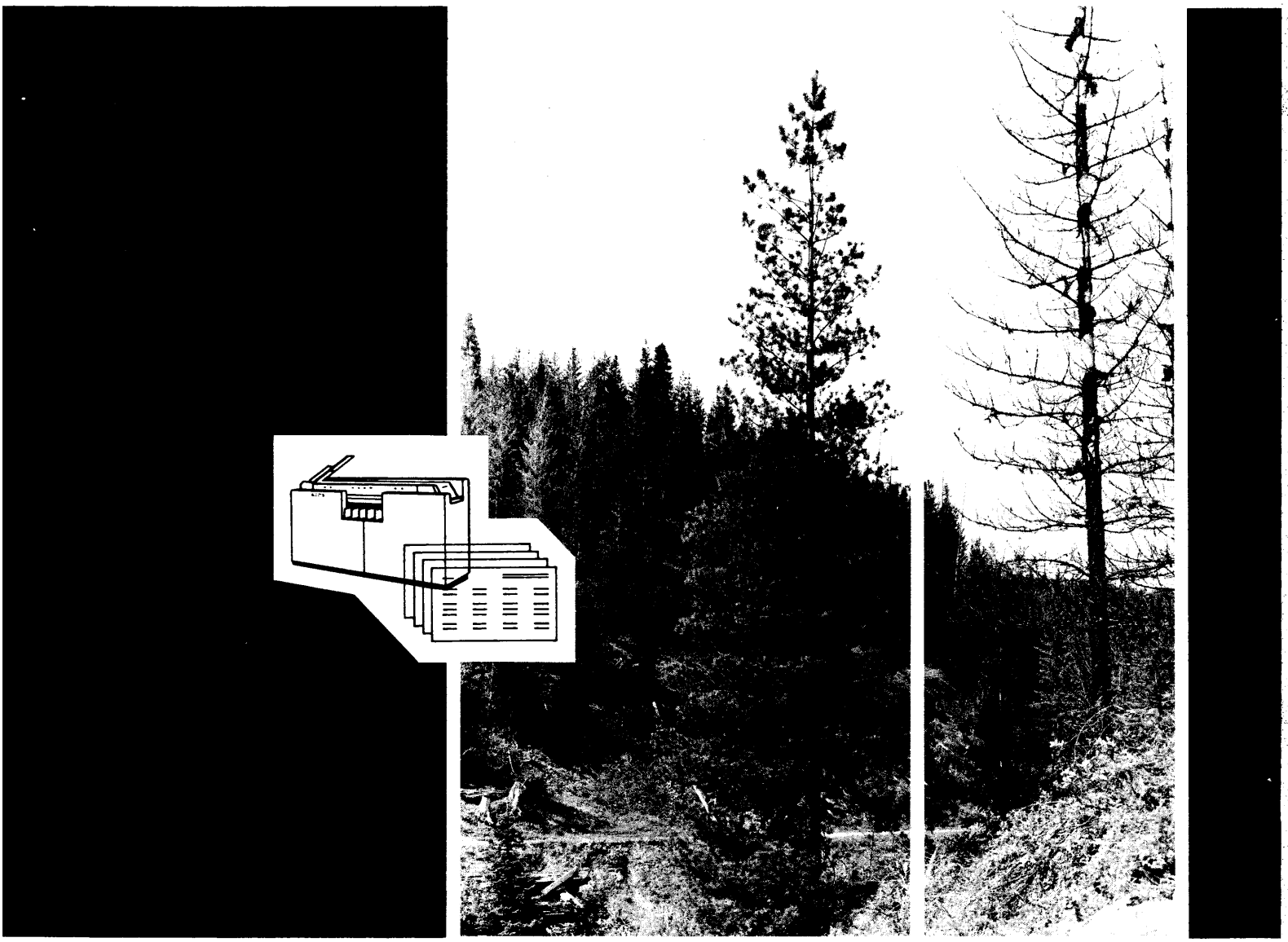

USDA Forest Service Research Paper INT-258
Intermountain Forest and Range Experiment Station
U.S. Department of Agriculture, Forest Service

RESEARCH SUMMARY

The major problem of managing white pines in North America is the blister rust disease caused by the introduced stem rust *Cronartium ribicola*. Populations of white pines exhibiting differing degrees of resistance as well as some proven management options are available for use in control strategies. But, since adaptative flexibility is of prime concern, a compromise must be reached between degree of resistance to a particular pest on the one hand and all the other factors of the environment on the other. An effective route to this compromise is integration of all genetic, biologic, and conventional control methodologies so as to maximize the number of management actions that work in a common direction.

Computer simulation is an efficient way to organize and analyze the knowledge available about complex systems. The research reported herein is an attempt at organizing knowledge about the complex blister rust system into a simulator that will ultimately supply site-by-site and stand-by-stand prescriptions of integrated management options. The model was formulated with the aid of a continuous systems simulation compiler, called SIMCOMP, that allows biologists having a minimal command of computer programing to maximize their input into model formulation.

The step-by-step formulation of the blister rust model is presented to illustrate model rationale and how use of SIMCOMP can facilitate incorporation of biologic knowledge. The detailed description also provides flow diagrams and quantitative relationships for implementation of the programing phase. Procedures for verification of the completed simulation and needs for additional research are also discussed.

CONTENTS

USDA Forest Service
Research Paper INT-258
January 1981

COMPUTER SIMULATION OF WHITE PINE BLISTER RUST EPIDEMICS

I. MODEL FORMULATION

G.I. McDonald, R. J. Hoff, and W. Wykoff

INTERMOUNTAIN FOREST AND RANGE EXPERIMENT STATION
U.S. Department of Agriculture
Forest Service
Ogden, Utah 84401

THE AUTHORS

GERAL I. McDONALD is principal plant pathologist on the Station's genetics and pest resistance research work unit at Moscow, Idaho. Dr. McDonald received his B.S. in forest management (1963) and Ph.D. in plant pathology (1969) from Washington State University, Pullman. He has been investigating the genetic interaction of the blister rust organism and its hosts as well as epidemiology of blister rust since he joined the Station in 1966.

RAYMOND J. HOFF is principal plant geneticist on the Station's genetics and pest resistance research work unit at Moscow, Idaho. Dr. Hoff received a B.A. in biology (1957) from Western Washington State University and a Ph.D. in botany (1968) from Washington State University, Pullman. He has been working on the development of western white pine resistance to blister rust and other pest problems with other conifers.

WILLIAM R. WYKOFF is a research forester on the Station's quantitative analysis of forest management practices and resources for planning and control research work unit at Moscow, Idaho. Mr. Wykoff received his B.S. in forest management (1970) from the University of Minnesota, St. Paul, and his M.S. in forest management (1975) from Washington State University, Pullman. Since joining the Station in 1974, he has worked on the development of tree growth models, and the implementation of these models in a stand development simulation program.

ACKNOWLEDGMENTS

The authors would like to express their sincere appreciation to those who contributed valuable technical assistance. Special thanks to Dr. Ralph Williams, USDA Forest Service, Region 1; Dr. Everett Hansen, Oregon State University; and Dr. Neil Martin and Dr. David Hamilton, USDA Forest Service, Intermountain Station.

INTRODUCTION

The application of computer simulation to the quantitative analysis of plant disease epidemics has received increased attention in recent years (Waggoner and Horsfall 1969; Zadoks 1971, 1972; Kranz 1974; Waggoner 1974; Strand and Roth 1976; Rouse and Baker 1978). Computer simulation requires quantification of pest propagules, host target, and weather variables. These measurements are then used to formulate equations that relate the biotic and abiotic variables.

Any specific modeling effort in biology is directed at one of the following four broad objectives: (1) compilation and summarization of the knowledge about a certain subject; (2) illustration or exemplification in support of a provisional theory; (3) illustration or exemplification to show the inadequacies or incorrectness of a provisional theory; and (4) selection of the most reasonable theory from a series of theories about a certain phenomenon (Reddingius 1974). White pine blister rust is an excellent candidate for the application of general objective (1). This epidemic is a complex biological phenomenon that has been intensely studied over many years producing a great amount of data. Thus, our modeling objective is to bring together the available knowledge to try to understand how blister rust epidemics behave under various natural and man-influenced circumstances. The ultimate objective of this effort is to develop low cost, integrated rust management plans. The objectives of this paper are to (1) describe the components of the blister rust system, and (2) to present a model of blister rust epidemics. Details of programing the model will be published in a separate Station General Technical Report.

Cronartium ribicola is a heteroecious full-cycle rust that infects to varying degrees all species of *Pinus* subgenus *Strobus*, section *Strobus*, and most species of *Ribes*.

In most of the forested areas of the world located in the north temperate zone, *Ribes* and *Pinus* species grow together. Currently the rust is present in most localities, but in the warmer drier regions, the disease is found infrequently.

Aeciospores are produced on pine in the spring when the *Ribes* plants are leafing out. The spores are windborne to the developing leaves where they germinate and infect the *Ribes* leaves. Infections begin producing urediospores in about 2 weeks. The urediospores reinfect *Ribes* leaves throughout the summer any time temperature and moisture conditions are favorable and viable spores are present. In northern Idaho, teliospores are present from July 1 to October 1 most years. They generally germinate immediately upon the presence of any moist period of at least 12 hours duration that occurs while viable teliospores are present. The sporidia produced by teliospore germination are windborne to the pine needles where they immediately germinate and infect the pine through stomata. Over the next 1 to 3 years, the fungus grows down the needle and penetrates the stem or branch. About 1 year after penetration of the stem, pycniospores are produced. The function of these spores has not been definitely shown, but they are believed to be spermatia--it is not known if the fungus is heterothallic or homothallic (McDonald 1978). The aeciospores are generally produced the year following pycnia production.

The fungus produces fusiform swellings and cankers on the branches and stems of susceptible trees. The cankers grow parallel (up and down) with the stems and branches at a rate of about 5-13 cm each way each year. The growth around the stem is about 3 cm each way each year, making the stem encirclement rate about 6 cm per year. Factors such as site, genotype of the host, and genotype of the rust may cause variation in the encirclement rate. Thus, the time needed to produce a canker that girdles a stem varies with the growth rate of the tree, growth rate of the rust, the diameter of the tree at the point that the fungus reached the stem, and possibly other genetic and environmental factors. This period can vary from a few weeks on small seedlings to 40 years or more on mature trees. After trees are girdled (even seedlings) it takes 3 to 10 years for the tree to die.

In many cases, trees do not die entirely. Tops are lost; branches die; and growth slows down as a result. But, it can be generally said that there is little effect on growth until shortly before death.

Heavy infection can cause defoliation of *Ribes* plants, but, in most areas in most years, the infection is not of sufficient magnitude to cause obvious damage to the *Ribes* population.

The Blister Rust Epidemic

The rust was introduced into the northeastern United States about 1900 on *P. strobus* seedlings shipped from France (Mielke 1943). The disease quickly spread through the range of *P. strobus*.

The rust was introduced into western North America about 1916. This introduction was apparently also on infected *P. strobus* seedlings from France (Hahn 1949). The disease quickly spread throughout the extensive stands of western white pine in the Cascade and Rocky Mountains. The economic management of *P. monticola* is presently out of the question without some sort of control strategy (Ketcham and others 1968).

THE OVERALL MODEL

The two approaches to ecosystem modeling that have been commonly employed are analytical models and simulation models (Hall and Day 1977). A simulation model was used for the white pine blister rust system because of our desire to incorporate as much biologic knowledge as possible.

Box-and-arrow diagrams and word models were used to define the system and then both mechanistic and descriptive equations were created to describe the relations between state variables or "boxes" (see also Hall and Day 1977). The rationale of box-and-arrow diagrams is illustrated in figure 1. Each compartment is a state variable and the movement of quantities (needles, spores, *Ribes* bushes, infections, trees, and so on) from one box to another is called a flow. The flows are controlled by forcing functions, donor-controlled interaction, and donor-recipient controlled interaction. State variables will be represented by numbers and(or) numbers and X's. Flows will be represented by J's.

SIMCOMP Method of Simulation

The computer programing system that was used is called SIMCOMP version 2.1 (Gustafson and Innis 1973). Their system is based on "box-and-arrow" flow diagraming as shown in figure 1.

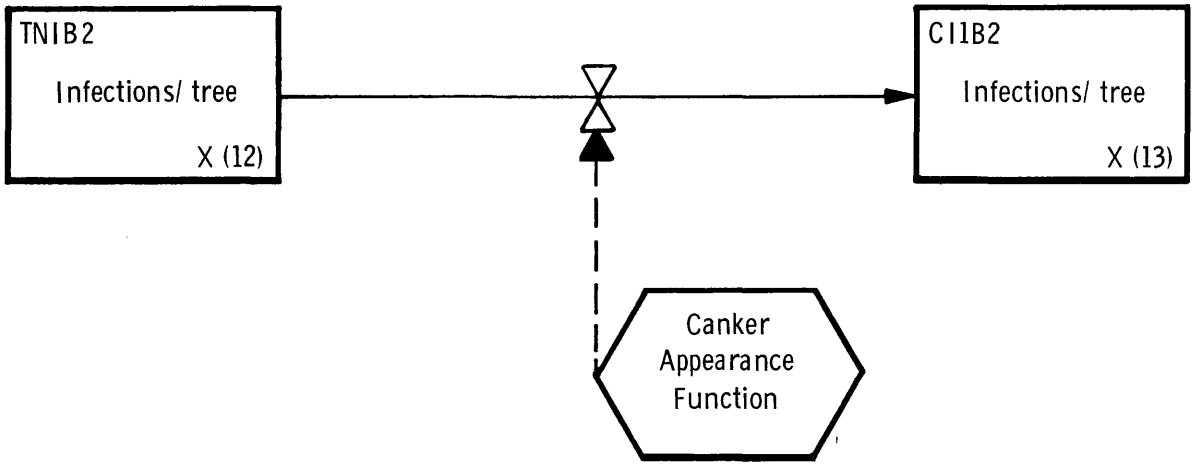

Figure 1.--Rationale of the box-and-arrow method of diagramming simulation models illustrated with flow $J_{(12\rightarrow13)}$ from state variable X(12) to state variable X(13). Solid line from box to box shows flow of matter and arrow shows direction of flow. Dotted line shows flow of information that controls flow of matter through butterfly valve.

The SIMCOMP approach has worked very well for us in providing guidance to the biologists (Geral I McDonald and R. J. Hoff) for development of the flow diagrams, and the SIMCOMP framework greatly facilitated communication between the biologists and the systems analyst (William R. Wykoff). Keep in mind as you read that the model was formulated to be programed by the SIMCOMP compiler.

Since the blister rust system is complex, submodels were developed that group state variables composed of the same materials, like bushes per hectare or infections per tree. The amount of these materials may be increased, decreased, or left the same as time changes. In some cases, the time change from state variable to state variable occurs on an annual cycle and, in other cases, many state variable changes occur within one annual cycle.

The model was organized into five separate submodels (fig. 2):

A. *Ribes* density (bushes per hectare)
B. *Ribes* infection (spores of infections per square centimeter of leaf surface)
C. Pine target (square centimeters of infective surface per tree)
D. Pine infection (infections per tree)
E. Stand infection (trees per hectare)

The model is developed with word and diagrammatic definitions of each flow within each submodel. Four appendixes provide the derivation of the mathematical formulas that specify the material and informational flows and the construction of some specialized functions and subroutines. These derivations were approached from the viewpoint of explaining natural processes rather than the expectation of a simple statistical fit (Jowett and others 1974). But, in many cases, lack of understanding forced us to accept a statistical fit or even an assumed relationship.

Figure 2 shows the relationships among the various components. The *Ribes* density submodel computes the number of bushes per hectare as a function of light intensity, which is in turn computed from the Total number of Living Trees per hectare (TLT) and Current Tree Height (CTH). The level of *Ribes* eradication can be imposed as a control measure or set at a given value to simulate some natural restriction on *Ribes* density. This submodel computes *Ribes* Density for each of the four major species in northern Idaho to produce four outputs: RD(1), RD(2), RD(3), and RD(4) (see table 1 for variable definitions).

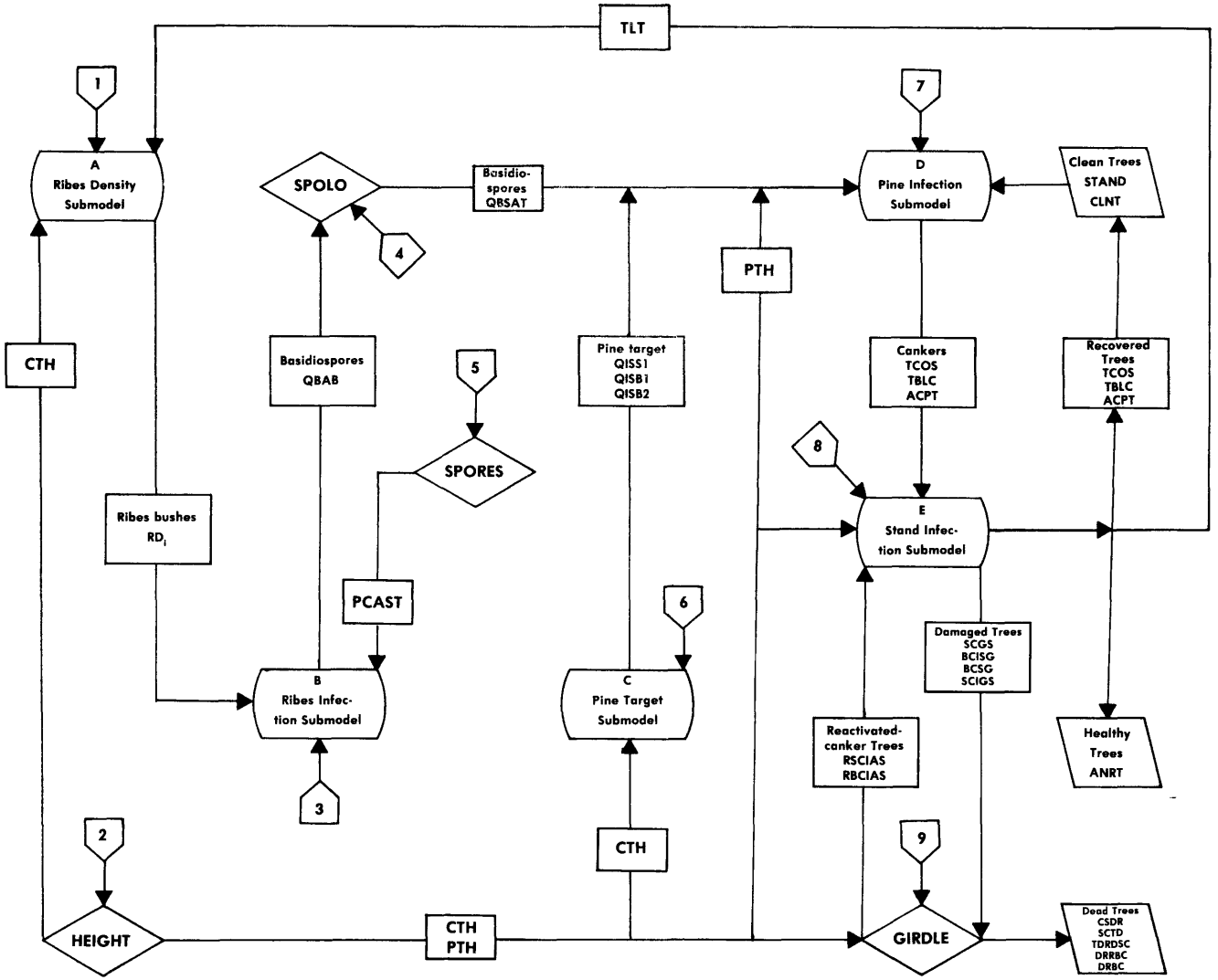

Figure 2.--Flow diagram of white pine blister rust model. Rectangular boxes contain computed variables; parallelograms contain inputs and outputs; and connectors indicate user-controlled variables defined as follows: connector 1 - table 1 variables; connector 2 - SITE and TIME from table 1; connector 3 - variables from table 2; connector 4 - GPF_i and $TARGET_i$ of table 2; connector 5 - DIP(DAA1), TCW_i and TSD of table 3; connector 6 - table 9 variables; connector 7 - table 12 variables; connector 8 - table 17 variables; and connector 9 - FER and ICIAS of table 17.

The *Ribes* infection submodel accepts user controlled (input) variables defined in table 3. (Tables numbered out of sequence are found under respective submodel discussions.) The output is the number of basidiospores per square centimeter available at the pine tree (QBSAT). The input variables are grouped into weather parameters, *Ribes*-species-specific-rust-growth parameters, and rust growth parameters. In all, 21 variables influence the simulation of rust development on the *Ribes* host.

Next, the pine host target is developed. Only one computed variable (current tree height) and two input variables (table 3) are used here. This submodel provides the target area of an average tree each year by needle age and needle location (bole and branch). The output is expressed as square centimeters of infection surface. Note that current tree height is also used and so site quality is an additional variable.

Individual pine tree infection is computed as the total number of cankers on an average tree in the stand (ACPT), the Total number of Lethal branch Cankers (TLC), and the Total number of Cankers derived from Stem-needles (TCOS) for each year of the simulation. Eight input variables (defined in table 4) interact with spore load (QBSAT) and Past Tree Height (PTH) to simulate the annual amount of new infection.

The infection that develops annually on the average tree is expanded to a stand basis by the stand infection submodel. In all, 10 input variables (table 5) interact with the computed variables from the individual pine infection submodel, and the height function to simulate dead trees, damaged trees, recovered trees, clean trees, and healthy trees. Trees that recovered because of permanent canker inactivation feed back to the individual pine infection submodel. Trees that are resistant are removed from the system. Simulation output can be expressed as the level of any state variable over time or a disease progress curve for mortality, lethal branch infection, stem or needle-derived bole infections, or total infections. Note also that Total of Living Trees (TLT) per hectare is fed back to the *Ribes* density submodel.

DIAGRAMMATIC AND WORD MODELS

The simulation includes specification of varying levels and kinds of host resistance and other control measures, as well as specification of various epidemiological fitness traits (Nelson 1973) of the rust. The objective was to change the variables in order to observe their influences on the simulated development of rust damage on pine stands. Duration, seasonal frequency, and season of occurrence of infection periods can be specified also. Consequently, host-, fungus-, and environment-related parameters can be varied independently and their individual influences on the outcome of simulated epidemics studied.

We are simulating infection on an average tree in a given stand. This average tree is characterized by an average target area, an average distance from basidiospore source to the tree, and, therefore, an average number of infections. The average infection level is then used to simulate infection of stand members on an individual basis. This simplification should work well since most white pine stands are even-aged. In this section, each flow will be defined in words, so that the biology of the model can be seen to be separate from the quantitative relationships.

A submodel consists of a grouping of state variables (boxes) all defined by the same units such as bushes per hectare, spores per bush, infections per tree, or square centimeters per tree. Each state variable is delineated by the subscripted capital letter X, a number, and an acronym (for example, BC1T). In the appendix description of the quantitative relationships, each flow will be quantified by an equation and each flow will be identified by a subscripted capital letter ($J_{5,1}$).

Ribes Density Submodel

Generalized source of *Ribes* bushes (fig. 3) is partitioned each year into number of *Ribes* bushes per hectare for each of four *Ribes* species (5→1)(5→2)(5→3)(5→4). *Ribes* bush populations are known to be influenced by amount of sunlight available. Some *Ribes* species are more responsive to sunlight than others; so the four principal *Ribes* species of northern Idaho are handled separately. Amount of sunlight reaching the forest floor depends largely on tree size and density. Second, *Ribes* bushes can be physically removed from the site or their populations reduced by other means. Thus, the number of bushes per hectare can be a function of management options. Third, the *Ribes* species are distributed according to their site requirements; a given site may not be suited for one or more of the species, requiring that density also be set independent of the sunlight relationship. All state variables and external variables relating to this submodel are defined in table 1 and each flow path is described in table 2.

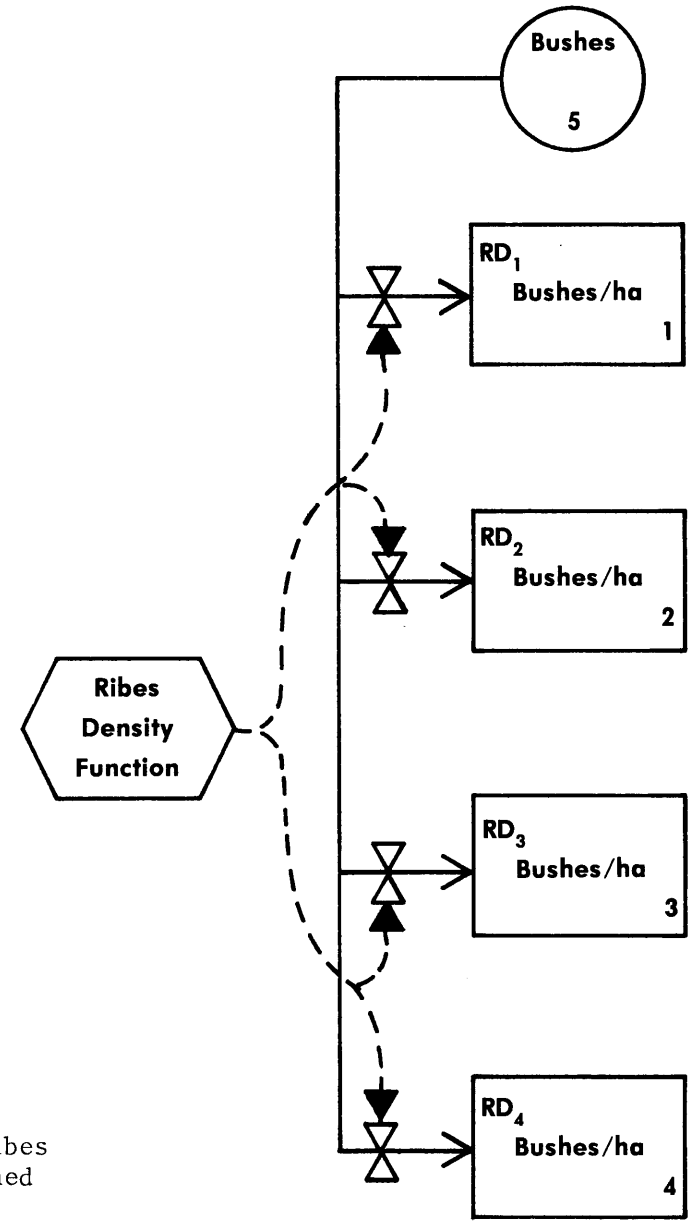

Figure 3.--Box-and-arrow diagram of the ribes density simulation submodel (terms defined in table 1).

Table 1.--*Definition of variables used in* Ribes *density submodel*

Variable			Definition
State variables:	i		
X(1)	RD_i	1	*Ribes* density, *R. hudsonianum* bushes per hectare
X(2)	RD_i	2	*Ribes* density, *R. inerme* bushes per hectare
X(3)	RD_i	3	*Ribes* density, *R. lacustre* bushes per hectare
X(4)	RD_i	4	*Ribes* density, *R. viscosissimum* bushes per hectare
X(5)	BUSHES		Unspecified source of *Ribes* bushes
User controlled variables:			
$ERAD_i$			If positive number = eradication level in bushes per hectare; 0 = *Ribes* species not present; -1 = *Ribes* population under natural control.
i			Index to *Ribes* species. 1 = *R. hudsonianum*, 2 = *R. inerme*, 3 = *R. lacustre*, 4 = *R. viscosissimum*.
SITE			Site index, total height at 50 years in feet.
TIME			Current stand age, years
Computed variables:			See appendix I

Table 2.--*Ribes density submodel flow description*

Flow path	Flow name	Flow description	Flow equation*
$J_{(5,1)}$	Ribes generation	Annual production of *R. hudsonianum*	$RD(1) = \begin{cases} 0.05 + 2.15\ PFS^{16.58} & ; ERAD(1) = < 0 \\ 0 & ; ERAD(1) = 0 \\ ERAD(1) & ; ERAD(1) = > 0 \end{cases}$
$J_{(5,2)}$	Ribes generation	Annual production of *R. inerme*	$RD(2) = \begin{cases} 1.45 + 4.35\ PFS^{11.84} & ; ERAD(2) = < 0 \\ 0 & ; ERAD(2) = 0 \\ ERAD(2) & ; ERAD(2) = > 0 \end{cases}$
$J_{(5,3)}$	Ribes generation	Annual production of *R. lacustre*	$RD(3) = \begin{cases} 40.0 + 190.0\ PFS^{10.96} & ; ERAD(3) = < 0 \\ 0 & ; ERAD(3) = 0 \\ ERAD(3) & ; ERAD(3) = > 0 \end{cases}$
$J_{(5,4)}$	Ribes generation	Annual production of *R. viscosissimum*	$RD(4) = \begin{cases} 40.0 + 660.0\ PFS^{27.03} & ; ERAD(4) = < 0 \\ 0 & ; ERAD(4) = 0 \\ ERAD(4) & ; ERAD(4) = > 0 \end{cases}$

*See Appendix I for discussion of flow equation derivation.

Ribes Infection Submodel

The *Ribes* infection submodel (fig. 4) is composed of four parts--one for each spore stage involved. The definitions of the variables used are given in table 3 and flows are described in table 4. Rust development and pine infection attributable to each of the four principal *Ribes* species of northern Idaho will be computed individually to create a composite spore load for each infection period by summation over all four *Ribes* species. Infection periods will be defined during the input of weather data. The model was made to respond to a variety of descriptions of infection period, which can be based on duration, date of occurrence, and average temperature.

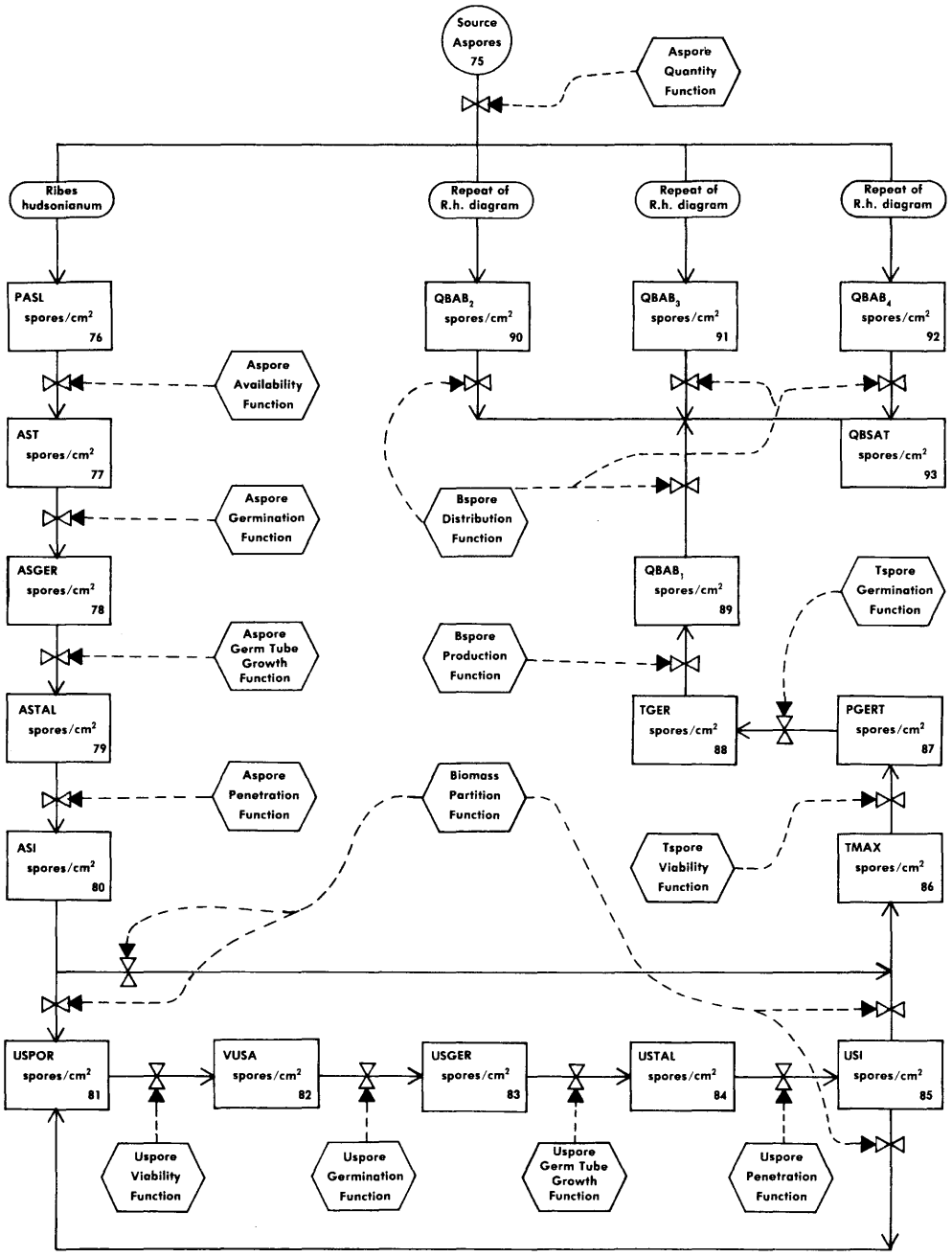

Figure 4.--Box-and-arrow diagram of *Cronartium ribicola* infection on *Ribes* species (terms defined in table 3).

Table 3.--*Definitions of variables used in the* Ribes *infection submodel*

Variable			Definition
State variables:		i	
X(75)	SOURCE		Unspecified source of aeciospores.
X(76)	PASL		Potential aeciospore load, spores per square centimeter.
X(77)	AST		Number of aeciospores per square centimeter trapped in a given infection period, spores per square centimeter of *Ribes* leaf (under surface).
X(78)	ASGER		Number of aeciospores per square centimeter that are expected to germinate, spores per square centimeter.
X(79)	ASTAL		Aeciospores expected to produce germ tubes of adequate length to cause infection, spores per square centimeter.
X(80)	ASI		Aeciospores expected to cause infections during a given infection period, spores per square centimeter.
X(81)	USPOR		Urediospores available for infection from both aecial and uredial infections, spores per square centimeter.
X(82)	VUSA		Viable urediospores, spores per square centimeter.
X(83)	USGER		Urediospores germinated during a given infection period, spores per square centimeter.
X(84)	USTAL		Urediospores expected to produce germ tubes of adequate length to cause infection, spores per square centimeter.
X(85)	USI		Urediospores expected to cause infections during a given infection period, spores per square centimeter.
X(86)	TMAX		Teliospores - maximum number available, spores per square centimeter.
X(87)	PGERT		Probable number of teliospores available for germination, spores per square centimeter.
X(88)	TGER		Teliospores expected to germinate during a given infection period, spores per square centimeter.
X(89)	$QBAB_i$	1	Quantity of basidiospores expected to be produced at *Ribes hudsonianum* bushes, spores per square centimeter.
X(90)	$QBAB_i$	2	Quantity of basidiospores expected to be produced at *Ribes inerme* bushes, spores per square centimeter.

(continued)

Table 3.--*Definitions of variables used in the* Ribes *infection submodel (continued)*

Variable		i	Definition
State variables:			
X(91)	$QBAB_i$	3	Quantity of basidiospores expected to be produced at *Ribes lacustre* bushes, spores per square centimeter.
X(92)	$QBAB_i$	4	Quantity of basidiospores expected to be produced at *Ribes viscosissimum* bushes, spores per square centimeter.
X(93)	QBSAT		Quantity of basidiospores expected at trees, spores per square centimeter.
User controlled variables:			
AGMAX			Temperature where aeciospore germination is maximum, degrees C.
$AIYR_i$			Aeciospore infection yield ratio expressed as infections per germinated aeciospore and indexed by *Ribes* species.
AMHL			Average maximum hourly load of aeciospores, spores per square centimeter per hour.
$BMASS_i$			Biomass of urediospores/teliospores produced by a single infection and indexed by *Ribes* species, m^3.
$BSYR_i$			Potential basidiospore yield ratio indexed by *Ribes* species, basidiospores/teliospore.
DAA1			Days after April 1 to midpoint of an infection period indexed to infection periods (0 to many/yr).
DAP			Date of aeciospore appearance expressed as days after April 1 (1/yr).
DIP(DAA1)			Duration of infection period, indexed by infection period, hours.
GPF_i			Growth point factor, indexed by *Ribes* species and expressed as *Ribes* bushes/clump.
i			Index to *Ribes* species. 1 = *R. hudsonianum*, 2 = *R. inerme*, 3 = *R. lacustre*, 4 = *R. viscosissimum*.
$TARGET_i$			*Ribes* target, indexed by species, expressed as cm^2/bush.
TCW_i			Average telial column width, indexed by species, expressed in microns.

(continued)

Table 3.--*Definitions of variables used in the* Ribes *infection submodel (continued)*

Variable	Definition
User controlled variables:	
TIP (DAA1)	Average temperature of an infection period, indexed by infection period, expressed as degrees C.
$TSAR_i$	Teliospores from aeciospores infection ratio, indexed by *Ribes* species expressed as proportion of spore biomass arising from aeciospore infections that is devoted to production of teliospores.
TSD	Average teliospore diameter, microns.
TSL	Average teliospore length, microns.
$TSUR_i$	Teliospores from urediospores infection ratio, indexed by *Ribes* species expressed as proportion of spore biomass arising from aeciospore infections that is devoted to production of teliospores.
UGMAX	Temperature where urediospore germination is maximum, degrees C.
$UIYR_i$	Urediospore infection yield ratio, indexed by *Ribes* species and expressed as infections per germinated spore.
USD	Average urediospore diameter, microns.
USL	Average urediospore length, microns.
Computed variables:	See appendix I

Table 4.--Ribes *infection submodel flow descriptions*

Flow path	Flow name	Flow description	Flow equation*
$J_{(75\rightarrow76)}$	Aeciospore generation	Computation of potential aeciospore load expressed in aeciospores per square centimeter per infection period	$PASL_i = AMHL \cdot DIP_i$
$J_{(76\rightarrow77)}$	Aeciospore availability	Computation of number of aeciospores available per square centimeter of *Ribes* leaf surface during a specified infection period	$AST_i = 1.954(A1^{2.6})e^{-A1^{3.6}} \cdot PASL_i$
$J_{(77\rightarrow78)}$	Aeciospore germination	Calculation of number of trapped aeciospores expected to germinate during a given infection period per square centimeter of leaf surface	$ASGER_i = AST_i \cdot GERMA$
$J_{(78\rightarrow79)}$	Aeciospore germ tube growth	Computation of number of germinated aeciospores per square centimeter of leaf surface expected to produce germ tubes of sufficient length for penetration of *Ribes*	$ASTAL_i = PGERAP \cdot ASGER_i$
$J_{(79\rightarrow80)}$	Aeciospore infection establishment	Computation of number of expected aeciospore germ tube penetrations that establish infection per square centimeter of lower leaf surface	$ASI_i = ASTAL_i \cdot AIYR_i$
$J_{(80\rightarrow81)}$	Urediospores from aeciospores and uredispores	Computation of urediospore production by infections caused by aeciospores	$USPOR_i = UMASS_i/(\pi \cdot USL \cdot USD^2) + BMASS_i \cdot (1-TSUR_i)$

(continued)

Table 4.--Ribes *infection submodel flow descriptions (continued)*

Flow path	Flow name	Flow description	Flow equation*
$J_{(81\rightarrow82)}$	Urediospore viability	Computation of number of germinable urediospores per square centimeter in a given infection period	$VUSA_i = 2.477(A4)^{1.5-(A4)^{2.5}} e^{\cdot USPOR_i}$
$J_{(82\rightarrow83)}$	Urediospore germination	Computation of number of urediospores that germinate during a given infection period	$USGER_i = VUSA_i \cdot GERMU$
$J_{(83\rightarrow84)}$	Urediospore germ tube growth	Calculation of number of germinated urediospores expected to produce germ tubes of sufficient length to penetrate	$USTAL_i = PGERAP \cdot USGER_i$
$J_{(84\rightarrow85)}$	Urediospore infection	Computation of number of urediospore infections per square centimeter of *Ribes* leaf caused by urediospore infections	$USI_i = USTAL_i \cdot UIYR_i$
$J_{(85\rightarrow81)}$	Urediospore infection from urediospores	Computation of the number of urediospores produced per square centimeter of *Ribes* leaf by urediospore infections	$USPOR_i = BMASS_i \cdot (1-TSUR_i)$
$J_{(80\rightarrow86)}$ $J_{(85\rightarrow86)}$	Teliospore generation	Computation of number of teliospores expected to arise from aeciospore and urediospore derived infections	$\bar{TMAX}_i = \frac{TSAR_i \cdot ASI_i \cdot BMASS_i}{\pi \cdot TSL \cdot TSD^2} + \frac{TSUR_i \cdot USI_i \cdot BMASS_i}{\pi \cdot TSL \cdot TSD^2}$

(continued)

Table 4.--Ribes *infection submodel flow descriptions (continued)*

Flow path	Flow name	Flow description	Flow equation*
$J_{(86\rightarrow87)}$	Teliospore viability	Computation of number of teliospores viable during a given infection period per square centimeter of leaf surface	$PGERT_i = TMAX_i \cdot 2.416 \cdot A9^{1.25} e^{-(A9)^{2.25}}$
$J_{(87\rightarrow88)}$	Teliospore germination	Computation of number of teliospores expected to germinate during a given infection period	$TGER_i = PGERT_i \cdot PCAST$
$J_{(88\rightarrow89)}$	Basidiospore generation	Computation of number of basidiospores produced for each square centimeter of underside leaf surface per infection period	$QBAB_i = TGER_i \cdot BSYR_i$
$J_{(89\rightarrow93;90\rightarrow93;91\rightarrow93;92\rightarrow93)}$	Basidiospore distribution	Computation of number of basidiospores per square centimeter of flat surface at the white pine tree	$QBSAT = \sum_{i=1}^{4} \left[\frac{QBAB_i \cdot PBIRX_i}{282,734.34(2RX-1)} - \frac{QBAB_i GPF_i \cdot (1-PET)}{100,000,000} \right] \cdot TARGET_i \cdot RD_i$

*See appendix I for derivation of flow equations

The infection period defines that period of favorable environmental circumstances during which spores are released, transported to an infection court, germinate, and establish a new thallus.

The two criteria used to define Duration of Infection Period (DIP) were (1) 5 consecutive hours of assumed 100 percent relative humidity as determined from hourly precipitation records where each hourly record was required to have at least 0.01 inches of rain, and (2) moisture in the woods was assumed to remain at or near 100 percent relative humidity for 2 hours after the 5-hour wet period if the period ended during darkness. Thus, the minimum infection period was 5 hours. Next, date of occurrence of the infection period was expressed as number of Days After April 1 to the midpoint of the period (DAA1). Average Temperature of an Infection Period (TIP) was obtained by summation of daily maximum and minimum temperatures divided by the number of records summed. The infection periods can be redefined so that one could investigate the influence of this definition on the simulated outcome or use data from a specified location.

The infection process will be divided into five major areas: trapping, spore viability, spore germination, germ tube growth rate, and probability of penetration (infection yield ratio). Details of trapping will be discussed for aeciospores, urediospores, and basidiospores. Viability is assumed to be controlled by a time-dependent function. Germination is divided into germination lag period (the time between onset of conditions for germination and beginning of germination); germination period (the time from beginning to end of germination); and germination percentage. All three of these facets of germination are easily measured, as is germ tube growth rate. The last process, probability of penetration, will be considered as a catchall. We will assume that only Infection Period Duration (DIP) and Infection Period Temperature (TIP) will influence the germination process. But all kinds of factors from rust and pine genotype to chemicals applied to control the rust will be assumed to influence probability of penetration. This probability can be measured by supplying optimum temperature and duration conditions, then varying all other factors. We have accordingly measured Basidiospore Infection Yield (BIY) and Aeciospore Infection yield (AIY) and have incorporated a place for Urediospore Infection Yield ratio (UIY), but have not measured it. It is expected that the model will be very sensitive to each of these values. Thus, they can all be used to make many kinds of adjustments to simulate the influence of control chemicals, weather, *Ribes* and pine resistance genes, and rust genetic variation. Each specific IY will be discussed in the appropriate place.

Within the commercial range of western white pine in Idaho, the four principal species of a total of 15 *Ribes* species are *R. hudsonianum (R. petiolare), R. viscosissimum, R. lacustre,* and *R. inerme* (Mielke and others 1937). Intensification occurs at different rates on *R. hudsonianum, R. inerme,* and *R. viscosissimum* (Mielke and others 1937), but little if any intensification occurs on *R. lacustre* (Mielke and others 1937; Buchanan and Kimmey 1938). Consequently, calculation of basidiospore loads must take into account *Ribes* species, in addition to *Ribes* population densities, aeciospore loads, and weather. Thus, each state variable is actually one of a set of four that will be indexed by i (Index to *Ribes* Species). This submodel will be described for *R. hudsonianum* (i=1).

The first problem was to develop a model describing the amount of *Ribes* leaf surface to be expected for each of the species. In general, the four *Ribes* species under consideration complete their growth by the first of July in northern Idaho (Mielke and others 1937). We assumed that the amount of *Ribes* material available on July 1 will be available while aeciospores are flying, which is generally about mid-May in northern Idaho. Much of the available data is on the basis of individual bushes. Mielke and others (1937) supply data on the number of leaves per bush for the four species and Lachmund (1934) supplies data on the average size of the leaves for the four species (table 5).

Table 5.--*Average number of leaves per bush and average size of leaves in square centimeters for four* Ribes *species*

Species	i	Number of leaves	Leaf size[1]	Number of leaves/bush[2]	Leaf surface/ bush
			cm^2		cm^2
R. hudsonianum	1	385	35.45	470.6	16.7×10^3
R. inerme	2	325	14.06	578.9	8.1×10^3
R. lacustre	3	342	6.68	907.3	6.1×10^3
R. viscosissimum	4	362	16.20	240.2	3.9×10^3

[1]Calculated from Lachmund (1934, table 2). Includes both open and shade forms.
[2]Calculated from figure 3 and table 5, Mielke and others (1937) and includes open, shade, and partial-shade forms.

We decided to model *Ribes* infection from the viewpoint of individual infections (spores) because of some interesting epidemiological perspectives that came out of the study of single aeciospore isolates of *C. ribicola* on detached *R. hudsonianum* leaves. These studies were designed to investigate the genetics of *C. ribicola*, but the following observed features of the life cycle of the rust were pertinent to our modeling effort:

1. Rarely does an aeciospore infection produce teliospores directly.

2. Infections started from urediospores produce a mixture of teliospores and urediospores.

3. The relative proportion of urediospores and teliospores seems to be influenced by leaf physiology because urediospore populations derived from a single aeciospore (rust genetics controlled) and placed on several single leaves from one *Ribes* clone (*Ribes* genetics controlled), each in a separate Petri dish and all held at 21°C, will produce a variable ratio dish to dish.

4. Temperature seems to be involved in some way because urediospore infections held at 13°C produce mostly telia, whereas those kept at 21°C produce mixes.

5. The average partitioning seems to be about a 1:1 ratio (urediospores: teliospores) of the spore yield capacity of each infection on a biomass basis at 21°C.

6. A given infection seems to have a definite life expectancy, thus constant spore production requires continued reinfection.

7. The stages in the life of an individual aeciospore infection seem to require 14 days incubation, urediospore production peaks at 25 days, trailing to nontransferable (nonviable) urediospores at about 35 days in sealed Petri dishes at 100 percent relative humidity.

8. The stages in the life of an individual urediospore infection are 14 days incubation followed by urediospore and teliospore appearance at 14 days and then peak urediospore and teliospore production between 25 and 28 days.

9. Teliospores are produced in the enclosed Petri dishes and germinate as soon as mature, whether they are held at a constant 21°C, kept at 13°C nights and 21°C days, or held at a constant 13°C.

These observations lead to a description of the life cycle of *C. ribicola* that is somewhat different from current belief (Van Arsdel and others 1956). The current thought is that a 13°-16°C night temperature is required to trigger formation of significant numbers of teliospores and that about 30 days are required from inoculation with aeciospores to formation of teliospores. Also, the teliospores typically show up about 2 weeks after the 13°C night temperatures are initiated. Based on our observations, we believe that the "trigger" is a temperature shock to the urediospores produced by the initial aeciospore infection and a temperature drop that causes the formation of dew needed for the urediospores to reinfect. Then the lower temperatures cause the new uredial infections to produce mostly teliospores. The net result is a new cycle of infections from urediospores, which in turn produce teliospores. In our experience with detached leaf culture of *C. ribicola*, we have tried repeatedly to obtain teliospores by using aecial infections and a temperature trigger. Poor yields were obtained until we began making urediospore inoculations. Then, teliospores were produced in as little as 14 days after urediospore inoculation, even under a constant 21°C.

Our work with detached leaf culture has also led to our strong feeling that a given infection produces spores and then dies. Thus, continuation of the rust over the summer requires the proper matching of periods favorable for infection and of viable inoculum. More on this later.

With that view of the life cycle of *C. ribicola* in mind, we went to the literature in search of more information. In 1918, L. H. Pennington and W. H. Snell studied uredial generations in the Adirondack region of New York State (reported by Spaulding 1922). They observed seven periods of urediospore production. The first generation started on May 28 and reached a peak on June 12, 14 days later. The second generation peaked about June 27, and the third peaked about July 12. In order to assess the timing accurately, one would have to have the timing of the infection periods. But, the appearance and general features of Pennington and Snell's periods seem to match well with stages of our hypothesized life cycle. Also, the appearance of telia in the above case matched our observations. Telia appeared first on June 28 with the second generation of urediospores and then appeared with all subsequent generations.

If a specific niching of viable urediospore populations and infection periods is required for the successful increase of *C. ribicola*, then several factors about the epidemics on *Ribes* become evident. First, each individual group of aecial infections has a set of future infection periods with which it must match for greatest buildup. Thus, the more cohorts started, the higher the chance of a matching weather sequence. With this thought in mind, some data from 1931 through 1936 (Stillinger[1]) were analyzed. Occurrence of wet periods and the level of *Ribes* infection were given for each of the 6 years. There appeared to be a high degree of correspondence between the length of dry period between wet periods and the level of infection. A 21-day cycle of wet periods throughout the summer seemed to be related to highest levels of teliospore production.

---

[1]Stillinger, C. R. 1936. Infection studies at Newman Lake, Washington 1936, p. 128-137. *In* 1936 annual report, Spokane Office of Blister Rust Control (Mimeographed). U.S. Dep. Agric. Bur. Plant Quar.

If the above is true, then the number and temporal distribution of periods of infection by aeciospores becomes important. Knowledge about the relative abilities of aeciospores and urediospores to spread the rust also becomes important. During the course of our investigations into single-spore cultures of the rust, we have transferred thousands of single aeciospores and hundreds of single urediospores. A fine glass needle about the same diameter as the spores being transferred was used. The aeciospores and urediospores exhibit strikingly different behavior patterns toward electrostatic forces and water. Aeciospores appear to have an active electrostatic behavior. These spores are either attracted to or repelled by the glass needle. Sometimes it is nearly impossible to remove them from the glass needle and at other times it is nearly impossible to pick them up. In regard to water, aeciospores seem to be repelled by water. It is very difficult to make an aeciospore adhere to the surface of a large (100μ diameter) water drop. They are most easily placed on a leaf surface covered with droplets about 10-15μ in diameter. They, of course, require free water for germination; but their electrostatic and water behavior patterns fit the theory of wind transport. Also, aeciospores seem to come from the aecium in a dehydrated state (they look like deflated footballs). They then hydrate (inflate) quickly when placed on a wet leaf.

On the other hand, urediospores show the opposite behavior. These spores are easy to pick up with the glass needle -- they appear to be much less active electrostatically. When placed on the surface of a water drop, they quickly leave the needle and slowly drift to the junction between the drop surface and the leaf surface. Also, urediospores seem to be turgid when in association with the sorus, but they quickly dry out with a complete loss of viability when placed in a dry environment. We have noted much better inoculation success when urediospores have been transferred en masse to water drops rather than to the wet surface of a leaf.

The water and electrostatic behavior differences between the two kinds of spores lead us to believe that aeciospores are a dispersion spore-type influenced greatly by the wind and that urediospores probably are moved very little by the wind, but are readily transported by insects and water. Thus, urediospore spread should be limited largely to bushes that were the site of an aeciospore infection. A search of the literature shows that the two spore stages function as expected. Viable aeciospores have been known to travel up to 400 miles (Mielke 1943). Urediospores have been trapped up to 1,000 yards from a known source (Spaulding 1922), but their effectiveness in causing disease at this distance is unknown. Snell (1920) reported that most urediospore spread was limited to the bush infected by aeciospores. It seems likely to us that spread is usually limited to within the bush and we will model accordingly.

Variation in incubation periods, spore yields, ratio of urediospores to teliospores in both aecial and uredial infections, spore echinulation patterns, and telial column length and width all could modify the epidemiological fitness (Nelson and McKenzie 1973; Nelson 1973) of the *Ribes* portion of the life cycle of *C. ribicola*. Changes here cause changes in the sporidial load faced by the pine host. Many opportunities may exist to modify and to monitor these epidemiological fitness traits. Although these aspects are not included, such knowledge should eventually be integrated into the rust management plans to fine tune the model.

Next, we wanted to develop a model of the level of infection on *Ribes* leaves or, more specifically, the level of basidiospore inoculum to expect in differing seasons and localities for each infection period. The level measured by percentage of leaf surface bearing telia could not be used. This measure varies a great deal, depending on the interaction of weather and site (Mielke and others 1937), and on the susceptibility of the *Ribes* leaves to aeciospore infection. Leaf susceptibility is related somewhat to leaf age and varies from species to species and from open to shade form leaves (Lachmund 1934). The model should be able to process *Ribes* species distribution patterns and environmental input data into predicted basidiospore loads season by season and locality by locality.

First, we assume that all the aecial infections from a single infection period form a single cohort. Then, each cohort can be thought of as developing according to the scheme shown in figure 5. Study of the figure shows the importance of pattern of infection period occurrence. Temporal variation of aeciospore, urediospore, and teliospore viability and occurrence, that could not be incorporated into the figure, are illustrated in figures 6 and 7. We assume that the urediospore and teliospore viability-occurrence curves are sharp. The assumption is based on data obtained from Spaulding (1922), Spaulding and Rathbun-Gravatt (1925b), and our experience with single aeciospore cultures. If our assumptions are correct, it is obvious that shifts of a few days one way or the other in the infection period peak can cause major differences in the amount of multiplication and the ultimate level of basidiospore

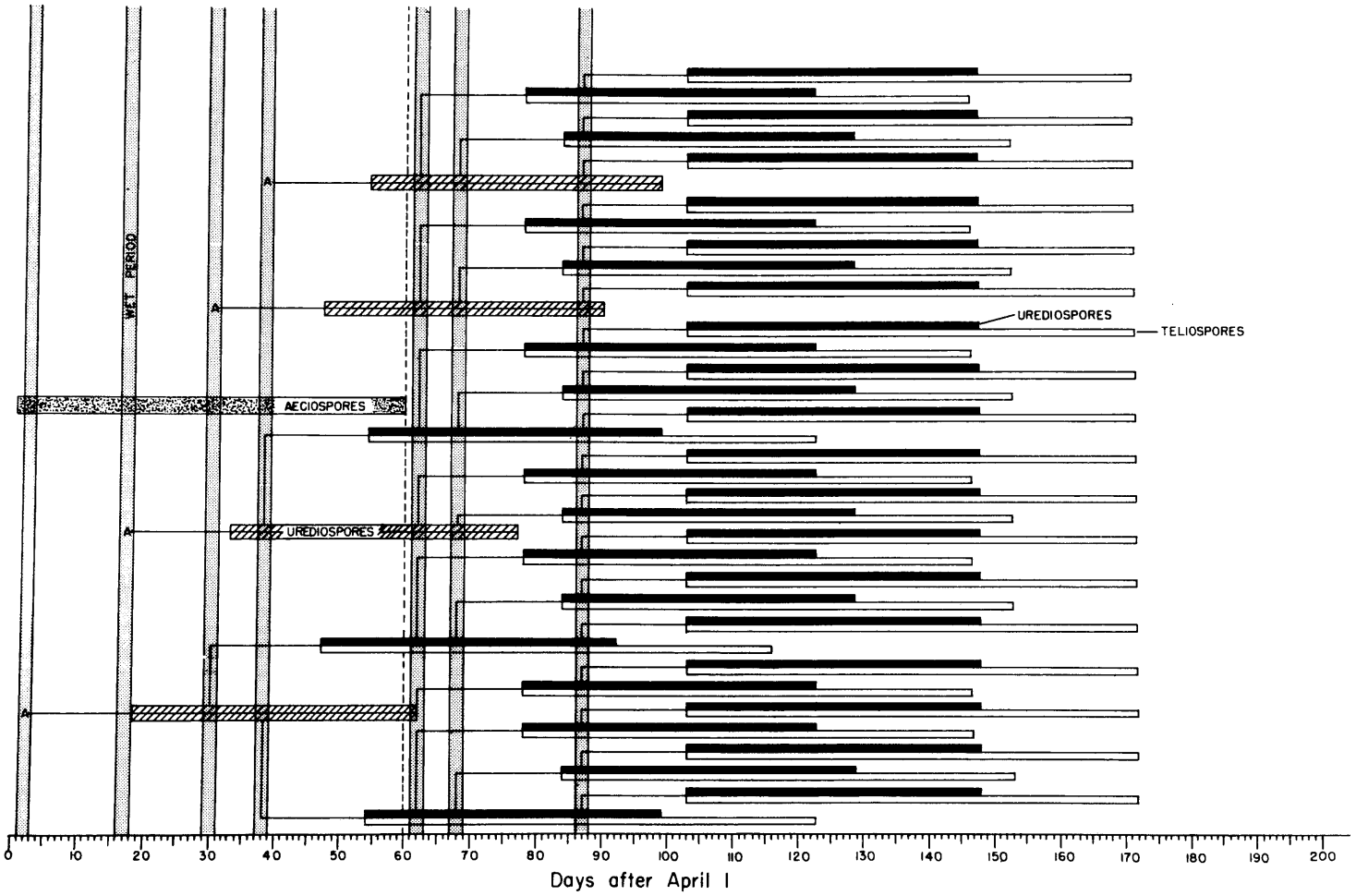

Figure 5.--Theoretical distribution of individual cohorts of *Cronartium ribicola* infection on *Ribes* sp. Assumptions: (1) aeciospore presence is April 1 to May 31; (2) aeciospore infections produce only urediospores; (3) urediospore infection produces 1:1 ratio of urediospores to teliospores; and (4) urediospore viability of one cohort set at 45 days and teliospore viability set at 70 days. Occurrence of wet periods as in northern Idaho (1934) and according to Paine (1947) low pine infection occurred.

inoculum. Figure 5 also shows why 1934 was a poor pine infection year (Paine 1947). A good early buildup was followed by an absence of wet periods when the teliospores were present. If instead, an infection period had fallen at about day 110 (late July) a massive buildup would have resulted. Then, an infection period of sufficient duration in mid-August would have resulted in high pine infection. The *Ribes* infection submodel (fig. 4) was developed to operate on the basis of infection periods that can be defined in different ways as already discussed. The current form makes use of days after April to midpoint of infection period (DAA1), Duration of Infection Period in hours (DIP), and average of maximum and minimum Temperatures for the Infection Period (TIP).

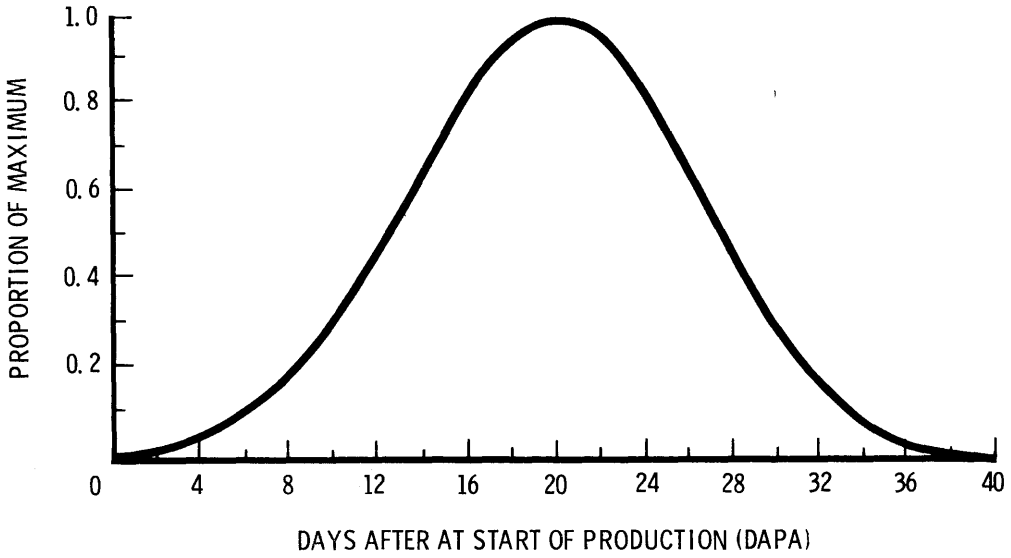

Figure 6.--Assumed distribution of *Cronartium ribicola* aeciospores as based on description of occurrence by Mielke and Kimmey (1935). Curve produced by Weibull function (equation 2 where: a = 0, b = 22.0, c = 3.6, and x = DAPA).

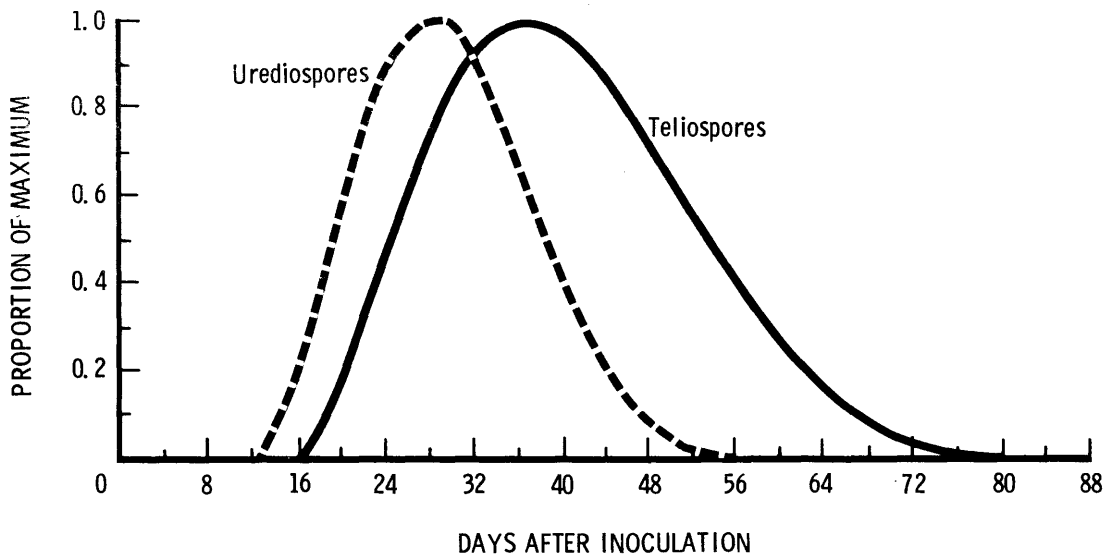

Figure 7.--Assumed distribution of urediospore and teliospore availability based on data and descriptions of Spaulding (1922) and Spaulding and Rathbun-Gravatt (1925b). (proportion urediospores = equation 2 where a = 12, b = 20, c = 2.5, w = 2.477, and x = DAYS; proportion teliospores = equation 2 where a = 16, b = 27.5, c = 2.25, w = 2.416, and x = DAYS).

The number of infections expected from an aeciospore load expressed as spores per square centimeter will be calculated for each species. If the amount of infection from each cohort of aeciospore infections is calculated separately, then the entire season can be simulated for each species. *R. hudsonianum* generally inhabits creek bottoms and small openings in the forest. Lloyd (1961) showed that dew is found in canyon bottoms more often than it is in upland areas and that once formed it lasts longer. Thus, we assumed that this species would be subject to longer infection periods (3 hours longer) than the other three, which are generally upland species. No infections will occur after an infection period of less duration than the time needed for spores to germinate and penetrate *Ribes* leaves.

The box-and-arrow diagram will now be described flow by flow in words. But, this submodel will cycle by infection periods and *Ribes* species whereas the others cycle once annually.

AECIOSPORE INFECTION

Computation of potential aeciospore load (75→76, fig. 4). Prediction of average number of infections per bush requires knowledge of aeciospore load, but this value is not presently available because it has not been measured. Aeciospore loads should be monitored for several years at a range of sites. In the absence of data, we will assume an Aeciospore average Maximum Hourly Load (AMHL) that sets maximum Potential Aeciospore Load (PASL) for an area.

Computation of number of aeciospores trapped per cm^2 *of* Ribes *leaf surface during a specified infection period* (76→77). This relationship was developed from the results of Mielke and Kimmey (1935), who listed aeciospore appearance dates, date of peak cast, and end of cast at seven sites over a number of years. We adjusted all their observations to a common blister-appearance time and calculated the average number of days to beginning of aeciospore cast (16 days), number of days to peak cast from first appearance (21 days), and duration of the cast (49 days). These features were used to develop the assumed availability curve shown in figure 6.

Calculation of proportion of trapped aeciospores expected to germinate during a given infection period (77→78). To incorporate infection-period temperature as well as duration into the model, aeciospore and urediospore germination tests were conducted. Fresh aeciospores or urediospores were mixed with distilled water and sprayed on water agar in Petri dishes. Fifteen inoculated plates were placed in incubators set at 5-degree intervals from 0° to 30°C so that one observation per temperature per hour from 2 hours to 16 hours and one observation at 24 hours after start of germination could be made. Each plate was discarded after percent germination (based on 100 spores) and germ tube length (based on 20 spores) were recorded. The results are presented as temperature-dependent plots in figures 8, 9, 10, 11, 12, 13, and 14. Curves in figures 7, 8, 11, 13, and 14 were developed using the Weibull function (eq. 2 appendix I) (Bailey and Dell 1973).

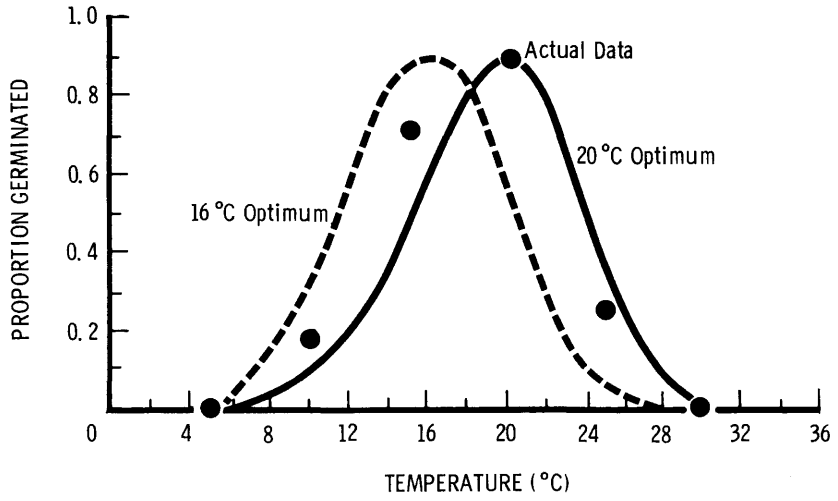

Figure 8.--Proportion germination of *Cronartium ribicola* aeciospores as a function of temperature. Solid line shows optimum at 20°C according to author's unpublished data and dotted line shows optimum at 16°C according to Van Arsdel and others (1956). Optimum is variable to simulate a variable epidemiological fitness trait, (proportion = equation 2 where: a = 3.0, b = WBA, c = WCA, w = 10.3, x = temperature).

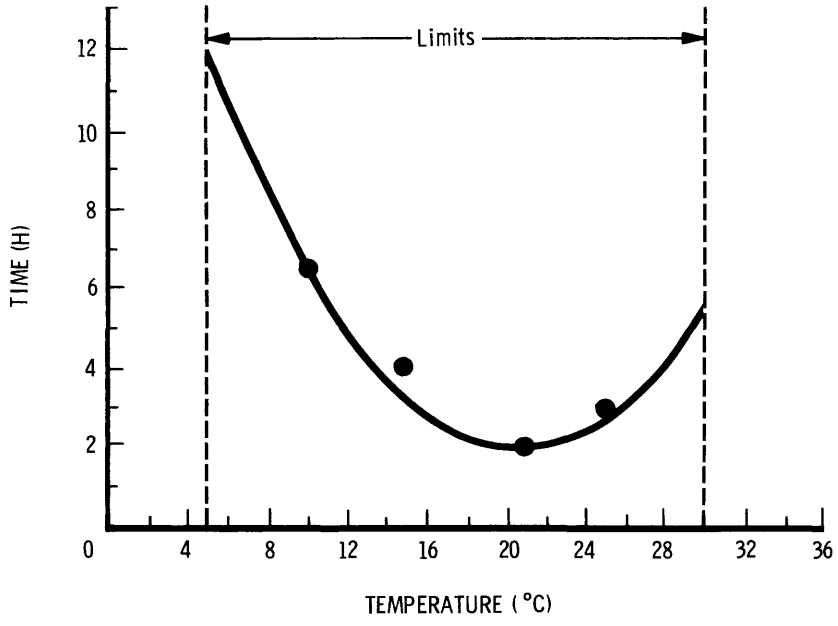

Figure 9.--Relationship between temperature and period of germination lag of *Cronartium ribicola* aeciospores. Data points from author's unpublished data; curve fit manually.

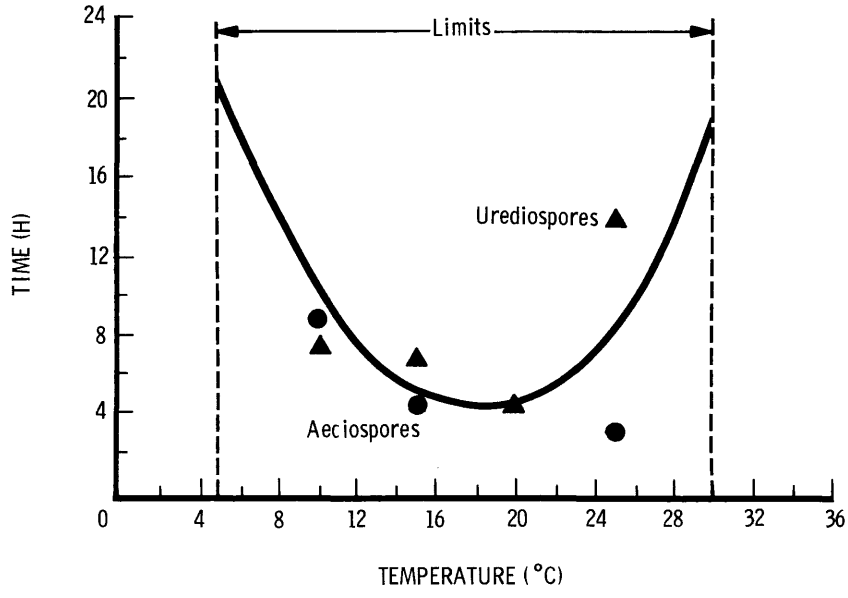

Figure 10.--Relationship between temperature and period of germination of *Cronartium ribicola* aeciospores and urediospores. Data points from author's unpublished data; curve fit manually.

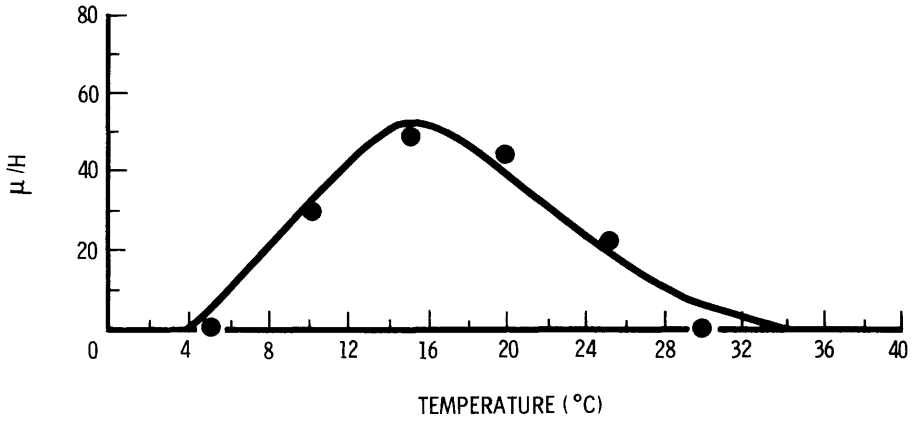

Figure 11.--Growth rate of *Cronartium ribicola* aeciospore germ tubes. Data points from author's unpublished data and curve produced by the Weibull function (equation 2 where a = 3.5, b = 15.0, c = 3.5, w = 126.37, and x = temperature).

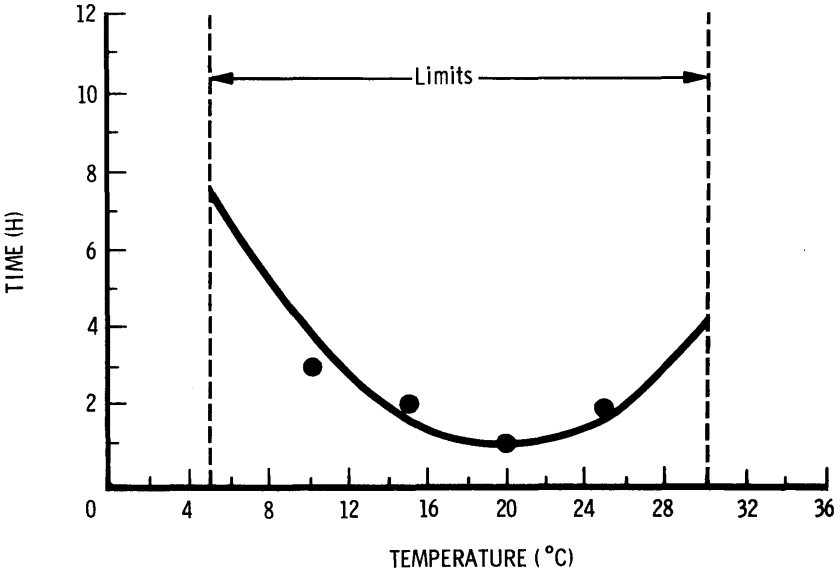

Figure 12.--Relationship between temperature and period of germination lag of *Cronartium ribicola* urediospores. Data points from author's unpublished data; curve fit manually.

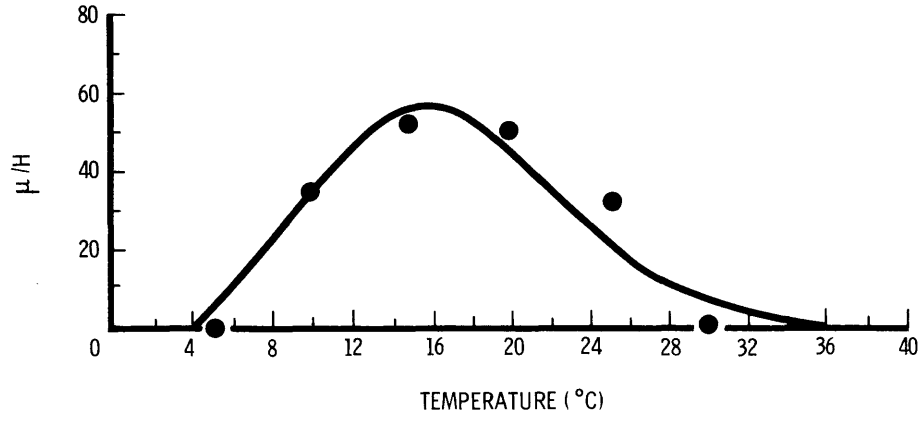

Figure 13.--Growth rate of *Cronartium ribicola* urediospore germ tubes. Data points from author's unpublished data and curve produced by Weibull function (equation 2, where a = 3.5, b = 15.0, c = 3.5, w = 136.23, and x = temperature).

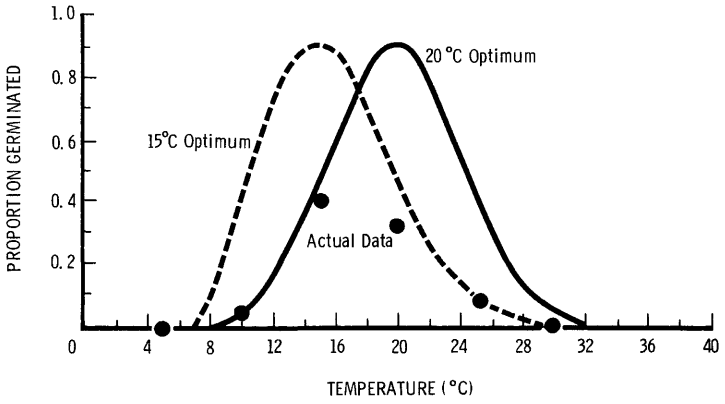

Figure 14.--Germination of *Cronartium ribicola* urediospores as a function of temperature. Dotted line shows optimum at 15°C according to author's unpublished data and solid line shows optimum at 20°C, according to Van Arsdel and others (1956). Optimum is variable to simulate a variable epidemiological fitness trait (curves simulated by Weibull function, equation 2, where a = 7, b = WBU, c = WCU, w = 10.3, x = temperature).

Three features of germination were utilized: first, the proportion germinated as a function of temperature (fig. 8); second, the period of germination (fig. 9); and third, the amount of time a population of spores required to complete germination as a function of temperature (fig. 10).

Computation of number of germinated aeciospores expected to produce germ tubes of sufficient length for penetration (78→79). It has been observed that germ tubes grow flat on the surface of *Ribes* leaves and that penetration occurs through stomata and then only when the germ tube passes directly over the stomatal opening (personal communication, J. Y. Woo). The germ tubes seem to grow to a maximum length of around 500 to 600μ (authors' unpublished data). Also, germ tubes of less than 100μ or more than 300μ in length are seldom seen to penetrate (personal communication, J. Y. Woo). Given a temperature dependent GERm Tube growth Rate of Aeciospores (GERTRA) (fig. 11), probability of penetration by a germinated spore should be a function of germ tube length and relative densities of stomata and aeciospores.

Computation of expected aeciospore germ tube penetrations that establish infection (79→80). We have determined Aeciospore Infection Yield Ratio (AIYR(ISP)) on detached *Ribes hudsonanium* leaves, but Lachmund's (1934) study of aeciospore infection provided us with some additional information. His data were presented as bar graphs of infection spots per square inch obtained from artificial inoculation of leaves in 10 age groups from four *Ribes* species. Values were read from the bar graphs, averaged over all leaf ages and leaf types (open form and shade form), and converted to infections per square centimeter (table 6). A second study (Pierson and Buchanan 1938a) provides a good comparison of aeciospore and urediospore infection levels. In the spring of 1976, we made 7,500 single spore transfers and obtained 69 takes (authors' unpublished data). If we assume a similar success ratio in the wild, we can expect 0.009 infections for every aeciospore trapped by the lower surface of *R. hudsonianum* leaves.

We felt that this single determination of infection yield would be insufficient; so some infection experiments were conducted on detached *R. hudsonianum* leaves. All the tests were based on two *Ribes* clones and aeciospores from a single canker. This canker was on a *Pinus flexilis* seedling that was inoculated in one of our large-scale progeny tests. Ten leaves were collected from each of two *Ribes* clones growing in a greenhouse. Each leaf was placed on a wet filter paper in a Petri dish. One rubber-cement-coated cover slip was placed next to the leaf and inside the Petri dish. A water suspension of aeciospores was sprayed onto the leaf and cover slip with an aerosol-powered chromatography sprayer. The Petri dish was then sealed and placed in a growth chamber held at a constant 17°C and 16-hour photoperiod of about 600 fc.

Germination of the spores was recorded after 24 hours and infection after 16 days as number of pustules per square centimeter of leaf surface. We assumed one pustule per penetration and the results are shown in table 7. Evidently there is some sort of specific genetic interaction between *Ribes* and *C. ribicola*, since we obtained good infection on clone 1 and no infection on clone 2. We do not know the extent of the genetic interaction or its influence on the epidemic.

Table 6.--*Relative levels of* Cronartium ribicola *aeciospore and urediospore infection on the four principal* Ribes *species of northern Idaho*

Species	ISP	Aeciospore infections		Urediospore infections
		Per cm^2 leaf	Relative	Per cm^2 leaf	Per cm^2 leaf
R. hudsonianum	1	[1] 16.89	1.00	[2] 3.8	[2] 5.7
R. inerme	2	[1] 14.57	0.86		
R. lacustre	3	[1] 7.13	.42		
R. viscosissimum	4	[1] 4.65	.27		

[1]Calculated from Lachmund (1934).
[2]Calculated from Pierson and Buchanan (1938a).

Table 7.--*Infection ratio of* Cronartium ribicola *aeciospores on detached leaves of* Ribes hudsonianum *obtained from two clones*

Leaf number	Clone 1				Clone 2		
	Percent germinated	Number germinated/cm^2	Infections/cm^2	Spores/infection	Percent germinated	Number germinated/cm^2	Infections/cm^2
1	38	250	21	11.9	43	295	0.0
2	53	420	20	21.0	55	160	0.0
3	57	415	90	4.6	54	135	0.0
4	70	605	9	67.2	56	145	0.0
5	60	175	13	13.5	60	135	0.0
6	62	225	34	6.6	70	190	0.0
7	61	215	0	0.0	66	135	0.0
8	72	245	10	24.5	51	155	0.0
9	62	255	14	18.2	45	75	0.0
10	73	225	1	225.0	44	140	0.0
Totals		3030	212			1565	0.0

Computation of urediospore production by infections caused by aeciospores (80→81). Our goal was to simulate curves of teliospore availability such as those published by Kimmey (1945). These curves are not available for our species and conditions. We also lack information on the role of leaf drop and relative yields of urediospores and teliospores by an infection developing from an aeciospore as discussed. Regarding leaf drop, we will assume for the present that our viability-occurrence curves (fig. 7) will be sufficient. Regarding urediospore-teliospore partitioning, we will include a variable ratio of urediospores to teliospore production for both uredial and aecial infections ($TSAR_i$ and $TSUR_i$) (see table 3 for definitions).

We relied on our single-aeciospore-culturing experience for many of the details of partitioning spore production. A single aeciospore infection on a detached *R. hudsonianum* leaf can produce about 12,000 urediospores, according to our visual estimates. We also estimate that a single urediospore infection under similar conditions can produce about 10 telial columns, if no urediospores are produced. If urediospores average 15μ x 32μ (Colley 1918), then 12,000 spores = $68x10^6\mu^3$ of spore volume. Also, we find that teliospores average about 10μ x 40μ (authors' unpublished data) and that infections on *R. hudsonianum* produce telial columns that average 100μ in diameter and 900μ in length. Thus, 10 telial columns = a yield of spore volume of $70x10^6\mu^3$. The two estimated values are in close agreement.

The size of the telial columns produced by *C. ribicola* on the different *Ribes* species varies. Mielke and others (1937) describe the size differences in qualitative terms. *R. hudsonianum* produced large and closely spaced columns. *R. inerme* produced somewhat more sparsely spaced, but longer columns. *R. viscosissimum* produced short stout columns more sparsely spaced than those of *R. inerme*. *R. lacustre* produced sparsely spaced columns that were longer than the others, but thinner. These qualitative descriptions were used to construct some estimated quantitative dimensions in conjunction with two pieces of quantitative data that were available. Colley (1918) states that telial columns average about 100μ in diameter and may be up to 2,000μ in length although both length and diameter vary greatly. Taylor (1922) estimates that 1 in^2 of fully infected *R. lacustre* leaf surface will produce 281,280 sporidia at 6,000 sporidia per column. These values lead to about seven columns per square centimeter (calculated by the authors).

Mielke and others (1937) describe telial production on the four *Ribes* species on a scale based on relative mass of telial columns per unit area. With *R. lacustre* as 1, *R. viscosissimum* was 2, *R. inerme* was 12, and *R. hudsonianum* was 20.

Teliospores are packed rather tightly into the columns and are of a somewhat irregular shape. If we measure the total length of a chain of teliospores and divide by the number in the chain, however, we find that teliospore length averages about 40μ. If we assume that spore size is invariate over *Ribes* species, then we can make some estimates about column dimensions based on our current information and estimate the number of teliospores per column for each *Ribes* species. The estimated dimensions are: *Ribes hudsonianum* 100μ x 900μ; *R. lacustre* 50μ x 1,200μ; *R. viscosissimum* 100μ x 450μ; and *R. inerme* 100μ x 1,200μ.

If the *R. hudsonianum* values are taken as 1, the relative mass values for the other species become (1) *R. lacustre* 0.05, (2) *R. viscosissimum* 0.1, and (3) *R. inerme* 0.6. Let us assume that these mass values represent a measure of the relative production capabilities of the different *Ribes* species. The rust should be studied on each *Ribes* species to determine the relative influence of *Ribes* species and environment on telial column parameters and spore biomass production. Some understanding of within-species variation and variation within different combinations of rust and *Ribes* is also needed. We will assume that all species produce the same size teliospores and urediospores, but that the productivity and telial column size and diameter varies among species. If *R. hudsonianum* can produce $70x10^6\mu^3$ of spore

volume per infection, then *R. lacustre* can produce $3.5x10^6\mu^3$ ($70x10\mu \cdot 0.05$), *R. viscosissimum* $7x10^6\mu^3$, and *R. inerme* $42x10^6\mu^3$. These values complete those necessary to model the rust on *Ribes*.

If each aeciospore infection is assumed to produce a given amount of biological material ($BMASS_i$), as discussed, this yield can be in the form of urediospores or teliospores. Our evidence indicates that infections resulting from aeciospores behave differently than infections arising from urediospores in regard to the relative proportions of urediospores and teliospores. We will use the input variables TelioSpores from Aeciospores Ratio ($TSAR_i$) and TelioSpores from Urediospores Ratio ($TSUR_i$) to control the partitioning of the infection production potential for the two kinds of infections on the four *Ribes* species. Germination lag and germ tube growth are used in the same way to model urediospore infection as to model aeciospore infection, but the functions are different as illustrated in figures 12 and 13.

Computation of number of germinable urediospores in a given infection period (81→82). Out of all the urediospores produced by a certain cohort, the proportion viable (UV) is determined by the spore-age relationship shown in figure 7.

Computation of number of urediospores that germinate during a given infection period per square centimeter of Ribes *target* (82→83). The proportion of viable urediospores per square centimeter of leaf surface that will be expected to germinate in any given infection period of unlimited duration will be provided by the function illustrated in figure 14. The interaction of rust genes and temperature is assumed to control this function.

Computation of number of germinated urediospores expected to provide germ tubes of sufficient length for penetration (83→84). The rationale is the same as for flow (78→79).

Computation of number of infections caused by urediospores during a given infection period (84→85). An infection yield ratio is used to control this flow as it was for flow (79→80).

Computation of number of urediospores arising from urediospore infection (85→81). Urediospores are produced by infections arising from urediospores as well as aeciospores. So, this portion of the model is recycled through this feedback flow.

PRODUCTION OF TELIOSPORES

Computation of number of teliospores expected to arise from aeciospore (80→86) *and urediospore* (85→86) *derived infections.* The number of potential telispores (TMAX) is calculated from a summation of spore biomass left after removal of urediospores. Remember that teliospores can come from infections that resulted from both aeciospore and urediospore infection; thus, the two flows are considered in tandom.

BASIDIOSPORE PRODUCTION

Computation of number of teliospores viable in a given infection period (86→87). Teliospore viability varies with age (fig. 7) and temperature during formation (Van Arsdel and others 1956); thus a viability function is necessary. In northern Idaho, the temperature seldom exceeds the limit critical to formation viability (35°C); so, we incorporated only the teliospore-age variable at this time.

Computation of number of teliospores expected to germinate in a given infection period (87→88). Teliospores germinate to produce basidiospores. Assuming that the number of teliospores per square centimeter of *Ribes* leaf is known for each *Ribes* species, what quantity of basidiospores can be expected? A model of teliospore germination was developed that yields percent of teliospores germinated (PCAST) as a function of infection period duration, teliospore column diameter, and teliospore diameter. The detailed construction of this model is given in appendix III.

Computation of number of basidiospores produced for each square centimeter of underside leaf surface of Ribes hudsonianum *per infection period* (88→89). Each germinating teliospore can produce a maximum of four basidiospores, but under natural conditions we know very little about how many are actually produced per teliospore. So, we elected to reserve a spot for an input variable called BasidioSpore Yield Ratio ($BSYR_1$), which is expressed as basidiospores per teliospore.

Computation of number of basidiospores produced for each square centimeter of underside leaf surface of R. inerme *per infection period* (88→90). This flow is a repeat of flow (88→89) with a repeat of all flows between 77 and 88 with changed parameters to match *R. inerme*.

Computation of number of basidiospores produced for each square centimeter of underside leaf surface of R. lacustre *per infection period* (88→91). Same explanation as previous flow.

Computation of number of basidiospores produced for each square centimeter of underside leaf surface of R. viscossisimum *per infection period* (88→92). Same explanation as previous flow.

DISTRIBUTION OF BASIDIOSPORES TO PINE TREES

Computation of number of basidiospores per square centimeter of flat surface at the white pine tree (89, 90, 91, 92→93). As already indicated, the model includes a repeat of the flows 75 through 89 for the remaining three major *Ribes* species. In several places, details differ like aeciospore and urediospore infection yield ratios, urediospore versus teliospore partitioning, telial column parameters, and duration of infection periods. After the expected number of basidiospores per hectare is computed for each of the four *Ribes* species, simulated spore load is summed over *Ribes* species and is distributed to pine trees on the basis of Average *Ribes*-growth-point (Bush) to Tree Distance ($ABTD_i$) and the number of bushes per Growth-Point or Growth-Point Factor (GPF_i). The separate spore loads (spores/bush) for each infection period are used to calculate spores per hectare by multiplying by the number of bushes per hectare (state variables 1, 2, 3, and 4, *Ribes* density submodel). $ABTD_i$ and GPF_i are then used to calculate the average spore load in spores per square centimeter at the trees.

Pine Host Target Submodel

This submodel (fig. 15) computes the target of an average tree as a function of site index, stand age, host genotype, and weather. The computed target is partitioned into current, 1-year-old, and 2-year-old branch needles and current and 1-year-old stem needles. Variable definitions for the target submodel are given in table 8 and flow descriptions are given in table 9.

Six characteristics of the pine target were incorporated into this model: number of needles, placement of needles (branch or stem), number of rows of stomata per needle, needle length, needle age, and pine genotype (resistance). These characteristics are fully discussed under the pine infection model.

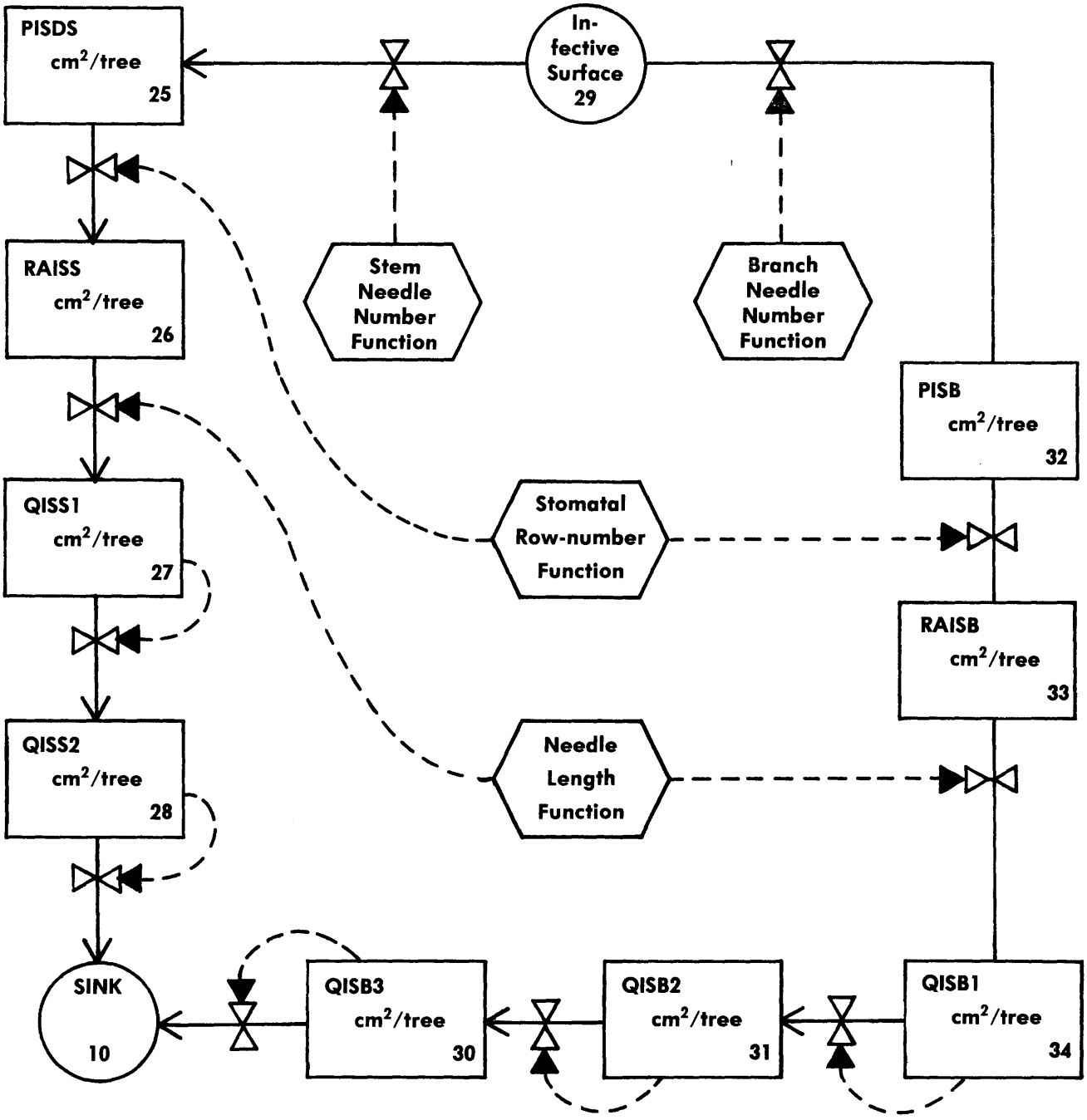

Figure 15.--Box-and-arrow diagram of pine-host target. Variable definitions are in table 8.

Table 8.--*Definition of variables used in the pine-host-target submodel*

Variable		Definition
State variables:		
X(10)	SINK	Sink that accepts dead needles.
X(25)	PISDS	Potential infective surface on direct stem needles, square centimeters per tree.
X(26)	RAISS	Stomatal row adjusted infective surface stem needles, square centimeters per tree.
X(27)	QISS1	Quantity of infective surface on stem needles in their first year, square centimeters per tree.
X(28)	QISS2	Quantity of infective surface on stem needles in their second year, square centimeters per tree.
X(29)	SOURCE	Unspecified source of infective surface.
X(30)	QISB3	Quantity of infective surface on branch needles in their third year, square centimeters per tree.
X(31)	QISB2	Quantity of infective surface on branch needles in their second year, square centimeters per tree.
X(32)	PISB	Potential infective surface branch needles, square centimeters per tree.
X(33)	RAISB	Row adjusted infective surface on branch needles, square centimeters per tree.
X(34)	QISB1	Quantity of infective surface on branch needles in their first year, square centimeters per tree.
User controlled variables:		
RSPN		Rows of stomata per needle, number rows/needle.
QNEEDL		Quantitative needle length factor, proportion of maximum needle length.
Computed variables:		See appendix I.

Table 9.--*Pine-target-submodel flow description*

Flow path	Flow name	Flow description	Flow equation*
$J_{(29\rightarrow32)}$	Branch needle generation	Computation of potential infective surface on current year branch needles	PISB = 3490 $CTH^{1.365}$
$J_{(32\rightarrow33)}$	Stomatal row adjustment	Potential infective surface in cm^2/tree on current year branch needles is adjusted for number of stomatal rows per needle	RAISB = 0.1 PISB·RSPN
$J_{(33\rightarrow34)}$	Needle length adjustment	Row adjusted IS on current year branch needles is adjusted for needle length	QISB1 = RAISB·QNEEDL
$J_{(34\rightarrow31)}$	Aging infective surface	Branch-needle IS on needles in their current year ages one year to give rise to IS on second-year branch needles	QISB2 = QISB1
$J_{(31\rightarrow30)}$	Aging infective surface	Branch-needle IS on needles in their second year ages one year to give rise to IS on third-year branch needles	QISB3 = 0.642·QISB2
$J_{(30\rightarrow10)}$	Needle death	Branch needles lost at end of third growing season due to natural death of needles	SINK = QISB3
$J_{(29\rightarrow25)}$	Stem needle generation	Computation of potential infective surface on current year stem needles	PISDS = $700(1.0-e^{-1.15\cdot CTH})$
$J_{(25\rightarrow26)}$	Stomatal row adjustment	Adjustment of potential IS on current year stem needles for number of stomatal rows	RAISS = 0.1·PISDS·RSPN
$J_{(26\rightarrow27)}$	Needle length adjustment	Stomatal-row-adjusted stem-needle IS is adjusted further for needle length by the stem-needle factor QSNEDL	QISS1 = RAISS·QSNEDL
$J_{(27\rightarrow28)}$	Aging infective surface	Computation of first-year aging infective surface on stem needles in their current year	QISS2 = QISS1
$J_{(28\rightarrow10)}$	Needle death	Stem needles lost at end of second growing season due to natural death	SINK = QISS2

*See appendix I for derivation of flow equations.

The concept of infective surface was developed to facilitate the modeling of the target area. The investigations of Clinton and McCormick (1919) and Chapman[2] indicated that infection by basidiospores occurred through the stomates. This was confirmed by Patton and Johnson (1967). The basidiospores land on a needle, germinate, and the germ tube grows in a random direction (Hansen 1972). When the tip of the germ tube happens to penetrate a stomate, it grows between the guard cells into the substomatal chamber, where it produces a substomatal vescicle, and then an infection hypha (fig. 16). The infection hypha penetrates a mesophyll cell and the infection is established. If one assumes that this entire process must be completed by utilization of energy stored within the basidiospore, then growth of germ tubes on pine needles should provide a clue to their growth potential. What is the average distance a spore can be away from a stomate and still have reserves to establish an infection? Germ tubes averaged about 100μ in length when spores were germinated on eastern white pine (Hansen 1972) or on water agar at pH 6.8 and 16°C (Bega 1957).

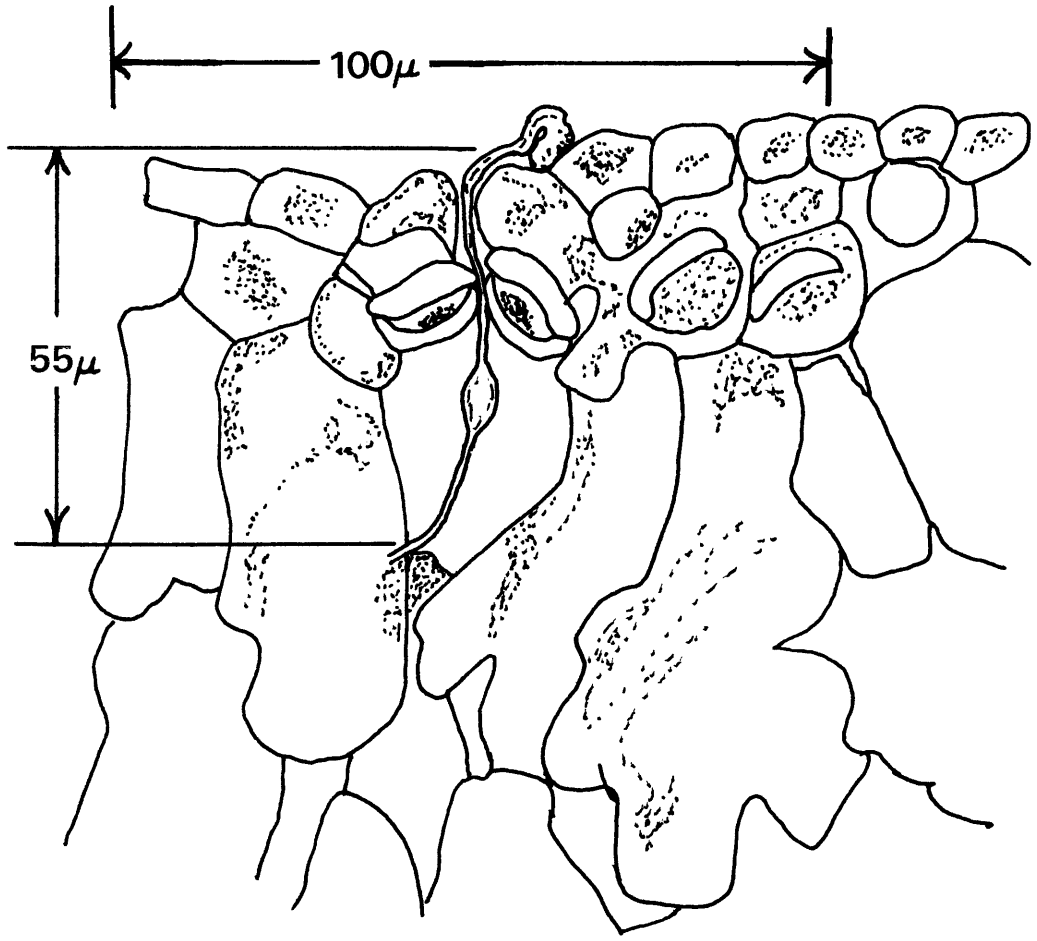

Figure 16.--Diagramatic representation of a *Cronartium ribicola* basidiospore infecting a pine needle.

[2]Chapman, C. M. 1934. A study of the movement of mycelium of *Cronartium ribicola* Fischer during the incubation period in *Pinus monticola* Dougl. *In* Blister rust work in the far West, p. 293-298. (Mimeographed) U.S. Dep. Agric., Div. Plant Dis. Control.

The distance from the top of the subsidiary cells to the bottom of the substomatal cavity averaged about 55μ on a few sections of western white pine needles (authors' unpublished data). This leaves about 50μ of growth potential. How can we envision the utilization of this potential? Since stomates are arranged in rows and the distance from the end of one stomate to the beginning of the next is about the same as the length of a stomate (20μ, authors' unpublished data), 50μ perimeters around succeeding stomata in a row overlap. Therefore, the important measure becomes the "infective width" of the stomatal row. We have assumed infective width to be 100μ (fig. 17). Infective surface is taken as the square centimeters of needle area within a tree that a spore can land on and have a chance to establish an infection. Factors influencing this parameter that must be considered in calculating target are needle length and number of rows of stomata.

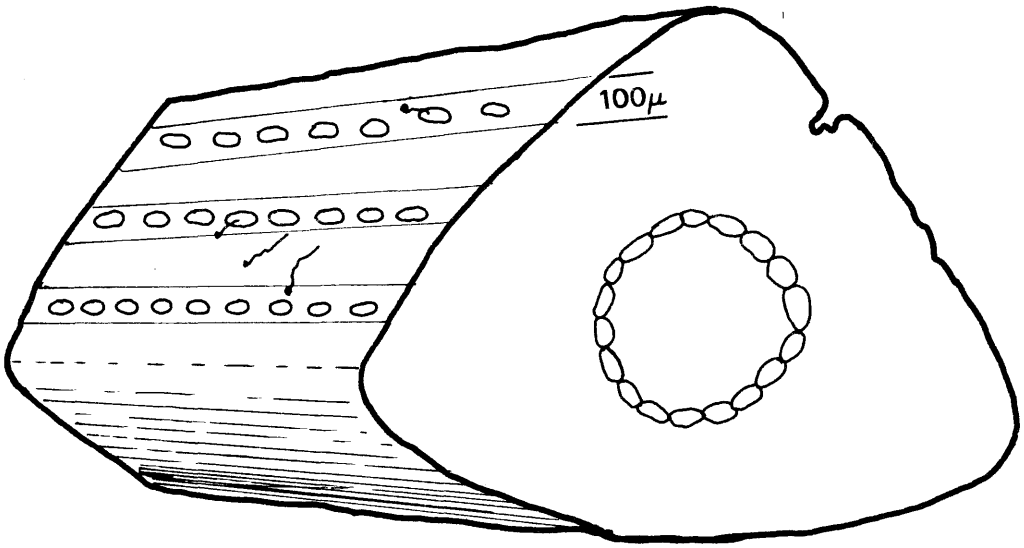

Figure 17.--The concept of infective surface is illustrated by this diagramatic representation of germinating basidiospores on the surface of a pine needle (infective surface in square centimeters per tree = average number of rows of stomata/needle x number of needles per tree x average length of stomatal row x 0.01 cm).

Computation of potential Infective Surface (IS) on current year branch needles (29→32). State variable 29 is a source of infective surface that is partitioned out each year to branch and stem needles according to the branch-needle and stem-needle growth functions. Potential Infective Surface Branch (PISB) is based on number of current year branch needles.

Potential branch-needle infective surface adjusted for stomatal-row-number (32→33). In this formulation, we have provision for a given value of Rows of Stomata Per Needle (RSPN) to be used for calculation of IS. This variable is important because it can apparently vary a great deal under the influence of both environmental and genetic factors.

Stomatal-row-adjusted branch-needle IS adjusted by a needle-length factor (33→34). Environment, genes, and tree age or size probably all influence needle length. This flow provides a place for such sources of variation.

Branch-needle IS on needles in their current year ages 1 year to give rise to IS on second-year branch needles (34→31). According to available data (Buchanan 1936), there are no losses of branch-needles between their first and second years, so the entire contents of QISB1 must be transferred to QISB2 (see table 8 for definitions).

Branch needle IS on needles in their second year ages 1 year (31→30). The equation mediating this flow was derived from Buchanan's (1936) needle-removal table. His sample showed that 64.2 percent of the branch needles of a particular cohort are retained for their third year.

Branch needle IS lost at the end of the third growing season due to natural death of needles (30→10). In western white pine, about 4 percent of the needles in the entire crown survive 4 years and in the upper crown 4-year survival is even lower (Buchanan 1936). Consequently, we assumed that all needles die and are cast at the end of their third season. All the contents of QISB3 are moved to the sink. Thus, new infections that occur on needles in their third season are assumed to be of no consequence.

Computation of potential stem needle IS (29→25). Needles are also located on the bole. These stem needles are of particular importance because infections originating here reach canker status directly on the bole. There is no canker mortality due to dying branches and, since the needles are located on the first year wood, boles are of small diameter so damage occurs quickly. For these reasons, stem needles are treated separately from branch needles. Infective surface flows from IS source (X29) to PISDS (Potential Infective Surface Direct-Stem).

Adjustment of potential IS for stem-needle (PISDS) (25→26). The use of RSPN was discussed under flow (32→33).

Stomatal-row adjusted stem-needle IS is adjusted for needle length by the stem-needle factor (QSNEDL) (26→27). QNEEDL, defined in table 8, is used to compute QSNEDL. This change is necessary because stem needles tend to be longer than branch needles.

Computation of 1-year aging of infective surface on stem needles in their current year (27→28). The assumption was made that none of the current year stem needles die before their second season. Thus, all of the IS in X(27) will be transferred to X(28) for the next cycle.

Infective surface moves to the sink after stem-needle death (28→10). Our field observations lead us to believe that stem needles generally die and are cast at the end of their second season. Thus, new infections on stem needles in their second season are cast before they can become cankers. This means that only first-year stem needles need be considered as targets.

We now have calculated infective surface values of first-year stem needles (QISS1), first-year branch needles (QISB1), and second-year branch needles (QISB2). These variables are transferred now to the pine infection submodel and combined with basidiospore load from the *Ribes* infection submodel to create a simulated amount of infection on an average tree.

Pine Infection Submodel

Pine infection is outlined in figure 18. This process is complex but the general aspects of pine infection delineated by Hirt (1935 and 1942) and Spaulding and Rathbun-Gravatt (1925a) have been preserved. Infections that occur on needles attached directly to the bole are of special significance as already discussed. For

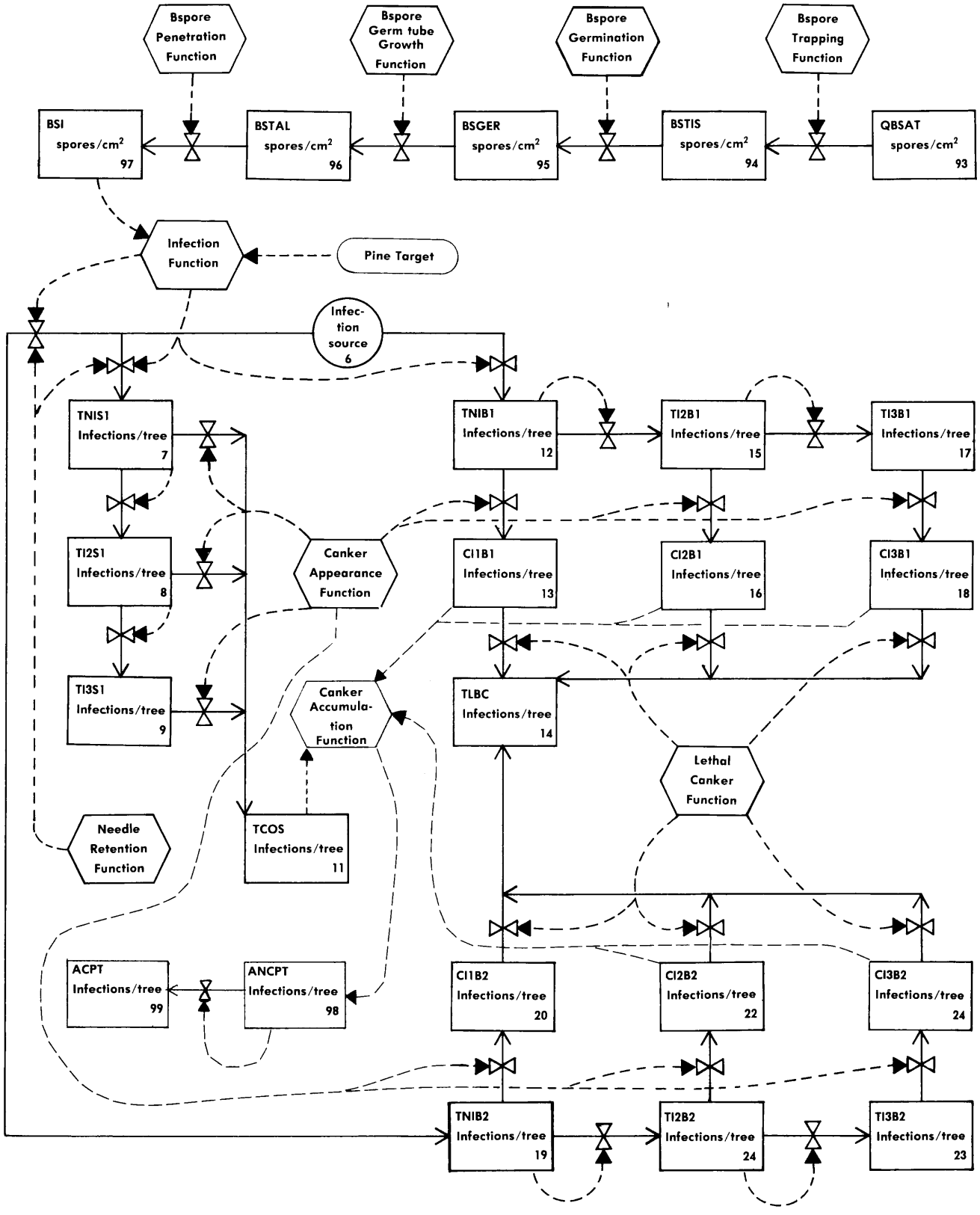

Figure 18.--Box-and-arrow diagram of *Cronartium ribicola* infection of the pine host.

review, they can begin the girdling process immediately and their numbers cannot be reduced by the death of branches; consequently, the silvicultural control treatment of pruning is not applicable to infections from this source. The probability of infection on stem needles becomes an important variable when estimating probable damage and working out control strategies. The definitions of the state variables found in this submodel are given in table 10 and descriptions of flows are in table 11.

Table 10.--*Definitions of variables used in the pine infection submodel*

Variable		Definition
State variables:		
X(10)	SOURCE	Unspecified source of pine infections.
X(11)	TNIS1	Total number of new needle infections in current year on stem needles infected in their first season.
X(12)	TI2S1	Total number of needle infections in current year that are in their second season and are in needles infected in their first season.
X(13)	TI3S1	Total number of needle infections in current year that are in their third season and are in needles infected in their first season.
X(14)	TCOS	Total number of cankers that appear on the stem in the current year from infections in stem needles.
X(15)	TNIB1	Total number of new needle infections in current year on branch needles in their first season.
X(16)	CI1B1	Number of canker infections from 1-year-old branch needle infections that were infected in their first year.
X(17)	TLBC	Total number of potentially lethal branch cankers that appear in current year.
X(18)	TI2B1	Total number of needle infections in current year that are in their second year and growing in branch needles that were infected in their first year.
X(19)	CI2B1	Number of canker infections from 2-year-old branch needle infections in needles that became infected in their first year.
X(20)	TI3B1	Total number of needle infections in current year that are 3 years old and growing in branch needles that were infected during their first year.
X(21)	CI3B1	Number of canker infections from branch needle infections in their third year and growing in needles that became infected during their first year.

Table 10.--*Definitions of variables used in the pine infection submodel (continued)*

Variable		Definition
X(22)	TNIB2	Total number of new needle infections in current year on branch needles in their second year.
X(23)	CI1B2	Number of canker infections from 1-year-old branch needle infections growing in needles that became infected during their second year.
X(24)	TI2B2	Total number of needle infections in current year that are 2 years old and growing in branch needles that became infected during their first year.
X(25)	CI2B2	Number of canker infections from 2-year-old branch needles that became infected in their second year.
X(26)	TI3B2	Total needle infections in their third season and growing in branch needles that became infected during their second growing season.
X(27)	CI3B2	Number of canker infections from 3-year-old branch needle infections growing in branch needles that became infected during their second growing season.
X(93)	QBSAT	Quantity of basidiospores at an average tree, basidiospores per square centimeter.
X(94)	BSTIS	Number of basidiospores trapped per unit infective surface, basidiospores per square centimeter.
X(95)	BSGER	Number of basidiospores expected to germinate after being trapped, basidiospores per square centimeter.
X(96)	BSTAL	Number of basidiospores expected to produce germ tubes of adequate length for penetration, basidiospores per square centimeter.
X(97)	BSI	Number of basidiospores expected to penetrate and establish infections, basidiospores per square centimeter.
X(98)	ANCPT	Average number of new cankers per tree each year.
X(99)	ACPT	Accumulated number of cankers per tree inbred by infection period.
User controlled variables:		
BIY		Ratio of spots to trapped and germinating basidiospores, spots per square centimeter:basidiospores per square centimber IS.
DIP(DAA1)		Duration of infection period, hours.

(continued)

Table 10.--*Definitions of variables used in the pine infection submodel (continued)*

Variable	Definition
FER	Fungus encirclement rate, meters/year.
NRF	Needle retention factor, year of branch needle retention.
QNLR	Needle lesion reduction resistance factor.
RGRN	Rust growth rate down the needle, mm/month.
SNAIF	Secondary needle age infection factor, proportionality constant.
TEF	Trapping efficiency factor of branch and stem needles.
TIP(DAA1)	Average temperature of an infection period, indexed by infection period, expressed as degrees C.
Computed variables:	See appendix I.

Table 11.--*Pine infection submodel flow descriptions*

Flow path	Flow name	Flow description	Flow equation*
$J_{(93\rightarrow94)}$	Basidiospore trapping	Computation of number of basidiospores trapped by a square centimeter of pine infective surface	BSTIS = QBSAT·TEF
$J_{(94\rightarrow95)}$	Basidiospore germination	Computation of number of trapped basidiospores expected to germinate during a given infection period	BSGER = BSTIS·GERMB
$J_{(95\rightarrow96)}$	Basidiospore germ tube growth	Computation of number of germinated basidiospores expected to produce germ tubes of sufficient length to penetrate	BSTAL = PGERBP·BSGER
$J_{(96\rightarrow97)}$	Basidiospore infection establishment	Computation of number of basidiospores penetrating to establish infection	BSI = BSTAL·BIY·QNLR
$\sum_{1}^{P} J_{(6\rightarrow7)}$	Basidiospore infections summed over infection periods	Calculation of number of new infections per tree for entire season on current-year stem needles	TNIS1 = $\sum_{1}^{P}$(BSI·0.5·QISS1)
$J_{(6\rightarrow12)}$	Basidiospore infections summed over infection periods	Calculation of number of new infections per tree on current-year branch needles	TNIB1 = $\sum_{1}^{P}$(BSI·0.25·QISB1)

(continued)

Table 11.--*Pine infection submodel flow descriptions (continued)*

Flow path	Flow name	Flow description	Flow equation*
$J_{(6\rightarrow19)}$	Basidiospore infections summed over infection periods	Computation of number of new infections per tree on second-year branch needles	$TNIB2 = \sum_{1}^{P}(BSI \cdot 0.25 \cdot SNAIF \cdot QISB2)$
$J_{(7\rightarrow11)}$	Canker appearance	Computation of number of incipient cankers from stem needles infected in their first year	$TCS1 = TNIS1 \cdot b^{-20(b^{-1.5})}$
$J_{(7\rightarrow8)}$	Needle infections aged	Computation of number of stem-needle infections that failed to reach canker status in 1 year	TI2SI = TNIS1-TCS1
$J_{(8\rightarrow11)}$	Canker appearance	Computation of number of 2-year-old stem needle infections that reached canker status in current year	$TCS2 = TI2S1 \cdot b^{-20(b^{-3.0})}$
$J_{(8\rightarrow9)}$	Needle infections aged	Computation of number of 2-year-old stem needle infection that failed to reach canker status in current year	TI3S1 = TI2S1-TCS2
$J_{(9\rightarrow11)}$	Canker appearance	Computation of number of 3-year-old stem needle infections that reach canker status in current year and summation of all stem-needle cankers to appear in current year	TCOS = TCS1 + TCS2 + TI3S1

(continued)

Table 11.--*Pine infection submodel flow descriptions (continued)*

Flow path	Flow name	Flow description	Flow equation*
$J_{(12\rightarrow13)}$	Canker appearance	Computation of number of 1-year-old needle infections in branch needles infected in their first year that reach canker status after 1 year	$CI1B1 = TNIB1 \cdot b^{-20(b^{-1.5})}$
$J_{(12\rightarrow15)}$	Needle infections aged	Computation of 1-year-old branch needles infected in their first year that failed to reach canker status in 1 year	TI2B1 = TNIB1-CI1B1
$J_{(15\rightarrow16)}$	Canker appearance	Computation of number of 2-year-old branch needle infections from needles infected in their first year that reach canker status in the current year	$CI2B1 = TI2B1 \cdot b^{-20(b^{-3.0})}$
$J_{(15\rightarrow17)}$	Needle infections aged	Computation of number of 2-year-old branch needle infections on needles infected in their first year that failed to reach canker status in current year	TI3B1 = TI2B1-CI2B1
$J_{(17\rightarrow18)}$	Canker appearance	Computation of number of 3-year-old branch needle infections that reached canker status in current year	CI3B1 = TI3B1

(continued)

Table 11.--*Pine infection submodel flow descriptions (continued)*

Flow path	Flow name	Flow description	Flow equation*
$J_{(13\rightarrow14)}$	Lethal-canker generation	Calculation of number of new lethal cankers from last year's incipient cankers from branch needle infections on needles in their first year	$CL1B1 = CI1B1 \cdot \left(\frac{0.24 \cdot FER \cdot PTH(I) + 0.6}{PTH(I)}\right)^{1.365}$
$J_{(16\rightarrow14)}$	Lethal-canker generation	Calculation of number of new lethal cankers from last year's incipient cankers from 2-year-old branch needle infections on needles infected in their first year	$CL2B1 = CI2B1 \cdot \left(\frac{0.24 \cdot FER \cdot PTH(I) + 0.6}{PTH(I)}\right)^{1.365}$
$J_{(18\rightarrow14)}$	Lethal-canker generation	Calculation of number of new lethal cankers from last year's incipient cankers from 3-year-old branch needle infections	$CL3B1 = CI3B1 \cdot \left(\frac{0.24 \cdot FER \cdot PTH(I) + 0.6}{PTH(I)}\right)^{1.365}$
$J_{(19\rightarrow20)}$	Canker appearance	Calculation of number of incipient cankers from 1-year-old infections on branch needles infected in their second year	$CI1B2 = TNIB2 \cdot b^{-20(b^{-1.5})}$
$J_{(19\rightarrow21)}$	Needle infections aged	Calculation of number of 1-year-old infections on branch needles that failed to reach canker status	$TI2B2 = TINB2 - CI1B2$

(continued)

Table 11.--*Pine infection submodel flow descriptions (continued)*

Flow path	Flow name	Flow description	Flow equation*
$J_{(21\rightarrow22)}$	Canker appearance	Calculation of number of incipient cankers from 2-year-old infections on branch needles infected in their second year	$CI2B2 = TI2B2 \cdot b^{-20(b^{3.0})}$
$J_{(21\rightarrow23)}$	Needle infections aged	Calculation of number of 2-year-old infections on branch needles that failed to reach canker status	$TI3B2 = TI2B2 - CI2B2$
$J_{(23\rightarrow24)}$	Canker appearance	Calculation of number of incipient cankers from 3-year-old infections on branch needles from 1-year-old needle infections on needles infected in their second year	$CI3B2 = TI3B2$
$J_{(20\rightarrow14)}$	Lethal canker generation	Calculation of number of new lethal cankers from last year's incipient cankers from 2-year-old branch needle infections on needles infected in their second year	$CL1B2 = CI1B2\left(\frac{0.24 \cdot FER \cdot PTH(I) + 0.6^{1.365}}{PTH(I)}\right)$
$J_{(22\rightarrow14)}$	Lethal canker generation	Calculation of number of new lethal cankers from last year's incipient cankers from 2-year-old branch needle infections on needles infected in their second year	$CL2B2 = CI2B2\left(\frac{0.24 \cdot FER \cdot PTH(I) + 0.6^{1.365}}{PTH(I)}\right)$

(continued)

Table 11.--*Pine infection submodel flow descriptions (continued)*

Flow path	Flow name	Flow description	Flow equation*
$J_{(24\rightarrow14)}$	Lethal canker generation	Calculation of number of new lethal cankers from last year's incipient cankers from 3-year-old branch needle infections on needles infected in their second year	$CL3B2 = CI3B2\left(\frac{0.24 \cdot FER \cdot PTH(I) + 0.6}{PTH(I)}\right)^{1.365}$
$J_{(6\rightarrow98)}$	Total new cankers	Calculation of number of new cankers that appear each year	$ANCPT = TCOS + CI1B1 + CI2B1 + CI3B1 + CI1B2 + CI2B2 + CI3B2$
$J_{(98\rightarrow99)}$	Canker accumulation	Calculation of accumulated number of cankers to appear on an average tree after a given period of exposure	$ACPT = ACPT + ANCPT$

*See appendix I for derivation of flow equations.

Computation of basidiospores trapped by a square centimeter of pine infective surface (93→94). After the basidiospores are produced, they must escape the *Ribes* canopy and penetrate the pine canopy. Both of these operations are dependent on the relationships among spore size, spore density, windspeed, and leaf size and shape. One way to gain an understanding of these relationships is to look at needles and leaves as spore traps and calculate the trapping efficiencies under different conditions (Gregory 1952). A paper by Edmonds (1972) provides the methodology for such calculations. Trapping efficiencies of pine needles and *Ribes* leaves are given in table 12. The movement of spores through the pine canopy is envisioned as follows: Any slight air movement will cause the spores to be moved around the needles rather than onto them because of the very low trapping efficiency of the needle. A few basidiospores would be trapped at 450 cm/sec (10 mi/h) where the efficiency reaches about 5 percent. At 900 cm/sec (20 mi/h) the efficiency reaches 25 percent. Thus windspeeds of 45 to 225 cm/sec (1 to 5 mi/h), which may be best for dispersal, may be worst for deposition. This leads to the conclusion that dispersal and deposition can be viewed as two completely different processes and that most basidiospores are probably deposited on the needles rather than trapped by impaction phenomenon. So long as the wind blows, the basidiospores remain in suspension, but during quiet periods the basidiospores settle out onto the pine needles. Another possibility is that rain will wash basidiospores out of the air even though the wind is blowing (Schrödter 1960). This subject brings up the question of the importance of variation of wind velocity in the total infection process of pines by *C. ribicola* basidiospores.

Table 12.--*Impaction efficiencies in percent for basidiospores with a diameter of 10μ and a specific gravity of 1*

Trap	Trap width	Horizontal windspeed			
		1 mi/h (45 cm/sec)	2 mi/h (90 cm/sec)	4 mi/h (180 cm/sec)	20 mi/h (900 cm/sec)
	cm				
Pine needle	0.1	<1.0	<1.0	2.5	25.0
Ribes leaf	7.0	<1.0	<1.0	<1.0	<1.0

Calculated from Edmonds 1972.

For example, wind during a wet period could prevent the spores from being deposited before they lose their viability and thus prevent disease development. A high wind, for example, 1 125 cm/sec (25 mi/h), could increase the efficiency of trapping by impaction in the tops of tall trees; consequently, wind profile could influence the amount of infection in short and in tall trees and in densely stocked and in thinly stocked stands.

Since basidiospores behave as a penetrator, not an impactor, the most meaningful measure of infection potential should be number of spores deposited on slides or stationary glass rods rather than some other type of spore sampler. One would want a trapping system that was inefficient in slow winds, but efficient under calm conditions.

The role of rain could be assessed by using the methodology that has been developed for trapping spores from rain (Rowell and Romig 1966; Roelfs and others 1970). The whole thing could be tied together by knowing the concentration of basidiospores in the air. This could be determined with a volumetric spore trap. It is conceivable that the character of the wind during a favorable infection period with respect to moisture and temperature could determine the effectiveness of the infection period.

All of our current available information on the infection yield ratio (spots per spore cast) has been obtained in the calm interior of infection tents with the basidiospores settling directly onto the pine foliage and glass-slide traps. Since most basidiospores of *C. ribicola* are probably deposited this way in nature, our simulation will assume a spore deposition model rather than an impaction model.

Computation of number of trapped basidiospores expected to germinate during a given infection period (94→95). Many factors can influence the likelihood that a spore will cause an infection even after it is trapped. The first consideration is that the basidiospore land where the germ tube can physically reach a stomata and cause an infection. We have attempted to solve this problem by our concept of infective surface, by considering only the needle surface from which a spore can reach a stomata. So, our next problem is basidiospore germination.

If the assumed relationships between germination and germ tube growth rate are the same for basidiospores as for aeciospores and urediospores, then probability of infection by basidiospores after they are trapped can be modeled in a similar fashion.

When sporidia were germinated on eastern white pine needles (Hansen 1972) under favorable temperature and moisture conditions, at least 95 percent germinated. Spores deposited on *P. lambertiana* in a saturated atmosphere and temperatures from 13°C to 22°C germinated at nearly the 95 percent rate over the range (Bega 1960). Since Bega (1960) found 100 percent germination of basidiospores on *P. monticola* and the above determination was also near 100 percent, we have assumed 100 percent germination between the temperatures 1°C and 24°C. Germination started at about 2 h after casting (Hansen 1972) and at 15°C and pH 3 to 4 was completed at 3 h (Bega 1960). These findings were incorporated into functions for germination lag and germination period (fig. 19 and 20). Hansen (1972) reported a germ tube growth rate of 3.5 μ/h for the first 30 h, and a decreasing rate for another 42 h on artificial membranes. Bega (1960) measured germ tube length on artificial media maintained at a pH of 4 at various temperatures. Length was measured 24 h after spore deposition. The hourly rate was determined by the authors and plotted (fig. 21). First, we needed the value for lag time between the onset of the infection period and completion of basidiospore germination. During this period, teliospores must germinate and the disseminated basidiospores must germinate and penetrate. It apparently takes about 6 to 7 hours for teliospores to begin to cast basidiospores, another 2 to 8 hours for the basidiospores to commence germination (fig. 19), and an additional 2 to 24 hours for the population of basidiospores to complete their germination (fig. 20). Then an additional 10 to 50 hours would be required for the germ tubes to grow and penetrate.

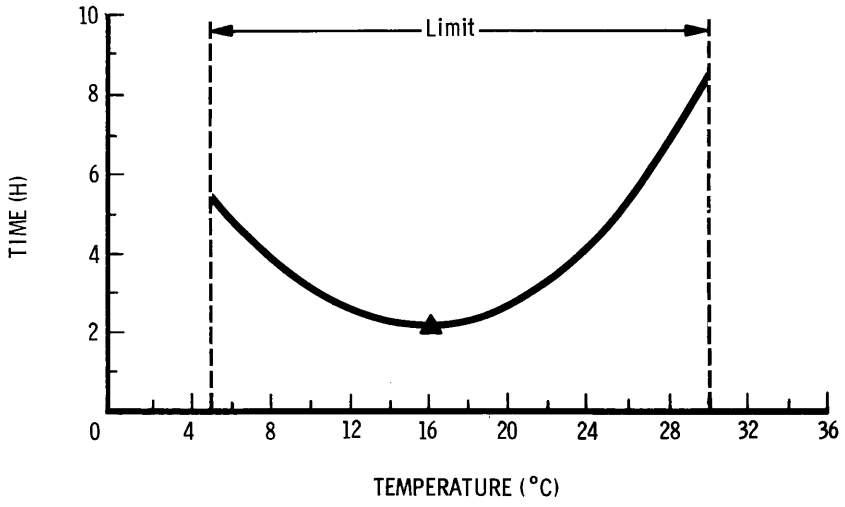

Figure 19.--Assumed relationship between temperature and period of germination lag of *Cronartium ribicola* basidiospores. Data point at minimum is from Bega (1960); and shape of curve is assumed to be the same as for *C. ribicola* basidiospores.

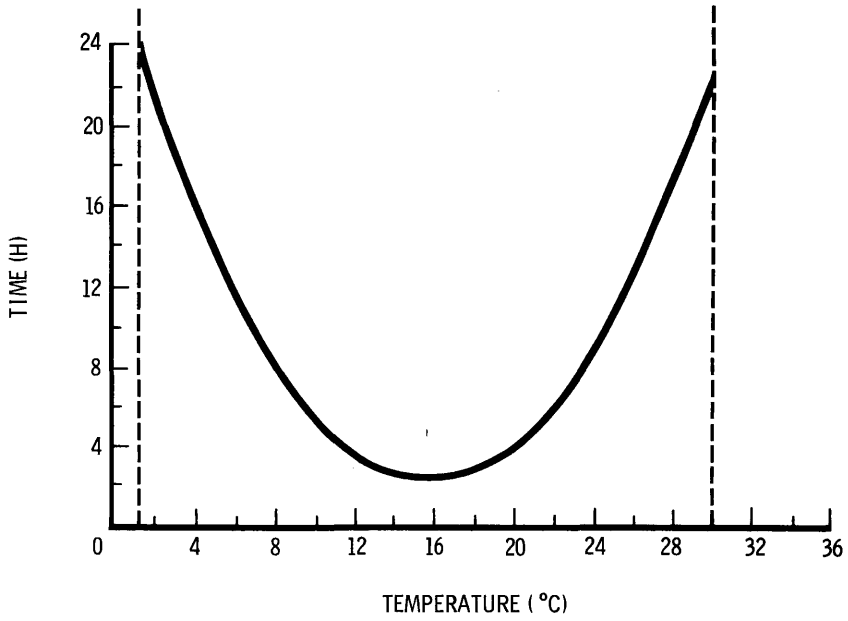

Figure 20.--Assumed relationship between temperature and period of germination of *Cronartium ribicola* basidiospores. Shape of curve estimated from author's unpublished data for aeciospores and urediospores and data from Bega (1960).

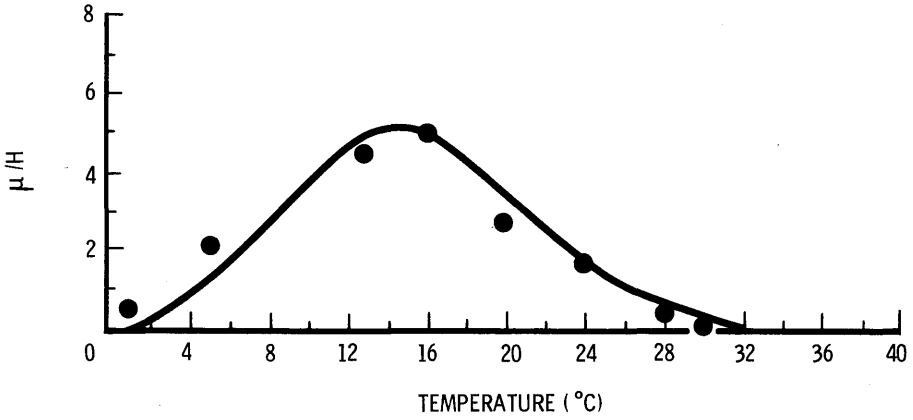

Figure 21.--Growth rate of *Cronartium ribicola* basidiospore germ tubes. Data points from Bega (1960) and curve from Weibull function where a = 0.02, B = 16.8, c = 2.8, W = 12.634, and X = temperature.

Computation of number of germinated basidiospores expected to produce germ tubes of sufficient length to penetrate (95→96). If probability of penetration is dependent on length of germ tube under ideal conditions, then the number of trapped and germinated BasidioSpores expected to produce germ Tubes of Adequate Length (BSTAL) to penetrate should be a function of infection period duration and temperature as both will influence germ tube length.

Computation of number of basidiospores penetrating to establish infection (96→97). It seems reasonable to assume that all the basidiospores that produce germ tubes of adequate length and are located on the infective surface will not reach the state of an established BasidioSpore Infection (BSI). What is the probability of a successful penetration? A measure of this probability is the ratio of spots found to spores trapped (Basidiospore Infection Yield ratio or BIY) under optimum conditions of temperature, moisture, and duration. BIY has been measured in the case of *C. ribicola* basidiospores on primary needles of *P. strobus* and on current year's secondary needles of *P. monticola*.

Hansen (1972) found that when he applied 100 spores per square millimeter to nine *P. strobus* seedlings, the ratio of spots to basidiospores trapped varied from 0.0 to 0.14 with an average of 0.004 (calculated by the authors on the assumption that Hansen inoculated 40 square millimeters of needle surface per seedling (Hansen 1972, p. 84 and 94). These nine seedlings were inoculated and then immediately placed in a

dew chamber. Ten more seedlings were inoculated, covered with moist plastic bags, and placed in the dew chamber. These trees yielded a ratio of 0.0005 to 0.011 and averaged BIY = 0.0043 spots per spore trapped (inoculated and ratio calculated as above). Thus, for primary needles of *Pinus strobus* the expectation is that the ratio of spots formed to basidiospores cast should be about 0.004 x average trapping efficiency, which equals 0.004 x 0.08 = 0.00033.

The ratio is stated in terms of spots per spores cast because all the available western white pine data are on this basis. In western white pine, one of our current studies at Moscow was inoculated in September 1973 by our standardized method (Bingham 1972a) except that rubber-cement-coated slides were stationed on a 2-foot grid throughout the inoculation. The slides were removed at the end of the inoculation. A lacto-phenol analin-blue fixing staining solution was placed on the slides and a cover slip added. Spores were then counted in a random sample of 10 fields of 0.175 mm^2 each on each slide. In June of 1974, spot types were tallied (see McDonald and Hoff 1975), and a sample of 20 slide stations was taken in order to obtain an estimate of the spot per basidiospore cast ratio. All trees within 1 foot of each of the 20 slides were studied. There were 20 planting spots within the prescribed distance from each slide, but some trees were clean (covered as controls) and some had died. In all, spots on 201 trees were used. All the spotted trees within 1 foot of each slide were used to calculate the ratio of spots to spores trapped on that slide. The average was 6.1 trees per slide. The average infection yield ratio (spots per square centimeter:spores cast per square centimeter) for each slide was used to calculate a mean BIY ($\bar{\chi}$ = 0.000087 ± 0.00001) of current year needles on 3-year-old trees. We will use the value of 0.000087 spots per basidiospore cast for current year western white pine needles.

There is apparently a resistance mechanism that causes a reduction in the rate of needle lesion frequency (Hoff and McDonald 1980). The difference between the average ratio of the four lowest-spotting families and the four highest-spotting families out of 120 families studied was 2.15 to 18.4. Thus spots were 8.56 times more frequent on the high spotters than on the low. More data on this important aspect of rust-resistance biology were collected for inclusion in this paper by analyzing records from the 1970 progeny test designed to screen resistant-tree seed orchard materials. Vaseline-coated slides were used to trap basidiospores during the artificial inoculation. Several hundred seedlings were included in each family. Number of basidiospores per square centimeter was calculated from the spore traps and number of spots per square centimeter of infective surface was determined on a sample of plants from each family (table 13). The ratios of spots to spores cast may or may not be comparable to the ratios already discussed because of the difference in spore trapping techniques; but the evidence clearly indicates that some families are high spotters and others are low spotters. The tenfold difference is in agreement with our earlier findings discussed above. The reduced-needle-lesion-frequency resistance mechanism was worked into the model as a BIY reduction factor, Quantity of Needle Lesion Reduction (QNLR). Thus, if we wanted to simulate the development of the rust on a population of trees characterized by the needle-lesion resistance factor, we would set QNLR as equal to 0.10.

Resistance mechanisms in the pine host are not the only possible factors that could reduce the BIY. As pointed out earlier, control chemicals, weather, rust genes, and other conditions could influence the ratio. These items will be introduced through the user-controlled variable BIY as they were in the case of aeciospore infection (AIYR(ISP)) and urediospores (UIYR(ISP)).

Calculation of number of new infections per tree on current-year stem needles (6→7). Since BSI was computed on the basis of current year secondary needles only, one more adjustment is needed to compute expected infection on stem needles. We do not know whether spores can be trapped only on upward surfaces or if all surfaces are equally effective traps. Our assumption is that only upward surfaces will trap. On

Table 13.--*Relationship between spore cast and frequency of spot formation for a group of full-sib families*

Degree of spotting	Families	Spore cast (spores/cm^2)	Lesion frequency (lesions/cm^2 infective surface)	Lesions/ trapped spore
Low spotters	19x17	2,660	0.16	0.00006
	208x207	2,500	.11	.00004
	20x21	3,000	.14	.00005
	69x185	2,660	.20	.00008
	86x166	2,000	.18	.00009
	84x155	2,000	.12	.00006
High spotters	176x215	3,160	1.47	0.0005
	159x78	2,410	1.72	.0007
	117x123	2,250	1.79	.0008
	237x202	1,750	1.06	.0006
	353x182	2,330	2.31	.0010

this basis, needle orientation on stem and branches was subjectively studied. The conclusion was that for stem needles 0.50 of the stomatal bearing surfaces were oriented upward and that 0.25 of the branch needle surfaces were likewise oriented. Thus, respective reduction will be made in amount of infection on each needle type.

Computation of number of new infections per tree on current-year branch needles (6→12). This flow is calculated the same as flow (6→7), except that the needle orientation factor is 0.25 instead of 0.5.

Computation of number of new infections on second-year branch needles (6→19). Primary foliage is known to be much more susceptible than secondary foliage (Patton 1967; authors' unpublished data). Also, data from Pierson and Buchanan (1938b) indicated that current-year needles of western white pine become spotted at a frequency 14.5 times less than 1- and 2-year-old needles. If this is so, then year-old secondary needles should have a BIY of 0.0013 (0.000087 x 14.5). This value is larger than Hansen's, but is in agreement with the findings over the years that *P. strobus* is more resistant than *P. monticola* (Bingham 1972b). Other results (Lachmund 1933) indicate that the current year's needles are much less susceptible to infection than older needles (table 14). Lachmund's finding was based on the detailed analysis of the pattern of appearance of young cankers after a particularly severe infection year. In all, 5,879 cankers were inspected and recorded as to the year of wood on which they occurred relative to the supposed infection year. The trees were described as "thrifty trees ranging from approximately 10 to 30 years of age." Lachmund's (1933) results show the following pattern of canker occurrence: current year wood, 0.10; 1-year-old wood, 0.53; 2-year-old wood, 0.31; and 3-year-old wood, 0.05. In order to interpret these findings, we must know the distribution of needles by needle-age class. The relative target contribution by each needle-age class was estimated from table 19 (see pine target submodel). The proportion of cankers on the wood that matched with current needles was divided by the proportion of target in that class to give cankers per unit of target as shown in column C of table 14. This analysis requires the assumption that needles are held to the end of their fourth growing season and that all the infections occurred in one season.

Table 14.--*Relative susceptibility of western white pine needles of different ages to* Cronartium ribicola *as measured by appearance of young cankers and needle spots*

Needle age at time of infection	A Cankers[1] 2 years after infection	B Needle[2] distribution 10 to 30 years	C Cankers/ unit target A/B	D Relative[3] difference	Spots[4]/ 100 cm^2	Relative difference
Current	0.1	0.43	0.23		1.3	
1 year	.53	.38	1.39	6.04	18.9	14.54
2 years	.31	.20	1.55	6.74	18.8	14.46

[1]Data obtained from Lachmund (1933).
[2]Data obtained from table 4, this paper.
[3]Value obtained by 1-year-old/current and 2-year-old/current.
[4]Data obtained from Pierson and Buchanan (1938b).

Pierson and Buchanan (1938b) reported on needle spotting on current and older needles. They potted seedlings 5 to 7 years old growing in the absence of the rust and placed them under heavily infected *Ribes* bushes during September and October. The trees were then placed in a greenhouse to allow for development of the rust. After 66 days, the number of spots was determined. The results were recorded as the number of spots per 100 square centimeters of needle surface.

In Lachmund's (1933) study, 1- and 2-year-old needles were six times more susceptible than current needles and in Pierson and Buchanan's (1938b) report 1- and 2-year-old needles were 14.5 times more susceptible.

Thus, we will use an input variable to account for the difference in susceptibility between current and older needles. Secondary Needle Age Infection Factor (SNAIF) will currently be set equal to the average difference (10.25) as shown by the data of Pierson and Buchanan (1938b) and Lachmund (1933).

Computation of number of incipient cankers (11) *from stem needles infected in their first year* (7→11). What will be the pattern of occurrence of canker appearance from any given year's infection? Little concrete information is available. Slipp[3] artificially inoculated branches of western white pine seedlings and saplings and followed the appearance of new cankers over time. The number to appear by the fourth year was taken as 100 percent and the distribution of the preceding year's cankers was calculated. At the end of 1 year, 7.5 percent were visible; 2 years, 80.4 percent; and 3 years, 98.8 percent.

Other results (author's unpublished) show a similar pattern with the added feature of genetic variation of incubation period. Two-year-old seedlings from 40 full-sib families were artificially inoculated in September. The following September the families varied in percent of their seedlings showing stem symptoms out of the

[3]Slipp, A. E. 1949. Canker development following artificial inoculation. Univ. Idaho, Moscow, 137 p. (Mimeographed)

total per family that showed stem symptoms by the fourth year after inoculation. The low family showed only 7 percent of the stem with stem symptoms and the highest family showed 60 percent. These data were used to construct curves of percentage cankered on years-after-inoculation. The relationship is shown in figure 22.

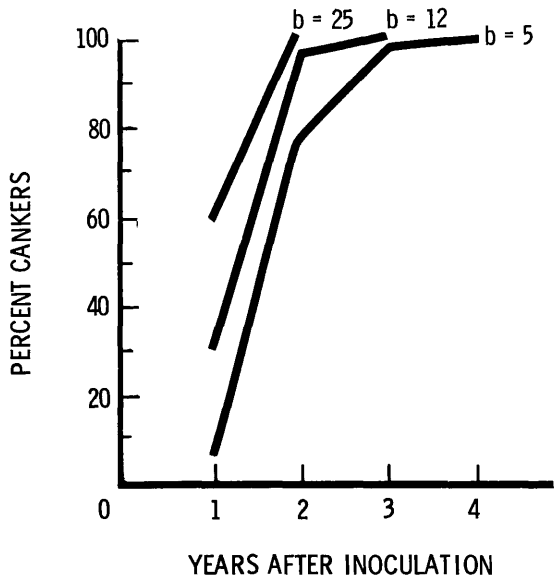

Figure 22.--Assumed rate of appearance of *Cronartium ribicola* cankers for three different rates of rust growth in needles of *Pinus monticola*.

Computation of number of stem-needle infections that failed to reach canker status in 1 year (7→8). This flow is self-explanatory. The needle infections that did not produce cankers are simply aged 1 year.

Computation of 2-year-old stem-needle infections that reached canker status in current year (8→11). The same relationships are used as in flow (7→11), but the variables have changed because of the additonal year.

Computation of number of 2-year-old stem-needle infections that failed to reach canker status in current year (8→9). This flow is the difference between needle infections in their second year (TI2S1) and the cankers that appeared from these infections (TCS2).

Computation of number of 3-year-old stem-needle infections (9) *that reach canker status in current year* (9→11). This flow is composed of all remaining infections.

Computation of number of 1-year-old needle infections in branch needles infected in their first year (12→13) *that reach canker status after 1 year* (13). This model uses the same relationship as flow (7→11).

Computation of 1-year-old branch-needle infections on needles infected in their first year that failed to reach canker status in 1 year (12→15). This flow is computed by obtaining the difference between year-old needle infections and their associated incipient cankers (CI1B1).

Computation of number of 2-year-old branch-needle infections from branch needles infected in their first year that reached canker status in the current year (15→16). This relationship is the same as in flow (8→11).

Computation of number of 2-year-old branch-needle infections on needles infected in their first year (15) *that failed to reach canker status in the current year* (15→17). Computation of the difference is again called for.

Computation of number of 3-year-old branch-needle infections (17) *that reached canker status in the current year* (17→18). The entire contents of X(17) flow to X(18).

Calculation of number of new lethal cankers (14) *from last year's incipient cankers from branch-needle infections on needles in their first year* (13→14). There is a relationship (fig. 23) between the probability that a branch canker will cause a bole canker (lethal canker) and the distance from canker to bole (Slipp 1953). The relationship has also been established, in the form of published curves (Childs and Kimmey 1938), between proportion of lethal cankers and tree height at time of infection. We constructed a composite curve (fig. 24) from the published data and one can readily see that proportion of cankers that are lethal is related to tree height at time of infection.

Since there is a definite relationship between tree height and branch length, there should be a relationship between a certain size of "crown cap" and proportion of cankers expected to be lethal. That is, there should be some length of crown from the top down that would be associated with the proportion of all cankers on a tree that eventually would reach the bole. This idea was tested by calculating the proportion of target (needles) in a crown cap 1 m in length. The result (fig. 24) was a close approximation of the composite lethal canker curve.

Calculation of number of new lethal cankers from last year's incipient cankers from 2-year-old branch-needle infections on needles infected in their first year (16→14). The explanation of this flow is analogous to flow (13→14).

Calculation of number of new lethal cankers (14) *from last year's incipient cankers from 3-year-old branch-needle infections on needles infected in their first year* (18→14). The explanation of this flow is analogous to flow (13→14).

Calculation of number of incipient cankers (20) *from 1-year-old infections on branch needles infected in their second year* (19→20). This flow is analogous to flow (12→13).

Calculation of number of 1-year-old infections on branch needles that failed to reach canker status (19→20). The explanation of this flow is analogous to flow (12→15).

Calculation of number of incipient cankers (22) *from 2-year-old infections on branch needles infected in their second year* (21→22). This flow is analogous to flow (12→13).

Calculation of number of 2-year-old infections on branch needles that failed to reach canker status (21→23). This flow is analogous to flow (12→15).

Calculation of number of incipient cankers (24) *from 3-year-old infections on branch needles infected in their second year* (23→24). This flow is analogous to flow (17→18).

Calculation of number of new lethal cankers (14) *from last year's incipient cankers from 1-year-old branch-needle infections on needles infected in their second year* (20→14). This flow is analogous to flow (13→14).

Calculation of number of new lethal cankers (14) *from last year's incipient cankers from 2-year-old branch-needle infections on needles infected in their second year* (22→14). This flow is analogous to flow (13→14).

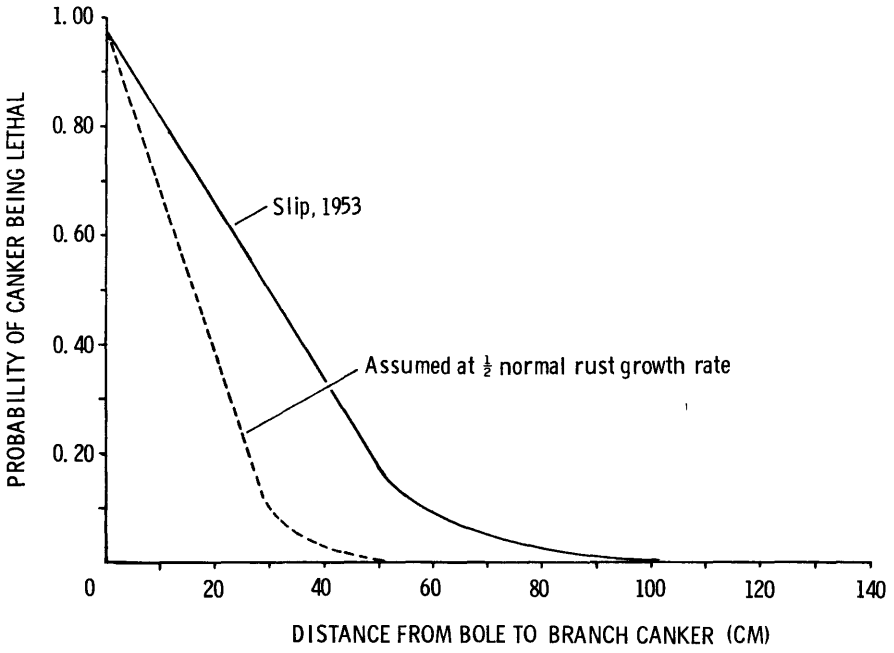

Figure 23.--Probability that *Cronartium ribicola* branch canker will cause a bole (lethal) canker on *Pinus monticola* as expected from Slipp's (1953) data and an assumed probability if normal rust growth rate were reduced by one-half.

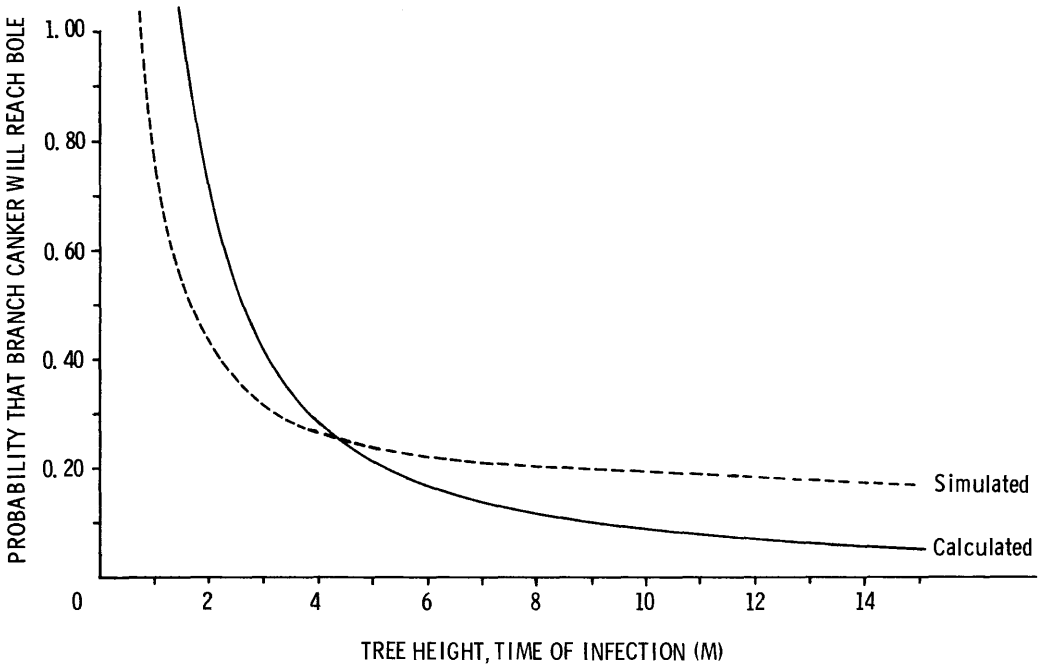

Figure 24.--Calculated (data from Childs and Kimmey, 1938) and target-area-simulated probability of a *Cronartium ribicola* branch-canker reaching the bole of a *Pinus monticola*.

Calculation of number of new lethal cankers (14) *from last year's incipient cankers from 3-year-old branch-needle infections on needles infected in their second year* (24→14). This flow is analogous to flow (13→14). After all flows have been calculated, the number of bole and lethal-branch cankers can be determined by summation.

Also, if needle retention could be reduced to 2 years instead of 3 on the branches and 1 year instead of 2 on the stem, there would be a great reduction in effective target. If the 3 years' branch needles are partitioned equally on the tree (table 19) and second-year needles are 10 times more susceptible than current-year needles, then elimination of second-year needles as a target would reduce effective target by 91 percent and there would be no effective target on the stem. Thus, we have included provisions for taking all stem needles and the second-year branch needles out of the model through the Needle Retention Factor (NRF) that can stop flows (6→7) and (6→12).

Calculation of number of new cankers to appear on average tree (98). This is a bookkeeping sort of flow. State variables 11, 13, 16, 18, 20, 22, and 24 are summed each year and placed in X(98).

Calculation of accumulated number of cankers to appear on an average tree (98→99). This flow serves to keep a record of all infections over all simulated years. The value in X(98) is added each year to the previous year's total.

Stand Infection Submodel

The preceding parts of the simulator all dealt with computation of the amount of rust infection on an average tree. The objective of the stand infection submodel is to expand the average infection to a stand and simulate disease progress curves for the stand. The factors assumed to influence the curves are host-growth rate, fungus-growth rate, host genotype, stand age, rust genotypes, natural canker inactivation (Kimmey 1969; Hungerford 1977), and the interaction of all the above and inoculum load over years. The box-and-arrow diagram (fig. 25) for stand infection illustrates the general concept, and the variables are defined in table 15 and flow descriptions are given in table 16.

This submodel is complex because of relatively large numbers of interconnected flows. The order of discussion will follow the flows beginning with (35→43) and ending at state variable (50), which is the part of the model dealing with seedlings. The next route will be (35→36) and pertains to stem cankers originating from stem needles. The branch (37→38→39) leads to death by cankers that remain always active and branch (37→45→46→47) leads to death by cankers that are temporarily inactive. The (35→44) route develops the branch canker relationships, and also contains both always active and temporarily inactive branch cankers.

Computation of number of infected seedlings (35→43). Branches on trees up to 1 m tall are so short that all cankers are considered lethal. So no distinction by type of canker is necessary and all cankered trees follow the same path.

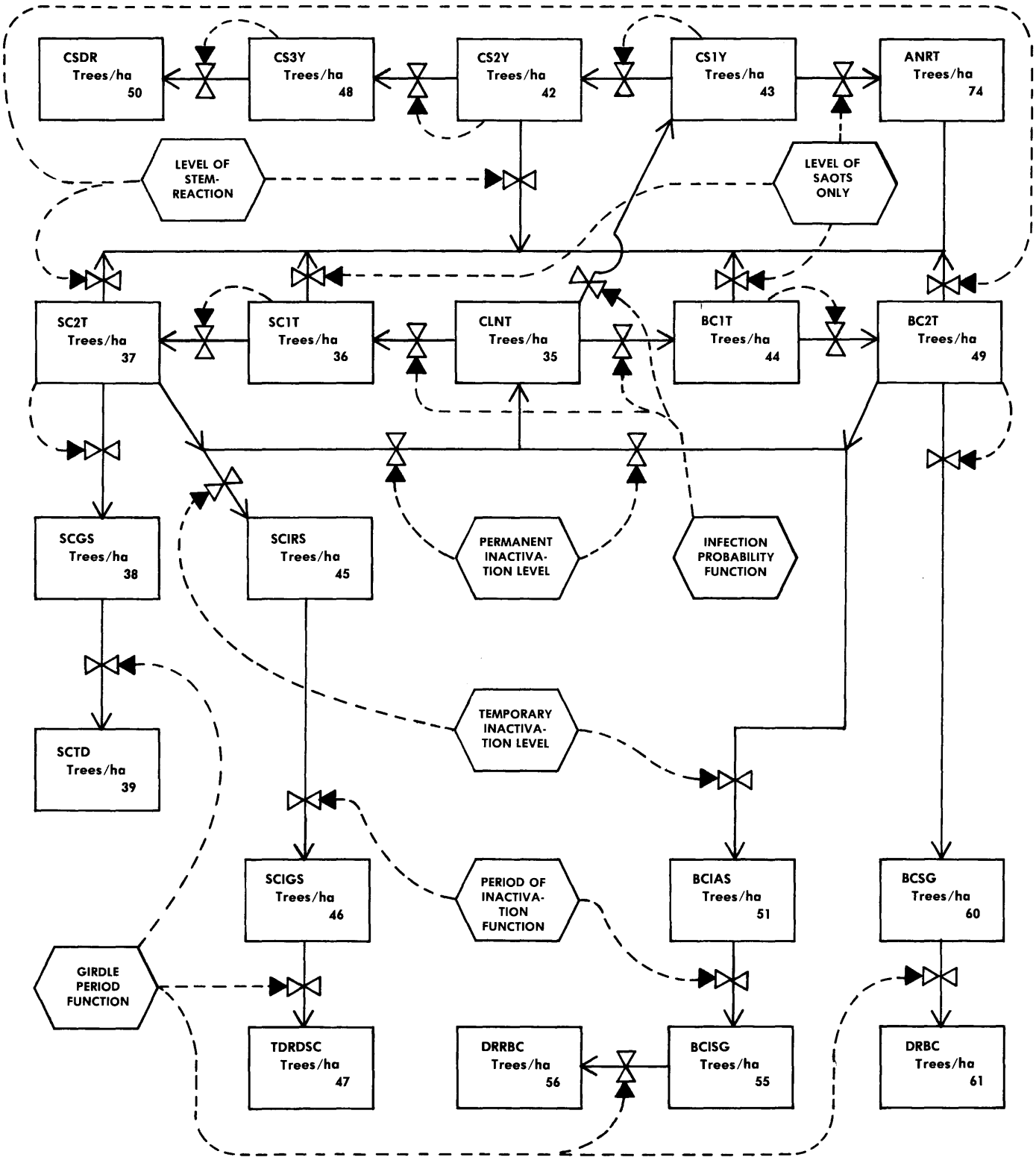

Figure 25.--Box-and-arrow diagram of *Cronartium ribicola* infection in *Pinus monticola* stands.

Table 15.--*Definition of variables used in stand infection submodel of the white pine blister rust simulation*

Variable		Definition
State variables:		
X(35)	CLNT	Number of clean trees in stand, trees per hectare.
X(36)	SC1T	Number of stem cankered first year trees, trees per hectare.
X(37)	SC2T	Number of stem cankered second year trees, trees per hectare.
X(38)	SCGS	Number of trees in stem canker girdle storage, trees per hectare.
X(39)	SCDT	Number of stem canker direct dead trees, trees per hectare.
X(42)	CS2Y	Number of cankered seedlings with second year cankers, trees per hectare.
X(43)	CS1Y	Number of cankered seedlings with first year canker, trees per hectare.
X(44)	BC1T	Number of branch cankered first year trees, trees per hectare.
X(45)	SCIAS	Number of trees in stem canker inactive storage, trees per hectare.
X(46)	SCIGS	Number of trees with stem canker and in girdle storage, trees per hectare.
X(47)	TDRDCC	Number of direct stem cankers, trees per hectare.
X(48)	CS3Y	Number of cankered seedlings third year cankers, trees per hectare.
X(49)	BC2T	Number of lethal branch cankered 2-year trees, trees per hectare.
X(50)	CSDR	Number of cankered seedlings dead from rust, trees per hectare.
X(51)	BCIAS	Number of trees with lethal branch cankers inactive and in storage, trees per hectare.
X(55)	BCISG	Number of trees with reactivated lethal branch cankers in storage for girdling, trees per hectare.
X(56)	DRRBC	Number of trees dead due to rust from reactivated lethal branch cankers, trees per hectare.
X(60)	BCSG	Number of trees with lethal branch cankers in storage for girdling, trees per hectare.

(continued)

Table 15.--*Definition of variables used in stand infection submodel of the white pine blister rust simulation (continued)*

Variable		Definition
X(61)	DRBC	Number of trees dead due to rust from lethal branch cankers, trees per hectare.
X(74)	ANRT	Accumulated number of rust resistant trees, trees per hectare.
User controlled variables:		
BCIL		Branch canker inactivation level, percent.
BCPIL		Branch canker permanent inactivation level, percent.
FER		Fungus encirclement rate, meters/year.
ICIAS		Inactive period for cankers inactive, years.
SCIL		Stem cankers inactivation level, percent.
SCPIL		Stem canker permanent inactivation level, percent.
SORL		Spots only resistance level, percent.
SRRL		Stem reaction resistance level, percent.
STAND		Initial stand in trees per hectare.
Computed variables:		See text

Table 16.--*Stand infection submodel flow descriptions*

Flow path	Flow name	Flow description	Flow equation*
$J_{(35\rightarrow43)}$	Seedling infection	Computation of number of infected seedlings per hectare	$CS1Y = CLNT(\frac{1.0}{1.0 + \frac{1.228}{ANCPT}})$
$J_{(43\rightarrow74)}$	Spots-only resistance	Computation of number of seedlings that possess spots-only resistance	SORT = CS1Y·SORL
$J_{(43\rightarrow42)}$	Infected seedlings age	Computation of number of infected seedlings that age one season	CS2Y = CS1Y-SORT
$J_{(42\rightarrow74)}$	Stem-reaction resistance	Computation of number of seedlings that possess stem-reaction resistance	SRRT = CS2Y·SRRL
$J_{(42\rightarrow48)}$	Infected seedlings age	Seedlings supporting 2-year-old cankers age 1 year	CS3Y = CS2Y-SRRT
$J_{(48\rightarrow50)}$	Infected seedlings age	Computation of number of seedlings 1 meter and under in height at time of canker appearance that die in the current year	CSDR = CS3Y + CSDR
$J_{(35\rightarrow36)}$	Stem infections	Computation of number of trees that have incipient stem needle cankers appear from a single season's infection	$SC1T = CLNT(\frac{1.0}{1.0 + \frac{1.228}{TCOS}})$

(continued)

Table 16.--*Stand infection submodel flow descriptions (continued)*

Flow path	Flow name	Flow description	Flow equation*
$J_{(36\rightarrow74)}$	Spots-only resistance	Computation of number of direct-stem infected trees that have spots-only resistance	SSORT = SC1T·SORL
$J_{(36\rightarrow37)}$	Infected trees age	Compilation of number of direct-stem-infected trees with cankers that will age 1 more year	SC2T = SC1T-SSORT
$J_{(37\rightarrow74)}$	Stem-reaction resistance	Computation of number of infected trees over 1 meter in height that exhibit stem-reaction resistance from stem-needle cankers	SSRRT = SC2T·SRRL
$J_{(37\rightarrow35)}$	Permanent inactivation	Computation of number of trees returned to CLNT due to permanent inactivation of stem cankers arising from stem needles	$TSCPI = (SC2T-SSRT)SCPIL^{SCPIT}$
$J_{(37\rightarrow45)}$	Temporary inactivation	Computation of number of trees infected with stem cankers from stem needles on which all cankers will be temporarily inactivated for the period ICIAS	$TSCTI = \bar{}(SC2T-SSRRT-TSCPI)SCIL^{SCPIT}$
$J_{(37\rightarrow38)}$	Girdle storage	Computation of number of trees supporting stem cankers that came from stem needles and are not resistant or do not have all cankers inactivated	SCGS = SC2T-SSRRT-TSCPI-TSCTI

(continued)

Table 16.--*Stand infection submodel flow descriptions (continued)*

Flow path	Flow name	Flow description	Flow equation*
$J_{(38\rightarrow39)}$	Girdle process	Computation of number of trees in SCGS that will die in a given year	SCTD = SCGT
$J_{(45\rightarrow46)}$	Reactivation process	Computation of number of trees that have at least one direct-stem-needle inactivated-canker reactivated	SCIGS = RSCIAS
$J_{(46\rightarrow47)}$	Girdle process of reactivated cankers	Computation of number of trees that have had inactive cankers reactivated that will die in a given year	TDRDSC = SCITD
$J_{(35\rightarrow44)}$	Branch infection	Computation of number of trees to have new lethal branch cankers appear in the current simulated year	$BC1T = (CLNT-SC1T+TSCPI)\cdot\left(\frac{1.0}{1.0+\frac{1.228}{TLBC}}\right)$
$J_{(44\rightarrow74)}$	Spots-only resistance	Computation of number of branch-cankered trees that have spots-only resistance	BSORT = BC1T·SORL
$J_{(44\rightarrow49)}$	Branch infections aged	Computation of number of branch-cankered trees that age 1 year	BC2T = BS1T-BSORT
$J_{(49\rightarrow74)}$	Stem reaction resistance	Calculation of stem-reaction resistance trees in the branch cankered population	BSRRT = BC2T·SRRL

(continued)

Table 16.--*Stand infection submodel flow descriptions (continued)*

Flow path	Flow name	Flow description	Flow equation*
$J_{(49\rightarrow35)}$	Permanent inactivation	Computation of number of BC2T trees that have all branch cankers permanently inactivated	$TBCPI = (BC2T + BSRRT)BCPIL^{BCPLT}$
$J_{(49\rightarrow51)}$	Temporary inactivation storage	Compilation of number of trees that will have all branch cankers temporarily inactivated for the period ICIAS	$TBCTI = (BC2T-BSRRT-TBCPI)BCIL^{RCPLT}$
$J_{(49\rightarrow60)}$	Girdle storage	Computation of number of trees that will go into storage for time it takes the rust to grow down the branch, girdle the stem and kill the tree	BCSG = BC2T-BSRRT-TBCPI-TBCTI
$J_{(60\rightarrow61)}$	Girdle process	Computation of number of trees in BCSG that will die in a given year	DRBC = BCTD
$J_{(51\rightarrow55)}$	Reactivation process	Computation of number of trees with all branch cankers that will have at least one canker reactivate	BCISG = RBCIAS
$J_{(55\rightarrow56)}$	Girdle process	Computation of number of trees that will be damaged by reactivated cankers in TGIRD2 years after cankers have been inactive for ICIAS years	DRRBC = BCITD

*See appendix I for derivations

The proportion of the stand infected in any one year is determined by a regression of proportion infected on average number of cankers per tree (fig. 26). The data for this regression were obtained from anywhere we could find mention of or could calculate percentage of the stand infected versus average number of cankers in the stand (Childs and Bedwell 1948; Childs and Kimmey 1938; Mielke 1943; Buchanan 1938; Macleod[4]; and authors' unpublished data). In all, 167 data points were found. All influencing factors such as tree size, number of years exposed, and site were ignored. Our curve was nearly the same as Childs and Kimmey's (1938) curve for infection by 5-foot height classes and was very close to Van der Plank's (1975) theoretical curve. We assume that the number of years of exposure has no bearing on this curve. That is to say, it makes no difference if a stand is exposed to 5 years of inoculum level L (total inoculum load = 5L) or to a single large inoculum load of 5L, the percentage of the stand infected would be the same in each case. Many of the data points used in the regression (assuming that 1 needle lesion = 1 canker) were from one application of heavy inoculum load on seedlings in the nursery under artificial conditions (authors' unpublished data). These points seem to match up with others that were obtained from field data on much larger trees exposed to many years of natural inoculum. We also arranged the data into age (size) classes, but no constant relationship was found. It seems that age and number of years of exposure are not as important as infection level. This regression is a very sensitive function in the model. Any predictive value the model may have would depend a great deal on the accuracy of the infection probability function.

We make the additional assumption as did Childs and Kimmey (1938) that the same general relationship must exist for lethal cankers as exists for all cankers.

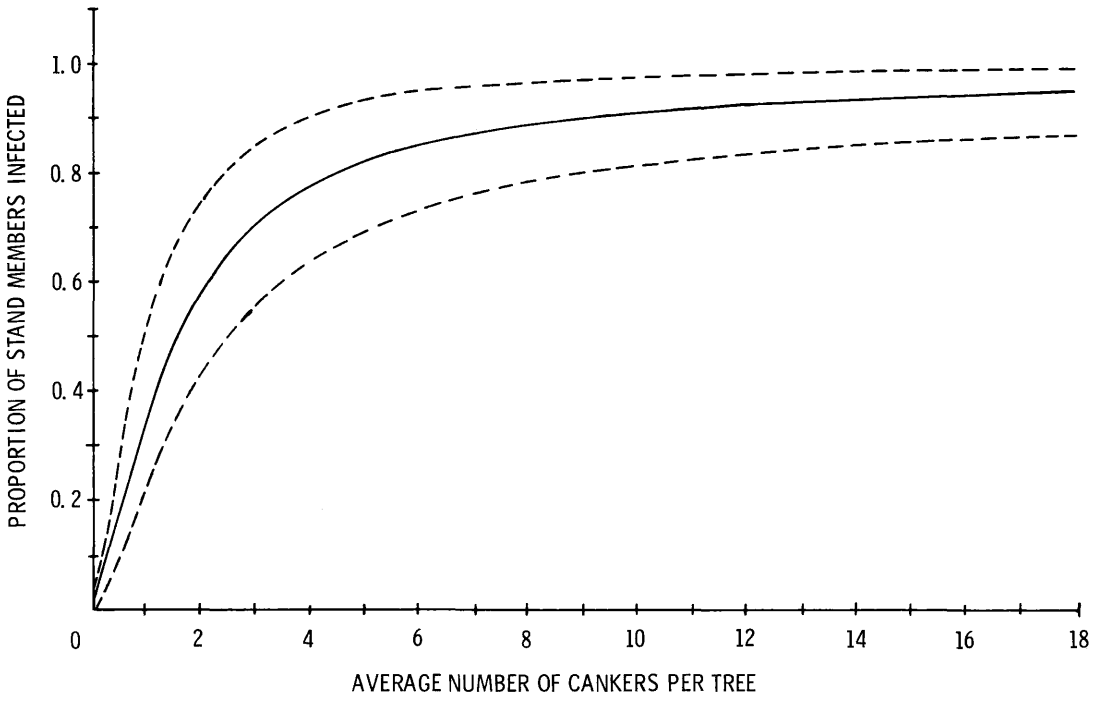

Figure 26.--Regression of proportion of *Pinus monticola* stand infected on average number of *Cronartium ribicola* cankers per tree. Dotted lines are 95 percent confidence limits.

[4]Macleod, R. L. 1937. Pine disease survey and scouting for blister rust in the inland empire, 1937, p. 112-116. *In* 1937 annual report Spokane office blister rust control. (Mimeographed) U.S. Dep. Agric., Bur. Plant Quar.

Computation of number of seedlings that possess spots-only resistance (43→74). The proportion of the stand exhibiting spots-only resistance (McDonald and Hoff 1970 and 1971) is given by the externally supplied variable--Spots Only Resistance Level (SORL). This resistance is actually expressed during the movement of the rust down the needles, but since the infection portion of the model simulates infection on an average tree, this needle resistance cannot be accounted for on an individual tree basis until this point in the simulation. Hence, the calculation is made and trees resistant by reason of the spots-only mechanisms are removed from X(43) before additional flows are calculated.

Computation of one season's aging of seedlings with 1-year-old cankers (43→42). The seedlings remaining after removal of resistant individuals are aged 1 year.

Computation of number of seedlings that possess stem resistance (42→74). The externally supplied variable, Stem Reaction Resistance Level (SRRL), is used to calculate this flow. SRRL is the proportion of the stand that can express a Stem-Reaction Resistance Level (see Hoff and others 1973). The flow is placed at this point in the simulator because it takes 2 years of canker development for the stem resistance to show up.

Seedlings supporting 2-year-old cankers age 1 year (42→48). The resistant trees are removed, and the remainder advanced 1 year. An important point to keep in mind is that only the first cankers on a tree count, since this is the canker that will be first to do damage.

Computation of the number of seedlings 1 m and under in height at time of canker appearance that die in the current year (48→50). Our experience shows that seedlings generally die within 3 years of canker appearance. The entire contents of X(48), trees that have been cankered 3 years, are flowed to X(50). In turn, X(50) is not emptied so that the number of seedlings simulated to have died from *C. ribicola* can be accumulated.

Compilation of number of trees when average stand height is over 1 m to have incipient stem-needle cankers appear from a single season's infection (35→36). If plants are over 1 m tall then a proportion of the uninfected stand (CLNT) is transferred to the first stem-needle cankered stage state variable X(36).

Computation of the number of direct-stem-infected trees that have spots-only resistance (36→74). Resistant individuals are moved to the resistant tree accumulation state variable (74).

Compilation of the number of direct-stem-infected trees with cankers that will age 1 more year (36→37). Needle-spots-only resistance removes trees from the population and the remaining infected trees develop for one additional year.

Computation of number of infected trees over 1 m in height that exhibit stem-reaction resistance from stem-needle cankers (37→74). The only difference between this flow and flow (42→74) is that the trees are assumed to be over 1 m in height for the current flow.

Computation of number of trees returned to CLNT due to permanent inactivation of stem cankers arising from stem needles (37→35). This flow deals with the problem of canker inactivation described by Kimmey (1969) and Hungerford (1977). Certain cankers are permanently inactivated while others remain inactive for a time then reactivate. This is treated as a probability. If the amount of permanent inactivation, or the amount of reactivation, the average number of direct stem cankers per infected tree, and the amount of inactivation are given, we can calculate the probability of a tree exhibiting only inactive cankers. The inactivation and reactivation

levels can be given as external variables and the average number of cankers per infected tree can be given by the calculations discussed above. Theoretically, if a tree has one direct stem canker and the probability of inactivation is 0.4, then the probability of that tree having only an inactive canker is 0.4 or if 10 trees have one canker each then four of those trees should have no active cankers. To digress for a moment, there are three things that can happen to a tree supporting cankers: (1) some cankers continue to grow; therefore disease development follows a normal course; (2) all the cankers are permanently inactivated and the infected tree would be classified as clean; (3) all the cankers are inactivated for a period of time and then one or more continue development.

Thus, the flows from state variable 37 to state variables 74, 35, and 45 are controlled by the probability of an infected tree having stem resistance, that all cankers have been permanently inactivated, or that all cankers have been temporarily inactivated.

Computation of number of trees infected with stem cankers from stem needles on which all cankers will be temporarily inactivated (37→45). The logic for calculating this flow is the same as outlined above.

Computation of number of trees supporting stem cankers that came from stem needles and are not resistant or have not been inactivated (37→38). This flow is computed as the remainder after removal of resistant trees and trees with inactive cankers.

Computation of number of trees in X(38) that will remain in X(38) for the period required to complete the girdling process (38→39). Period required for bark cankers established from stem-needle infections to girdle the bole is determined by a function called GIRDLE (appendix IV). TGIRD1 computes the storage period for stem-needle infections and TGIRD2 computes the period for branch-needle infections. Thus, the time required for girdling is calculated separately for cankers originating from stem and from branch needles. Computation of the storage period for stem-needle cankers is based on current tree height, past tree height, rust encirclement rate, tree circumference growth rate, and the length of time that elapses before death occurs after the girdle is complete.

Computation of number of trees with all direct stem-needle cankers temporarily inactivated and placed into storage for the duration of the inactivation period (45→46). So little is known about the inactivation process that we have assigned an external variable (ICIAS) to define the inactive period.

Computation of the number of trees that have had inactive cankers for the period ICIAS and now have reactivated cankers that will be stored until the girdling process is complete (46→47). The flow simply holds the infected trees with no change for the period ICIAS as set by the user.

Computation of the number of trees to have new lethal branch cankers appear in the current simulated year (35→44). After trees supporting stem-needle cankers have been removed from CLNT, we must next account for trees supporting lethal branch cankers.

Computation of number of branch-cankered trees that have spots-only resistance (44→74). The rationale for this flow is the same as flow (43→44).

Computation of number of branch-cankered trees that age 1 year (44→49). After the resistant trees are removed, the infected trees are transferred to X(49).

Calculation of stem-reaction resistance trees in the branch-cankered population (49→74). The rationale for this flow was discussed under (42→74).

Computation of number of BC2T trees with permanently inactivated branch cankers. Such trees have returned to the uninfected state for reinfection (49→35). An externally supplied variable sets the level of permanent branch canker inactivation.

Compilation of number of trees that will have all branch cankers temporarily inactivated for the period ICIAS (49→51). Most of the rationale has been discussed. An external variable sets the level of temporary branch canker inactivation and another external variable sets the length of the inactive period for both branch-needle and stem-needle cankers.

Computation of number of trees that will go into storage for the time it takes the rust to grow down the branch, girdle the stem, and kill or top-kill the tree (49→60). This flow simply sets up the value that is to be stored. The next flow executes the storage process.

Computation of number of trees in BCSG that will die in a given year (60→61). The rationale for this flow is discussed under flow (38→39).

Computation of number of trees on which all branch cankers have been inactivated and on each of which at least one canker will be reactivated (51→55). The period is defined by the external variable ICIAS.

Computation of number of trees that will be damaged by reactivated cankers in TGIRD2 years after cankers have been inactive for ICIAS years (55→56). This flow adds the inactive period ICIAS to the INDX time already computed in order to simulate the tree growth that occurred during ICIAS. The circumference of the point of entry is now larger; therefore, girdling will take longer.

DISCUSSION

Verification

You have seen the step-by-step process of model formulation. The next step will be programing the model for computer operation. Our programing objective will be to allow for the annual status of any state variable to be plotted and to incorporate various operational modes from complete random selection of infection weather to control of infection year and stand age when infection occurs so that various "what if" games can be played. After programing, the simulation will have considerable research value. But, before being used to directly assist in management decisions, it must be verified. The steps that should be taken range from calibration-prediction tests to verification of individual components through experimentation.

The simulator is nothing more than a hypothesis about the real world and, as such, it can never be complete. But, it should be able to assist us in our reading of real situations and predicting alternate outcomes. Obviously, we cannot predict weather, but we can read weather and other input data and compare actual and predicted results. Many such predictions could be made and the simulator could be modified as data are accumulated. At the conclusion of the general verification procedure, the range of the simulator's applicability and capability should be well understood.

Verification should include mapping *Ribes* and pine populations, monitoring aeciospore production and rust buildup on *Ribes* (bush by bush), and recording weather data such as days after April 1 to midpoint of an infection period, infection period duration, average temperature of infection period, and pattern of infection period occurrence. Occurrence of incipient cankers should then be recorded each year for a

period of years. The input data (weather; pine host parameters, such as stocking age, needle length, and number of stomatal rows; and *Ribes* bush species and density) would be used to predict the levels of the various applicable state variables. Some outputs such as basidiospore load need not be measured directly, because the objective would be to predict pine damage from easily measured parameters. Aeciospore load does need to be measured directly, because we do not have a value of aeciospore load that is a required input parameter. *Ribes*, pine, rust, and weather variables would be entered for a given year over a number of different sites that would vary in aspect, elevation, site quality, pine age, *Ribes* density, and *Ribes* species composition. In 5 to 10 years, the simulator could be verified, calibrated, and ready for use by forest managers.

Additional Research

The model formulation phase of the blister rust simulator has highlighted many areas in need of additional research. Areas of greatest need will be discussed in order of their appearance in the model formulation. The first major function HEIGHT (appendix II) was modeled on the basis of a very small amount of data. The mensurational literature contains little on annual height increment of western white pine. In fact, the whole area of the relationship between tree growth and target area needs additional work. For example, there is one report relating some crown parameters to number of needles (Buchanan 1936) in white pine; but more data are needed in order to address the effects of site quality, aspect, elevation, slope, and competing vegetation. In addition, little is known of the influences of environment on needle length and number of rows of stomata, both of which appear to have a considerable influence on effective target.

The relationships shown in figures 27 through 30 are crude empirical functions of the influence of sunlight on *Ribes* density. These important relationships could be refined experimentally for many different *Ribes* species and sites. These are important relationships to understand because with understanding there is an opportunity for us to manage pine stocking density, which can have a direct effect on *Ribes* density. Conversely, stands opened by the death of trees susceptible to blister rust may result in increased *Ribes* density. Some work has been done on these ecological relationships (Wellner 1946), but much more is needed to fully integrate these possibilities into a rust management plan and to make this model more realistic.

Greater breadth of data is needed to round out our understanding of the four important physical aspects of pine target--needle number, needle length, number of stomatal rows, and period of needle retention. We need to know more about the relative contributions of both environment and genetics to variation of these traits because there may be some opportunities for breeding or stand manipulation to shift stands to an unfavorable condition for the rust. It might be possible to regulate needle length and number of stomatal rows by stocking density and/or species mixes, as well as by breeding. Aspect and nutrient status of the site could also influence these characters. We should acquire enough understanding so that we do not inadvertently make one or more of the factors more favorable to the rust. Period of needle retention is of special importance and will be discussed more fully here.

More knowledge is needed concerning the *Ribes* target as well. How do various site conditions influence number of leaves per bush, size of leaves, and stomatal frequency? How does *Ribes* genetic susceptibility vary from site to site and species to species? For example, in our detached leaf inoculations, hundreds of urediospore transfers were made to four clones of *Ribes hudsonianum*. One clone became infected at about the 85 percent rate; another was positive about 50 percent of the time; but the two remaining clones remained disease-free. Research is needed on the hypothesis that this situation could be explained by a group of specific races of the rust, because the two clones that will not accept our restricted rust population were lightly infected in the field.

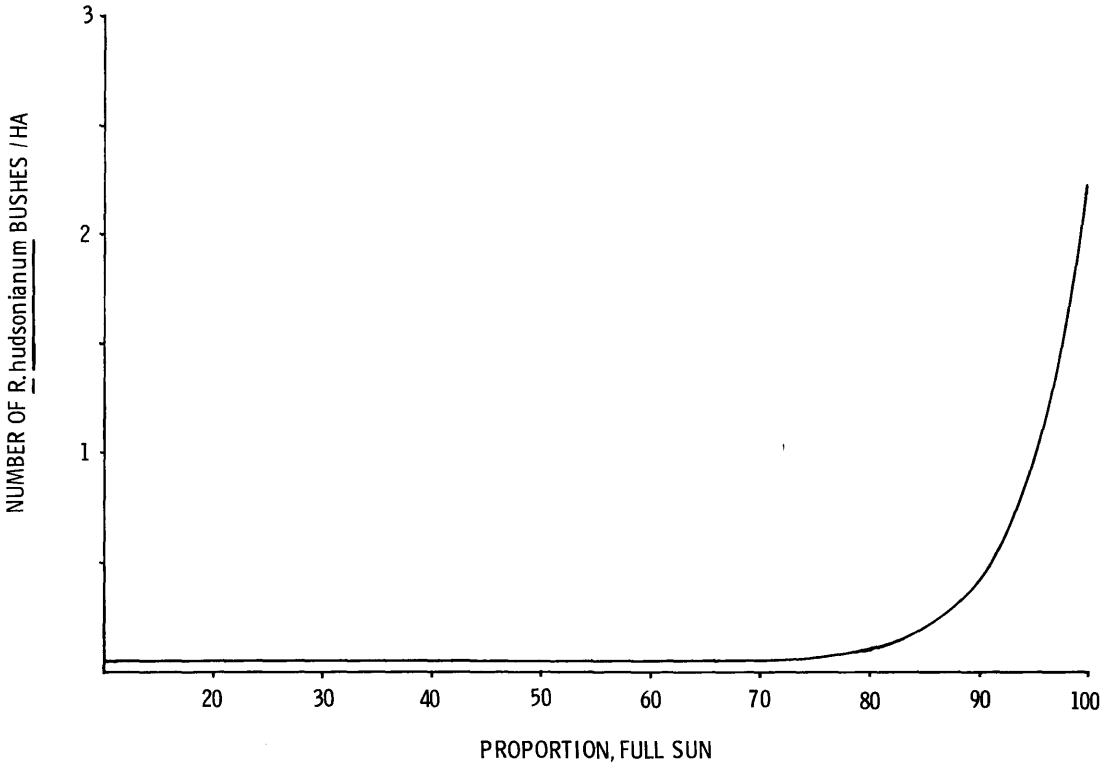

Figure 27.--Number of *Ribes hudsonianum* bushes per hectare as a function of proportion-full-sun.

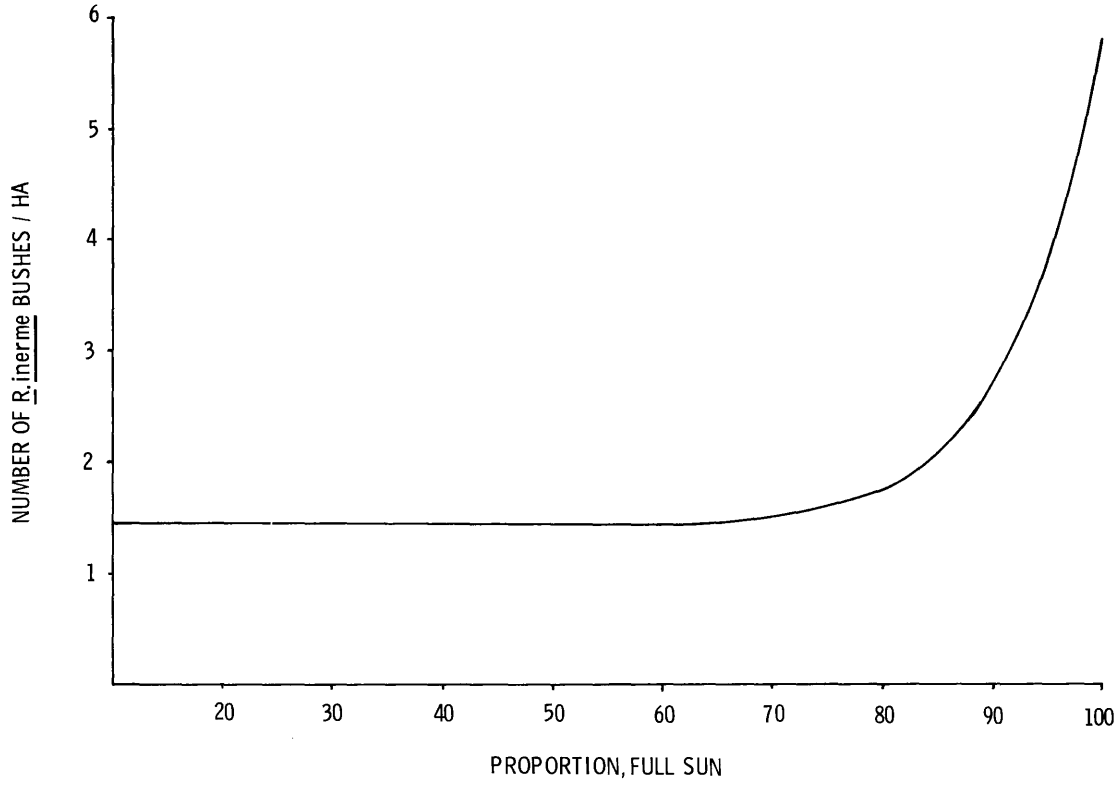

Figure 28.--Number of *Ribes inerme* bushes per hectare as a function of proportion-full-sun.

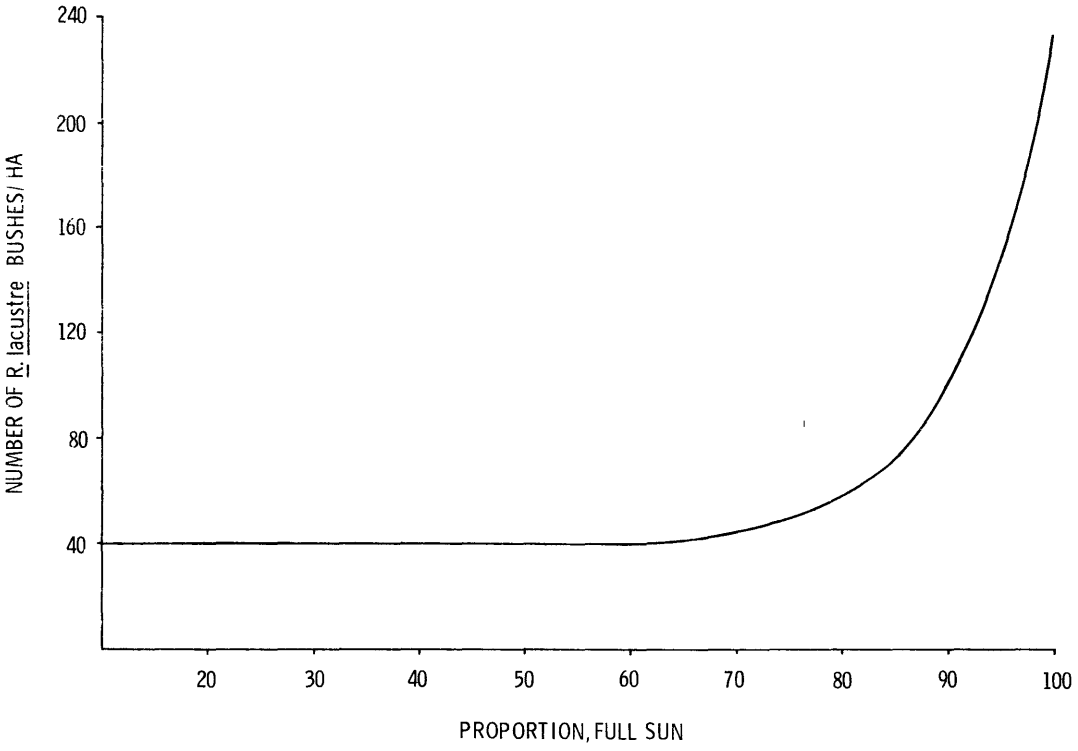

Figure 29.--Number of *Ribes lacustre* bushes per hectare as a function of proportion-full-sun.

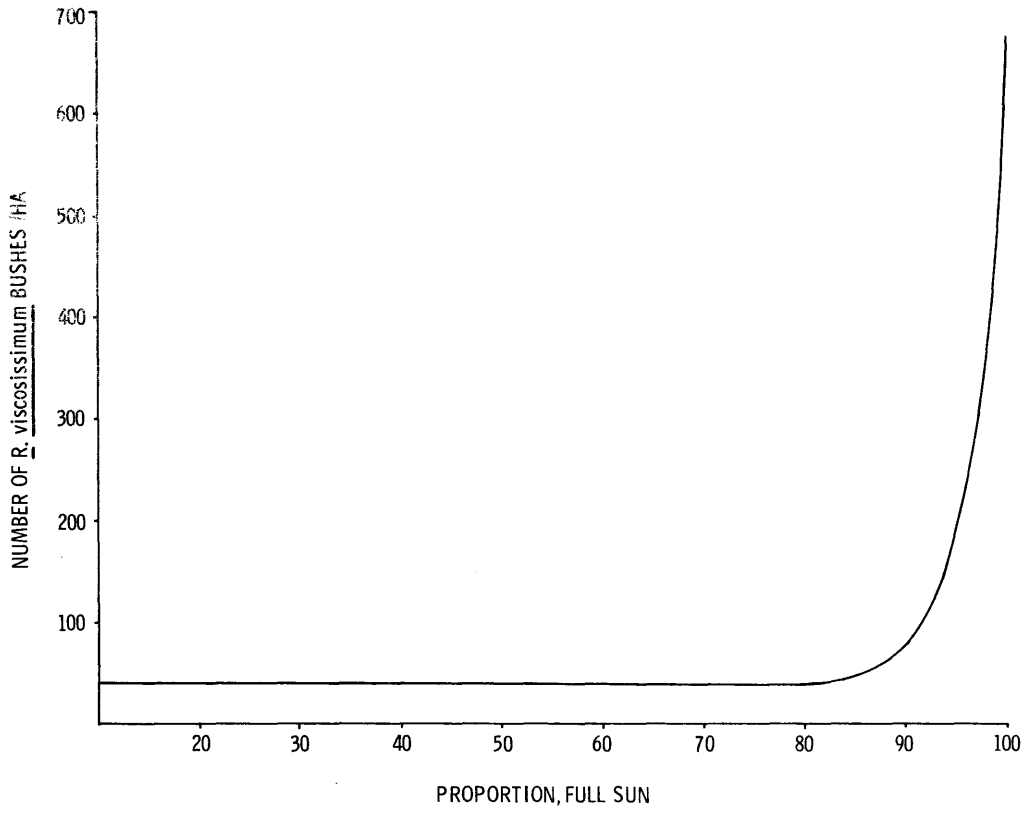

Figure 30.--Number of *Ribes viscosissimum* bushes per hectare as a function of proportion-full-sun.

In addition to the above, we performed a survey of *C. ribicola* infections on *R. viscosissimum* at the West Fork of Merry Creek outplanting site (Bingham and others 1973) on August 5, 1977. We randomly selected 92 bushes from a strip across the center of the outplanting. Of the 92 bushes inspected, 46 were disease free; 16 supported very sparse infections, and 20 were heavily infected. All three kinds of bushes appear to be located at random. Heavily infected bushes were always surrounded by disease-free or lightly infected bushes (see Hahn 1928).

These two observations and Hahn's (1928) findings under greenhouse conditions indicate that rust resistance probably exists in *Ribes* populations. How widespread is it, what are the genetic and environmental components of its variation, and can we manage stands of white pine so as to increase the resistance in *Ribes* or at least not decrease it?

Very little is known about the patterns of aeciospore dispersal and viability. Aeciospore inoculum density should be measured at a number of sites and those levels related to nearby aeciospore sources. We need more information about the duration of aeciospore viability and period of release, and little is known about the aeciospore infection process. Can we expect to exercise any control over aeciospore loads or do we want to try?

This modeling effort has uncovered a series of questions about both aeciospore and urediospore infection processes. A model of infection is presented simply to suggest a framework to facilitate additional studies. The ideas about individual infection life cycles and productivity should be subjected to experimentation. We should learn how these aspects of *C. ribicola* are controlled and how they contribute to the epidemic. Are there opportunities for management or pitfalls to be avoided?

Some aspects needing research are influence of temperature and moisture on aeciospore and urediospore germination percentage, period of germination lag, period of germination, and germ tube growth rate on both water agar and leaves. Additional knowledge is needed about the relative patterns of spore attachment and stomatal location. How are electrostatic forces involved in the infection process? How important are the various methods of spore dispersion (wind, water, and animals) to natural inoculation with urediospores?

In spite of all the past work on and the importance of teliospore production, it still remains an uncontrollable variable. One cannot routinely produce teliospores in a laboratory setting. The factors that influence teliospore production in the field are not really known. Can aecial infections produce teliospores or are urediospore infections required? What triggers the initial formation of teliospores? Once an individual infection begins producing teliospores, can it subsequently produce more urediospores?

In addition to knowing the trigger(s) that change urediospore production to teliospore production, we need more data on variation in telial column length, diameter, and growth density. There appears to be a strong *Ribes* species component to all these factors, and an environmental component probably also contributes. Knowledge about these rust traits is important because column size and density influence rate of release of basidiospores which have a direct bearing on the number of basidiospores released per infection period. For example, if the same number of teliospores were "packaged" in many long, slender columns as opposed to a few long thick columns, the long slender columns would enjoy a considerable advantage in causing pine infections during short infection periods because of a higher basidiospore release rate. *Ribes lacustre* tends to produce long slender columns and also appears to cause more damage than would be expected on the basis of telial column density. Perhaps the rust on *R. lacustre* can make more efficient use of short infection periods. How many other subtle differences in the rust might exist both within and

between *Ribes* species? How much of this variation could be used to our advantage, and how much constitutes pitfalls that can hinder our efforts to develop a workable strategy of rust management?

Another area of teliospore biology that is in need of further research is germination and basidiospore production ratio. What conditions influence germination of teliospores and the number of basidiospores produced per teliospore germinated? This information is needed for incorporation into the model and may be of value in developing alternative control measures. Also a better understanding is needed to facilitate screening of pine populations for resistance by way of more efficient use of available inoculum. Many of the traits concerned with teliospore production and germination may be amenable to some sort of manipulation procedure, either genetic or environmental.

The basidiospore dispersion portion of this model was based more on simple assumptions than available knowledge about the movement of fungal spores in the air could lead to. But, specific empirical knowledge about *Cronartium ribicola* basidiospore dispersion was used to make the simplified assumptions. Since a more sophisticated approach would require a large additional effort, the simplified model should be tested before further work is done on basidiospore dispersal.

Despite many reports (Patton and Johnson 1967; Hansen 1972; Hansen and Patton 1977; Hirt 1942) the infection of pine by basidiospores is poorly understood. Results of artificial inoculations are extremely variable. According to the theoretical treatment by Van der Plank (1975), there should be a tight linear relationship between the amount of inoculum and the amount of disease. Regarding blister rust on western white pine, this relationship appears to be very loose (authors' unpublished results), as shown by the fact that the value defined as basidiospore infection yield ratio (BIY), which is the slope of the regression of infections on inoculum load, is highly variable.

Many factors can influence this ratio, and most have already been discussed. The primary research needs are: (1) to measure the influence of temperature and moisture on percentage of basidiospore germination, germination lag period, germination period, germ tube growth rate, and germ tube morphology; (2) to measure the influence of pine genotype and *Ribes* species on the above rust traits; and (3) to determine the role of needle surface waxes and electrical charges on spore trapping in different environmental conditions and on various host genotypes.

Another area needing attention is the transport of the spore to the near vicinity of the needle. What role does wind play? We have noticed considerable variation in basidiospore size. Does this variation of basidiospore size interact with atmospheric conditions to cause variations in amounts of disease in such a way that management options can reduce losses? Does basidiospore size variation relate in some way to racial variation of *C. ribicola*? How does needle orientation influence amounts of infection? What are the genetic and environmental components of the variation in needle orientation?

The relative susceptibility of secondary needles of different ages is a feature of the blister rust system that is of primary concern, because the literature reports that current-year needles are up to 14 times less susceptible than needles in their second or third year. If this is true, then a very appealing control option would be to defoliate trees to rid them of 2- and 3-year-old needles after a heavy infection season. Differential defoliation chemicals such as Ethephon (Griffing and Ursic 1977) need to be tested. Breeding western white pine for 2-year branch needle and 1-year stem needle retention is also possible. If one were to develop this idea, we believe the first task should be to investigate differential susceptibility more fully. Some knowledge about the effects of differential defoliation on growth is already available (Linzon 1958).

Available knowledge about the rate of appearance of cankers from needle infections and growth of cankers down branches is limited to the original white pine population. Natural selection by the rust over the past 40 years for increased resistance in the pine could have caused large changes in these relationships. So, current wild pine populations may behave differently than expected. These relationships should also be considered in artificial breeding programs. Currently, they are not. Delayed appearance of the rust in the stem could lead to greater losses of infections when needles are naturally shed. A factor that might work in opposition is that infected needles in the absence of needle-shed resistance may be selectively retained by the tree.

The portion of the simulator that partitions branch infections into harmless branch cankers and lethal branch cankers is based on limited data. This portion should be studied further if sensitivity analysis demonstrates that it is an important relationship. We need a better understanding of how natural inactivation, biological agents, resistance, and environment influence a canker's capacity to grow from the branch into the bole. These relationships have an important bearing on the management options one might select. Breeding for a rate of reduced rust growth or development of genetic and cultural means to increase tree growth rate could greatly influence amount of rust damage.

The key function in the stand infection submodel was derived from the regression of proportion infected on average number of trees infected. It appears that this is another highly sensitive relationship in the model. A much larger data base is needed for the regression of stand infection on average number of cankers per tree. Even though the curve illustrating this function is close to the theoretical curve given by Van der Plank (1975) for diseases in general and by Childs and Kimmey (1938) for random blister rust infection in a homogeneous stand, we still need to know how the environment, tree size, tree age, inoculum load, pine genotype, and pine species influence this function.

Knowledge about natural inactivation is very limited; also, a minimum amount of effort was expended on this portion of the simulation. There should be, however, a good deal more effective way to represent even the amount of information that is available. Since we do know that inactivation, both permanent and temporary, occurs (Hungerford 1977), sensitivity analysis should be used to determine the importance of canker inactivation before additional effort is expended on recasting the model or acquiring new knowledge. Management options ranging from breeding to utilization of biological control agents might apply here.

The representation of girdling of boles could use a more complete treatment of canker placement in the crown and a better calculation of period of growth down the branches to the stem. Again, due to lack of knowledge, a simplistic representation was developed to provide a place for this aspect of the disease. If additional modeling efforts are deemed necessary in the future, a more complete model can be substituted.

A very important piece of information that is related to many aspects of the whole model is growth rate of the fungus. We have made the assumption that growth rate of the fungus is independent of growth rate of the host. Since we have no information on the influence of site or other factors on fungus growth rate, the parameter (FER) is a user-controlled variable. Because of the potential importance of this variable, it should receive high priority in any future modification or use of this simulator.

The current form of the blister-rust simulator is an initial and most incomplete representation of the real system. But, it still provides a partial definition of the boundaries of the blister-rust system. Definition should lead to a clearer

concept of how a change (application of a management option) in one part of the system is connected to a change in another part. Such understanding can greatly facilitate our ability to formulate experiments, to gain knowledge about the system, and to develop management prescriptions that will reduce the impact of the rust on ecosystems containing white pines.

PUBLICATIONS CITED

Bailey, R. L., and T. R. Dell.
1973. Quantifying diameter distributions with the Weibull function. For. Sci. 19:97-104.

Bega, R. V.
1957. Effect of environment on sporidia in *Cronartium ribicola*. Ph.D. thesis. Univ. Calif., Davis. 91 p.

Bega, R. V.
1959. The capacity and period of maximum production of sporidia in *Cronartium ribicola*. Phytopathology 49:54-57.

Bega, R. V.
1960. The effect of environment on germination of sporidia in *Cronartium ribicola*. Phytopathology 50:61-69.

Bingham, R. T.
1972a. Artificial inoculation of large numbers of *Pinus monticola* seedlings with *Cronartium ribicola*, p. 357-372. *In* Biology of rust resistance in forest trees: proceedings of a NATO-IUFRO advanced study institute, August 17-24, 1969. U.S. Dep. Agric., Misc. Publ. 1221, 681 p.

Bingham, R. T.
1972b. Taxonomy, crossability, and relative blister rust resistance of five-needled white pine, p. 271-278. *In* Biology of rust resistance in forest trees: proceedings of a NATO-IUFRO advanced study institute, August 17-24, 1969. U.S. Dep. Agric., Misc. Publ. 1221, 681 p.

Bingham, R. T., R. J. Hoff, and G. I. McDonald.
1971. Disease resistance in forest trees. Annu. Rev. Phytopathol. 9:433-452.

Bingham, R. T., R. J. Hoff, and G. I. McDonald.
1973. Breeding blister rust resistant western white pine. VI. First results from field testing of resistant planting stock. USDA For. Serv. Res. Note INT-179, 12 p. Intermt. For. and Range Exp. Stn., Ogden, Utah.

Brickell, J. E.
1970. Equations and computer subroutines for estimating site quality of eight Rocky Mountain species. USDA For. Serv. Res. Pap. INT-75, 22 p. Intermt. For. and Range Exp. Stn., Ogden, Utah.

Buchanan, T. S.
1936. An alinement chart for estimating number of needles on western white pine reproduction. J. For. 34:588-593.

Buchanan, T. S.
1938. Blister rust damage to merchantable western white pine. J. For. 36:321-328.

Buchanan, T. S., and J. W. Kimmey.
1938. Initial tests of the distance of spread to and intensity of infection on *Pinus monticola* by *Cronartium ribicola* from *Ribes lacustre* and *R. viscosissimum*. J. Agric. Res. 56:9-30.

Chapman, H. H., and W. H. Meyer.
1949. Forest mensuration. 522 p. McGraw-Hill: New York, Toronto, London.

Childs, T. W., and J. L. Bedwell.
1948. Susceptibility of some white pine species to *Cronartium ribicola* in the Pacific Northwest. J. For. 46:595-599.

Childs, T. W., and J. W. Kimmey.
1938. Studies on probable damage by blister rust in some representative stands of young western white pine. J. Agric. Res. 57:557-568.

Clinton, C. P., and F. A. McCormick.
1919. Infection experiments of *Pinus strobus* with *Cronartium ribicola*. Conn. Agric. Exp. Stn. Bull. 214, p. 428-459.

Colley, R. H.
1918. Parasitism, morphology, and cytology of *Cronartium ribicola*. J. Agric. Res. 15:619-659.

Edmonds, R. L.
1972. Collection efficiency of rotorod samplers for sampling fungus spores in the atmosphere. Plant Dis. Rep. 56:704-708.
Gregory, P. H.
1952. Fungus spores. Trans. Br. Mycol. Soc. 35:1-18.
Griffing, C. G., and S. J. Ursic.
1977. Ethephon advances loblolly pine needle cast. For. Sci. 23:351-354.
Gustafson, J. D., and G. Innis.
1973. SIMCOMP 2.1 user's manual and maintenance document. U.S. IBP Grassl. Biome Tech. Rep. 217, 96 p. Colo. State Univ., Fort Collins.
Hahn, G. G.
1928. The inoculation of Pacific Northwest *Ribes* with *Cronartium ribicola* and *C. occidentale*. J. Agric. Res. 37:663-683.
Hahn, G. G.
1949. Further evidence that immune *Ribes* do not indicate physiologic races of *Cronartium ribicola* in North America. Plant Dis. Rep. 33:291-292.
Haig, I. T.
1932. Second-growth yield, stand, and volume tables for the western white pine type. U.S. Dep. Agric., Tech. Bull. 323, 68 p.
Hall, C. A. S., and J. W. Day, ed.
1977. Ecosystem modeling in theory and practice. 684 p. John Wiley and Sons, Inc., New York.
Hansen, E. M.
1972. Germination behavior and vesicle formation by *Cronartium ribicola* and the infection of *Pinus strobus*. Ph.D. thesis. Univ. Wisc., Madison. 118 p.
Hansen, E. M., and R. F. Patton.
1977. Factors important in artificial inoculation of *Pinus strobus* with *Cronartium ribicola*. Phytopathology 67:1108-1112.
Hirt, R. R.
1935. Observations on the production and germination of sporidia of *Cronartium ribicola*. State Univ. Coll. For., Syracuse Univ. Tech. Publ. 46, 25 p.
Hirt, R. R.
1942. The relation of certain meteorological factors to the infection of eastern white pine by the blister-rust fungus. State Univ. Coll. For., Syracuse Univ. Tech. Publ. 59, 65 p.
Hirt, R. R.
1964. *Cronartium ribicola*, its growth and reproduction in the tissues of eastern white pine. State Univ. Coll. For., Syracuse Univ. Tech. Publ. 86, 30 p.
Hoff, R. J., and G. I. McDonald.
1980. Resistance to *Cronartium ribicola* in *Pinus monticola*: reduced needle lesion frequency. Can. J. Bot. 58:574-577.
Hoff, R. J., G. I. McDonald, and R. T. Bingham.
1973. Resistance to *Cronartium ribicola* in *Pinus monticola*: structure and gain of resistance in the second generation. USDA For. Serv. Res. Note INT-178, 8 p. Intermt. For. and Range Exp. Stn., Ogden, Utah.
Hungerford, R. D.
1977. Natural inoculation of blister rust cankers on western white pine. For. Sci. 23:343-350.
Jowett, D., J. A. Browning, and B. L. Haning.
1974. Non-linear disease progress curves, p. 115-136. *In* Epidemic of plant disease: mathematical analysis and modeling. J. Kranz, ed. Springer-Verlag, New York.
Ketcham, D. E., C. A. Wellner, and S. S. Evans, Jr.
1968. Western white pine management programs realigned on northern Rocky Mountain national forests. J. For. 66:329-332.
Kimmey, J. W.
1945. The seasonal development and the defoliating effect of *Cronartium ribicola* on naturally infected *Ribes roezli* and *R. nevadense*. Phytopathology 35:406-416.

Kimmey, J. W.
1969. Inactivation of lethal-type blister rust cankers on western white pine. J. For. 67:296-299.
Kimmey, J. W., and W. W. Wagener.
1961. Spread of white pine blister rust from ribes to sugar pine in California and Oregon. U.S. Dep. Agric. Tech. Bull. 1251, 71 p.
Kranz, J.
1974. The role and scope of mathematical analysis and modeling in epidemiology. p. 7-54. *In* Epidemics of plant disease: mathematical analysis and modeling. J. Kranz, ed. Springer-Verlag, New York.
Lachmund, H. G.
1933. Resistance of the current season's shoots of *Pinus monticola* to infection by *Cronartium ribicola*. Phytopathology 23:917-922.
Lachmund, H. G.
1934. Seasonal development of Ribes in relation to spread of *Cronartium ribicola* in the Pacific Northwest. J. Agric. Res. 49:93-114.
Linzon, S. N.
1958. The effect of artificial defoliation of various ages of leaves upon white pine growth. For. Chron. 34:50-56.
Lloyd, M. G.
1961. The contribution of dew to the summer water budget of northern Idaho. Bull. Am. Meteorol. Soc. 42:572-580.
McDonald, G. I.
1978. Segregation of "red" and "yellow" needle lesions types among monoaeciospore lines of *Cronartium ribicola*. Can. J. Genet. Cytol. 20:313-324.
McDonald, G. I., and R. J. Hoff.
1970. Resistance to *Cronartium ribicola* in *Pinus monticola*: early shedding of infected needles. USDA For. Serv. Res. Note INT-124, 8 p. Intermt. For. and Range Exp. Stn., Ogden, Utah.
McDonald, G. I., and R. J. Hoff.
1971. Resistance to *Cronartium ribicola* in *Pinus monticola*: genetic control of needle-spots-only resistance factors. Can. J. For. Res. 1:197-202.
McDonald, G. I., and R. J. Hoff.
1975. Resistance to *Cronartium ribicola* in *Pinus monticola*: an analysis of needle-spot types and frequencies. Can. J. Bot. 53:2497-2505.
Marquardt, D. W.
1966. Least-squares estimation of nonlinear parameters. IBM Share Libr. Dist. No. 309401.
Mielke, J. L.
1943. White pine blister rust in western North America. Yale Univ., Sch. For. Bull. 52, 155 p.
Mielke, J. L., and J. W. Kimmey.
1935. Dates of production of the different spore stages of *Cronartium ribicola* in the Pacific Northwest. Phytopathology 25:1104-1108.
Mielke, J. L., T. W. Childs, and H. G. Lachmund.
1937. Susceptibility to *Cronartium ribicola* of the four principal *Ribes* species found within the commercial range of *Pinus monticola*. J. Agric. Res. 55:317-346.
Mitchell, R. G.
1974. Estimation of needle populations on young, open-grown Douglas-fir by regression and life table analysis. USDA For. Serv. Res. Pap. PNW-181, 14 p. Pac. Northwest For. and Range Exp. Stn., Portland, Oreg.
Nelson, R. R.
1973. Pathogen variation and host resistance, p. 40-48. *In* Breeding plants for disease resistance: concepts and applications. R. R. Nelson, ed. Penn. State Univ. Press, University Park and London.

Nelson, R. R., and D. R. MacKenzie.
1973. The detection and stability of disease resistance, p. 27-39. *In* Breeding plants for disease resistance: concepts and applications. R. R. Nelson, ed. Penn. State Univ. Press, University Park and London.
Paine, L. A.
1947. Evaluation of the role of weather in recurrent intensification of white pine blister rust in western white pine. M.S. thesis. Univ. Idaho, Moscow. 44 p.
Patton, R. F., and D. W. Johnson.
1967. Mode of penetration of needles of eastern white pine by *Cronartium ribicola*. Phytopathology 60:977-982.
Pierson, R. K., and T. S. Buchanan.
1938a. Age of susceptibility of *Ribes petiolare* leaves to infection by aeciospores and urediospores of *Cronartium ribicola*. Phytopathology 29:709-715.
Pierson, R. K., and T. S. Buchanan.
1938b. Susceptibility of needles of different ages on *Pinus monticola* seedlings of *Cronartium ribicola* infection. Phytopathology 28:833-839.
Reddingius, J.
1974. Models in biology: a comment. The Am. Nat. 108:393-394.
Roelfs, A. P., J. B. Rowell, and R. W. Romig.
1970. Sampler for monitoring cereal rust urediospores in rain. Phytopathology 60:187-188.
Rouse, D. I., and R. Baker.
1978. Modeling and quantitative analysis of biological control mechanisms. Phytopathology 68:1297-1302.
Rowell, J. B., and R. W. Romig.
1966. Detection of urediospores of wheat rusts in spring rains. Phytopathology 56:807-811.
Schrödter, H.
1960. Dispersal by air and water-the flight and landing, p. 169-227. *In* Plant pathology: an advanced treatise. Vol. III. The diseased population epidemics and control. J. G. Horsfall and A. E. Dimond, eds. Academic Press, New York and London.
Slipp, A. W.
1953. Survival probability and its application to damage survey in western white pine infected with blister rust. Univ. Idaho, For., Wildl., and Range Exp. Stn., Res. Note 7, 13 p. Moscow, Idaho.
Snell, W. H.
1920. Observations on the distance of spread of aeciospores and urediospores of *Cronartium ribicola*. Phytopathology 10:358-364.
Spaulding, P.
1922. Investigations of the white pine blister rust. U.S. Dep. Agric. Bull. 957.
Spaulding, P., and A. Rathbun-Gravatt.
1925a. Conditions antecedent to the infection of white pines by *Cronartium ribicola* in the northeastern United States. Phytopathology 15:573-583.
Spaulding, P., and A. Rathbun-Gravatt.
1925b. Longevity of the teliospores and accompanying urediospores of *Cronartium ribicola* Fischer in 1923. J. Agric. Res. 31:901-916.
Strand, M. A., and L. F. Roth.
1976. Simulation model for spread and intensification of western dwarf mistletoe in thinned stands of ponderosa pine saplings. Phytopathology 66:888-895.
Taylor, M. W.
1922. Potential sporidia production per unit in *Cronartium ribicola*. Phytopathology 12:298-300.

Van Arsdel, E. P., A. J. Riker, and R. F. Patton.
1956. The effects of temperature and moisture on the spread of white pine blister rust. Phytopathology 46:307-318.
Van der Plank, J. E.
1975. Principles of plant infection. 216 p. Academic Press: New York and London.
Waggoner, P. E.
1974. Simulation of epidemics, p. 137-160. *In* Epidemics of plant disease: mathematical analysis and modeling. J. Kranz, ed. Springer-Verlag, New York.
Waggoner, P. E., and J. G. Horsfall.
1969. EPIDEM: a simulation of plant disease written for a computer. Conn. Agric. Exp. Stn. Bull. 698.
Wellner, C. A.
1946. Recent trends in silvicultural practice on National Forests in the western white pine type. J. For. 44:942-944.
Wellner, C. A.
1948. Light intensity related to stand density in mature stands of the western white pine type. J. For. 46:16-19.
Zadoks, J. C.
1971. Systems analysis and the dynamics of epidemics. Phytopathology 61:600-610.
Zadoks, J. C.
1972. Methodology of epidemiological research. Annu. Rev. Phytopathol. 10:253-276.

APPENDIXES

APPENDIX I

Quantitative Models

The derivation of relationships among state variables will be detailed in this section. Forcing functions, donor-controlled or donor-recipient controlled interactions, are developed for each flow within a given submodel. Each flow will be discussed under a subheading composed of the flow name. In referring to the box-and-arrow diagrams, remember that the dotted lines show where various functions apply when it is possible to have one derivation apply to the relationship between more than one set of state variables. Only the flow equations and their derivation are discussed in this section.

RIBES DENSITY SUBMODEL

Ribes Generation

The principal derivation in this submodel was the *Ribes* density function for each of the four major *Ribes* species; but before we begin that derivation we must look at the computaton of Proportion Full Sun (PFS), which depends on tree height and density. Tree height is computed by function HEIGHT from site and age data as discussed in appendix II. Stocking density and tree height are used to model stand basal area in square meters per hectare. Basal area was defined as the total cross sectional area of stems 1 inch and larger at breast height per unit of land area, where

$$\text{Cross sectional area} = \pi d.b.h.^2/4,$$
$$= 0.786\ d.b.h.^2.$$

We assumed that the height calculated by function height is the average height for all trees in the stand being simulated (Current Tree Height [CTH]), and that the d.b.h. of a tree of height CTH is the average d.b.h. for the stand. D.b.h. as a function of tree height was obtained from a regression of total tree height on d.b.h. (Deitschman, Glenn H., unpublished, this Station):

$$\text{D.b.h. in meters} = \frac{CTH - 1.14}{75.59}.$$

Current Basal Area per hectare (CBA) is estimated by multiplying stems per hectare by the average cross sectional area as follows:

$$CBA = TLT \cdot 0.786\ ([CTH-1.14]/75.59)^2$$

where

TLT = Total number of Living Trees per hectare (computed variable).

An empirical function that relates PFS (Proportion Full Sunlight) to basal area (Wellner 1948) was used as follows:

$$\text{Light intensity (PFS)} = e^{-(0.02 \cdot CBA)}.$$

The blister rust eradication program accumulated extensive records on the numbers and species of *Ribes* plants removed during the first working. These records are summarized in table 17 for the Kootenai, Cabinet, Clearwater, St. Joe, Coeur d'Alene, and Kaniksu National Forests of northern Idaho and western Montana (Swanson[5]). The data were recorded by stand type (open reproduction, dense reproduction, open pole, dense pole, open mature, dense mature, and burn), without definitions. In order to associate a light level with *Ribes* density, a few assumptions were made using white pine stand tables (Haig 1932). We assumed reproduction to be under 20 years old, pole-sized material to average 50 years of age, and mature trees to average 140 years of age. Open reproduction was assumed to be stocked at 200 trees per acre, open pole, 100 trees per acre, and open mature, 25 trees per acre. Armed with these assumptions, we calculated the levels of light intensity for each type of stand (table 17). This method assumed a constant relationship between shading and basal area, which we know is not strictly true, but presently we have no better information.

Table 17.--*Number of* Ribes *bushes eradicated per hectare during the years 1929 to 1937 in northern Idaho National Forests*

Stand type	Proportion full sun[1]	*R. lacustre*	*R. viscosissimum*	*R. petiolare*	*R. inerme*
Open reproduction	0.99	217	613	1.0	6.3
Dense reproduction	.82	77	69	.4	3.0
Open pole	.96	103	93	.6	3.4
Dense pole	.43	52	31	.05	1.3
Open mature	.91	160	82	.9	1.4
Dense mature	.22	29	8	.05	1.6
Burn	1.00	169	670	2.2	4.6

[1]Relative amount of sunlight reaching the forest floor. See text for method of determination.

[5] Swanson, H. E. 1937. *Ribes* eradication, Inland Empire, 1937. p. 23-25. *In* 1937 annual report Spokane office blister rust control. (Mimeographed) U.S. Dep. Agric., Bur. Plant. Quar.

Finally, we fit a power function to the data in table 17 to derive the relationship giving bushes per hectare as a function of proportion of full sunlight (fig. 27, 28, 29, and 30). Each species follows the same general trend, but the specific curve for each is different. The general function (*Ribes* density function) that seems to best fit the available data is:

$$RD_i = a_{2i} + a_{2i}\ PFS^{a_{2i}}$$

where

(a_{0i}, a_{1i}, a_{2i} = estimated parameters;

for

R. hudsonianum i = 1, $a_{01} = 0.05$, $a_{11} = 2.15$, $a_{21} = 16.58$,

R. inerme i = 2, $a_{02} = 1.45$, $a_{12} = 4.35$, $a_{22} = 11.84$,

R. lacustre i = 3, $a_{03} = 40.0$, $a_{13} = 190.0$, $a_{23} = 10.96$,

R. viscosissimum i = 4, $a_{04} = 40.0$, $a_{14} = 660.0$, $a_{24} = 27.03$.

These relationships are illustrated in figures 27, 28, 29, and 30. If a *Ribes* eradication program had been applied in the case of *Ribes viscosissimum* the input variable would be $ERAD_4$ (eradication level of *R. viscosissimum* in bushes per hectare) instead of being computed by the density function. This value is less than 0 when no eradication program is underway, 0 when this species is absent, and some value greater than 0.0 that is equal to the number of bushes per hectare left after the eradication has been performed. If eradication was not practiced or the bush density was not set, then the empirical function just derived that relates *Ribes* density to Proportion of Full Sunlight (PFS) comes into play. The ribes density submodel and the various management options are summarized in equation 1:

$$J_{(5\rightarrow 1,\ 2,\ 3,\ \text{or}\ 4)} = \begin{cases} a_{0i} + a_{1i}PFS^{a_{2i}} & ;\ \text{for } ERAD_i < 0 \\ 0 & ;\ \text{for } ERAD_i = 0 \\ ERAD_i & ;\ \text{for } ERAD_i > 0. \end{cases} = RD_i \qquad (1)$$

RIBES INFECTION SUBMODEL

Aeciospore Infection

Aeciospore generation.--The derivation of this flow equation is simple. The assumed or measured value of Aeciospore Maximum Hourly Load (AMHL) is multiplied by the duration of the infection period (DIP) in hours to give the potential spore load in aeciospores per square centimeter for the designated infection period. Thus:

$$J_{(75\rightarrow 76)} = AMHL\ DIP_i$$

$$= PASL_i$$

where

PASL = Potential Aecispore Load

i = index to *Ribes* species.

Aeciospore availability.--We felt that a normal curve best fitted the pattern of occurrence of aeciospores over time (fig. 6), and that the Weibull function (Bailey and Dell 1973) adequately described this distribution:

$$y = e(c/b)((x-a)/b)^{c-1} \cdot e^{-((x-a)/b)^{c}} \qquad (2)$$

where

a,b,c = variable parameters
e = base natural log
x = known parameter
y = unknown parameter.

In order to use the above approach, we needed to develop some way to determine date of appearance of aeciospores. In the spring of 1976, we collected aeciospores in our nursery beds located at Moscow, Idaho; in a natural stand near Clarkia, Idaho; and in a natural stand at the Priest River Experimental Forest. Blisters appeared in early April at Moscow and in early May at Clarkia and Priest River. These times of appearance were matched with the summation of average daily temperature (maximum and minimum averaged). In each case, blisters appeared when the average temperature summed to 80°C degree days in no more than 10 days after a 24-hour average of less than 4°C. These criteria can be used to establish an expected appearance date from published weather records. Our experience indicated that about 7 days after appearance, the first blisters break. Hence, Date of first Aeciospore aPpearance (DAP) will be recorded as date of blister appearance + 7 days and will be expressed as days after April 1 (also see Hirt 1964, p. 14). The aeciospore availability function (fig. 6) is used to compute proportion of the peak spore load that is available on a specified date.

The number of AecioSpores Trapped per square centimeter during a given infection period (AST) is calculated as a function of days after appearance of the aeciospores as shown in figure 6, using the parameters listed in fig. 6 and equation (2):

$$J_{(76,77)} = W(A1^{2.6}) \cdot e^{(-A1^{3.6})} \cdot PASL$$
$$= AST_i$$

where

A1 = DAYINF/22.0,
W = 1.954
= c/b from equation 2 times a constant to scale function to maximum value of 1; this parameter will also be used in other versions of the Weibull function,

DAYINF = DAA1 - DAP.

Aeciospore germination.--The first problem was to model germination of the available aeciospores as a function of temperature and assumed rust genotype. Rust genetics is introduced by assuming that optimum germination temperature is strongly inherited (fig. 8) and is controlled by input variable AGMAX as shown below:

$$PAGER = 10.295\ (WCA/WBA) \cdot A2 \cdot (WCA-1.0)\ e^{-(A2)^{WCA}}$$

where

PAGER = Proportion of available Aeciospores on the underside of *Ribes* leaves that are expected to GERminate, given an infection period of unlimited duration and a given average temperature (TIP),

WCA and WBA = parameters that control position of the peak (the genetic response from the rust),

A2 = (TIP - 3.)/WBA,

TIP = average temperature of the infection period.

WCA and WBA are parameters that control the shape of the Weibull function. We derived equations that give parameters WCA and WBA as a function of population mode:

$$WBA = 7.095 + 0.19242*GMA + 0.025314*GMA^2$$

and

$$WCA = 0.857046 + 0.172618*GMA + 0.002759*GMA^2$$

where

GMA = Mode
= AGMAX-3.

The constant, 3, is subtracted from AGMAX to adjust the mode as given by the Weibull function to the x-axis. As illustrated in figure 8, optimum germination temperature of rust aeciospores can be varied.

Next a model of germination as a function of infection period duration was developed. Ultimately rust genetic variation could be incorporated here, too, but at present it is not. Proportion of GERMinated Aeciospores (GERMA) is assumed to be controlled by both temperature and duration of the infection period (DIP). According to our data, the GERmination Lag period of Aeciospores (GERLA) varies with temperature as shown in figure 9. A parabola provides a good empirical first approximation of this relationship. GERmination Period of Aeciospores (GERPA), that is the time required to complete germination once it has started, also varies with temperature (fig. 10), and appears to fit the parabolic function:

$$GERLA = 0.04*(TIP^2) - 1.67*TIP + 19.43 \quad (3)$$
$$GERPA = 0.1*(TIP^2) - 3.57*TIP + 35.86 \quad (4)$$

where

TIP = average temperature of infection period in degrees C,

GERLA = time required for germination to begin in hours,

GERPA = time required to complete germination after it has begun in hours.

We can model expected germination as a function of DIP, if we assume that any given population will germinate according to the standard normal distribution with a range equal to GERPA encompassing ± 3 S.D. and a mean of GERPA/2.0. Then proportion germinated of the population will be a function of duration and temperature of the infection period:

$$GERMA = CNORMP(A,B,C)*PAGER$$

where

GERMA = proportion germinated,

CNORMP = normal distribution function obtainable on most computers,

A = DIP - GERLA,

B = GERPA/6.0,

C = GERPA/2.0.

The flow is computed by multiplying the number of aeciospores trapped (AST) by the proportion expected to germinate (GERMA):

$$J_{(77,78)} = AST_i * GERMA$$
$$= ASGER_i$$

Aeciospore germ tube growth.--If the length of the germ tube is a function of GERm Tube growth RAte (GERTRA) and duration of germ tube growth (DIP-GERLA), then GERm Tube Length of Aeciospores (GERTLA) becomes:

$$GERTLA = GERTRA \cdot (DIP-GERLA). \quad (5)$$

Since length of tubes should be distributed normally, the function CNORMP was used to compute proportion of GERminated Aeciospores with germ tube of proper length to Penetrate (PGERAP):

PGERAP = CNORMP(GERTLA, 33.3, 200.0),

where

GERTLA = average length attained by germ tube when infection period ends,

33.3 = microns per standard deviation for the range 100μ to 300μ,

200.0 = average of the distribution.

Then number of AecioSpores germ Tubes of Adequate Length (ASTAL) is computed by:

$$J_{(78,79)} = PGERAP * ASGER_i$$
$$= ASTAL_i$$

Aeciospore infection establishment.--The average aeciospore infection yield ratio for *R. hudsonianum* ($AIYR_i$) used in the model is the average of the experimentally determined values (table 7) already discussed:

$$AIYR_i = 0.05$$

where

i = *R. hudsonianum* index = 1,

0.05 = constant obtained by dividing 11 infections per square centimeter by 230 spores/cm^2.

This means that we should expect one aeciospore out of every 20 germinated aeciospores on the leaf surface of *R. hudsonianum* to penetrate and establish an infection. Many factors such as leaf age, moisture and temperature conditions, rust genotype, *Ribes* genotype, and *Ribes* species should influence this value. Consequently, much more study should be devoted to the determination and use of this infection yield ratio. Using the *R. hudsonianum* ratio we obtained and the information in

table 6, we computed the following values: for *R. inerme*, ($AIYR_2$ = 0.037); for *R. lacustre*, ($AIYR_3$ = 0.018); and for *R. viscosissimum*, ($AIYR_4$ = 0.012). The number of AecioSpore Infections (ASI) derived per square centimeter of leaf surface on *R. hudsonianum* is:

$$J_{(79,80)} = ASTAL_i \cdot AIYR_i$$
$$= ASI_i.$$

Urediospore Infection

Urediospores from aeciospores and urediospores.--The simulation of the number of urediospores produced by each aeciospore infection of a given cohort that will be available for causing new infections during a given infection period is determined by:

$$UMASS_i = ASI_i \cdot BMASS_i \cdot (1.0-TSAR_i)$$

where

ASI_i = number of aeciospore infections per square centimeter of leaf underside surface of a given species (i=1 to 4) established in each infection period from 12 to 60 days previous to the current period,

$BMASS_i$ = production capability of the rust on a given *Ribes* species in cubic microns (for *R. hudsonianum*, $70x10^6\mu^3$),

$TSAR_i$ = proportion of $BMASS_i$ to be devoted to teliospores,

$UMASS_i$ = total mass of urediospores present in current infection period.

Then the calculation of UredioSPORe production from aecial infection on a given *Ribes* species ($USPOR_i$) is:

$$J_{(80,81)} = UMASS_i/(\pi \cdot USL \cdot USD^2) + BMASS_i \cdot (1-TSUR_i)$$
$$= USPOR_i$$

where

π = 3.141,

USL = UredioSpore Length in microns,

USD = UredioSpore Diameter in microns,

$BMASS_i$ = spore production capability of given infection,

$TSUR_i$ = proportion of $BMASS_i$ produced by uredial infection that is devoted to teliospore production,

and

$BMASS_i \cdot (1-TSUR_i)$ = movement of $USPOR_i$ from X(85) and represents urediospores produced by uredial infections (see $J_{(85,87)}$).

Urediospore viability.--This flow is based on equation 2 and the parameters given in figure 7 for urediospore viability (UV); so that:

$$UV = 2.477(A4)^{1.5}e^{-(A4)^{2.5}}$$

where

A4 = (DAYS-12.0)/20.0,

DAYS = DAA1(M) - DAA1(L),

and

$DAA1_M$ = current infection period date in days after April 1,

$DAA1_L$ = last infection period date in days after April 1.

Also, this flow must be programed so that all cohorts of urediospores are computed separately, because each cohort will have a different UV. But all viable urediospores will contribute to the next round of infection (see fig. 5). In simplified form:

$$J_{(81,82)} = UV \cdot USPOR_i = VUSA_i. \quad (6)$$

Urediospore germination.--This flow is calculated by multiplying state variable 82 by proportion of viable spores expected to germinate during a given infection period. The computation begins:

$$PUSGER = 9.577\ (WCU/WBU)A5^{(WCU-1.0)}e^{-(A5)^{WCU}}$$

where

PUSGER = Proportion of viable UredioSpores produced by one cohort of aecial or uredial infections per square centimeter that will GERminate in a given infection period of unlimited length and temperature of TIP.

WCU and WBU = curve shape parameters set by UGMAX (a user controlled variable from table 3) using same equations as for WCA and WBA, except GMU = UGMAX-7,

A5 = (TIP-7.0)/WBU.

The remainder of this flow is calculated as in flow (77→78). But the constants of the equation for urediospore germination lag (GERLU) change (fig. 12):

$$GERLU = 0.03(TIP)^2 - 1.19(TIP) + 12.8 \quad (7)$$

The constants of the equation for urediospore germination period (GERPU) remain the same as for GERPA (equation 4). Thus:

GERMU = CNORMP(A,B,C)•PUSGER,

A = DIP - GERLU,

B = GERPA/6.0,

C = GERPA/2.0.

Finally:

$$J_{(82,83)} = VUSA_i \cdot GERMU$$
$$= USGER_i .$$

Urediospore germ tube growth.--The equations are the same as flow (78→79) except that some constants change. The GERm Tube Growth Rate (GERTRU) equation for urediospores (fig. 13) is:

$$GERTRU = 136.23(A3)^{2.5} e^{-(A3)^{3.5}} \quad (8)$$

The GERm Tube Length attained by Urediospore germ tubes (GERTLU) is the product of growth rate (GERTRU) times growth period (DIP-GERLU):

$$GERTLU = GERTRU*(DIP-GERLU) \quad .$$

Then Proportion of GERminated Urediospores with germ tubes of proper length to Penetrate (PGERUP) is:

$$PGERUP = CNORMP(GERTRU, 33.3, 200.0)$$

and number of UredioSpores with germ Tubes of Adequate Length ($USTAL_i$) is:

$$J_{(83,84)} = PGERAP \cdot USGER_i$$
$$= USTAL_i .$$

Urediospore infection--We have assumed that the Urediospore Infection Yield Ratio, $UIYR_i$, will have a range of values different from $AIYR_i$; although we have no observations. The number of infections expected from any one cohort of aecial infections will be provided by:

$$J_{(84,85)} = USTAL_i \cdot UIYR_i$$
$$= USI_i .$$

Urediospores infection from urediospores.--Since infections caused by all cohorts of aecial infections must be accounted for, the calculations from X(81) to X(85) must be repeated for all viable aecial cohorts (see fig. 5). Then, since the urediospores arising from urediospore infections are assumed to be identical to urediospores arising from aeciospore-caused infections, all the calculations from X(81) to X(85) must be repeated again. Since the different uredial cohorts will be of different ages, and urediospore viability is assumed to be a function of cohort age (fig. 7), each repeat will have a different urediospore viability value (UV in equation 6). The same is true for the aeciospore-derived-infection repeats of the last flow. All these infections are accumulated in state variable X(85), UredioSpore Infections (USI). Also, each repeat of urediospore-derived infection can have a new partitioning of the spore biomass. The variable TSUR is used as follows:

$$J_{(85,81)} = BMASS_i \cdot (1-TSUR_i)$$
$$= USPOR_i \quad .$$

Teliospore Production

Teliospore generation.--These flows are computed by calculating the sum of the teliospore biomass produced for a given cohort and then dividing by the expected size of a teliospore to yield the number of teliospores Thus:

$$J_{(80,86)} = \frac{TSAR_i \cdot ASI_i \cdot BMASS_i}{\pi \cdot TSL \cdot TSD^2}$$

$$J_{(85,86)} = \frac{TSUR_i \cdot USI_i \cdot BMASS_i}{\pi \cdot TSL \cdot TSD^2}$$

$$TMAX_i = J_{(80,85)} + J_{(85,86)}$$

where

$\pi = 3.141$,

TSL = teliospore length in microns,

TSD = teliospore diameter in microns.

Teliospore viability.--The proportion of available teliospores in any given infection period TMAX is multiplied by the teliospore viability function to give the number of Potential GERminated Teliosores (PGERT):

$$J_{(86,87)} = TMAX_i \cdot 2.416 \cdot A9^{1.25} e^{-(A9)^{2.25}}$$
$$= PGERT_i$$

where

$A9 = (DAYS-16)/27.5$.

Teliospore germination.--Number of Teliospores expected to GERminate (TGER) is calculated by:

$$J_{(87,88)} = PGERT_i \cdot PCAST \qquad \text{(see fig. 7)}$$
$$= TGER_i$$

where PCAST = proportion of viable teliospores that germinate in a given infection period (see appendix III for derivation).

Basidiospore generation.--Thus, the Quantity of Basidiospores produced At *Ribes* Bushes ($QBAB_i$) is computed:

$$J_{(88,89;\ 88,90;\ 88,91;\ 88,92)} = TGER_i \cdot BSYR_i = QBAB_i$$
$$= QBAB_i$$

where

i = 1 to 4 to index the four major *Ribes* species.

Basidiospore distribution.--The basidiospores produced by the rust on the *Ribes* plants are windborne to the pine hosts. As is characteristic of all wind-disseminated pathogens, the number of spores reaching a given target is primarily dependent on the distance from the target to the spore source (Schrödter 1960). Many other factors can influence the spore load-distance relationship like number of spores released, size and shape of spores, horizontal wind velocity, turbulence, and the density of point sources over a given area. We are not in a position to consider any atmospheric influences in this paper; so we are limited to spore number, source density, and physical spore characteristics. A theoretical treatment of the interaction of spore traits and flight pattern is also beyond the scope of this paper; however, these problems can be simplified through empirical use of Buchanan and Kimmey's (1938) plot of number of cankers per unit of needles exposed as a function of distance from a point source of basidiospores.

Their empirical relationship was used to develop the distribution function. Since we use the concept of infection on an average tree, the number of basidiospores deposited on the average tree should be a function of dilution due to distance from spore source to tree in a given area. The criteria imposed for calculation of the average distance were regular spacing of the pine host and of the point basidiospore sources (*Ribes* bushes). This restriction would not be necessary if data were available on the relative spatial relationships of both hosts. The average distance was graphically determined (fig. 31) for a set of different stocking densities of pine and point *Ribes* sources and was found to be largely independent of pine stocking at the densities tested and to be very dependent on point source stocking density (table 18). Thus, average tree to point source distance was determined for a range of *Ribes* stockings from 5.9 bushes/ha to 2,500 bushes/ha and a pine stocking of 2,500/ha. A plot of number of *Ribes* growing points per hectare yielded a curvilinear relationship (fig. 32). Growing points per hectare were used in place of bushes because *Ribes* bushes tend to grow in clusters and the concept of points gives more modeling flexibility as will be seen later. The average *Ribes* to tree distance was expressed as follows:

$$ABTD = e^{-(.503 \cdot \ln(RGP) + 3.65)} \qquad (9)$$

where

ABTD = average distance in meters,

e = base of natural logarithm,

ln(RGP) = natural log of the number of *Ribes* Growing Points per hectare,
= RD_i.

Table 18.--*Sample of graphically determined average distance from pine tree to* Ribes *growth point for four combinations of stocking*

Pine trees/ hectare	*Ribes* bushes/ hectare	Average tree to bush distance
Number	*Number*	*Meters*
2,500	39	6.08
2,500	6.25	15.29
1,111	44	6.25
1,111	5.90	15.51

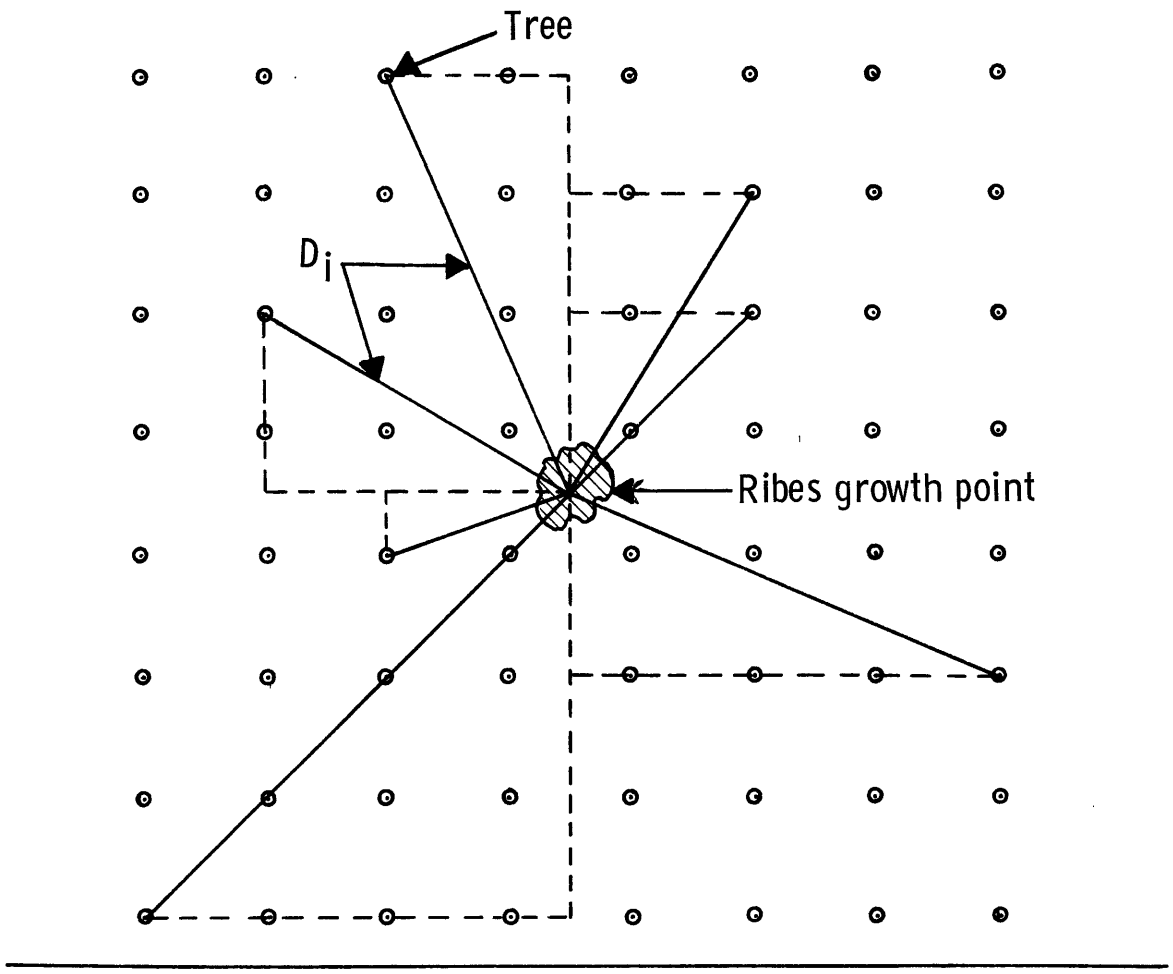

Figure 31.--Illustration of method used to calculate average spore source to target distance.

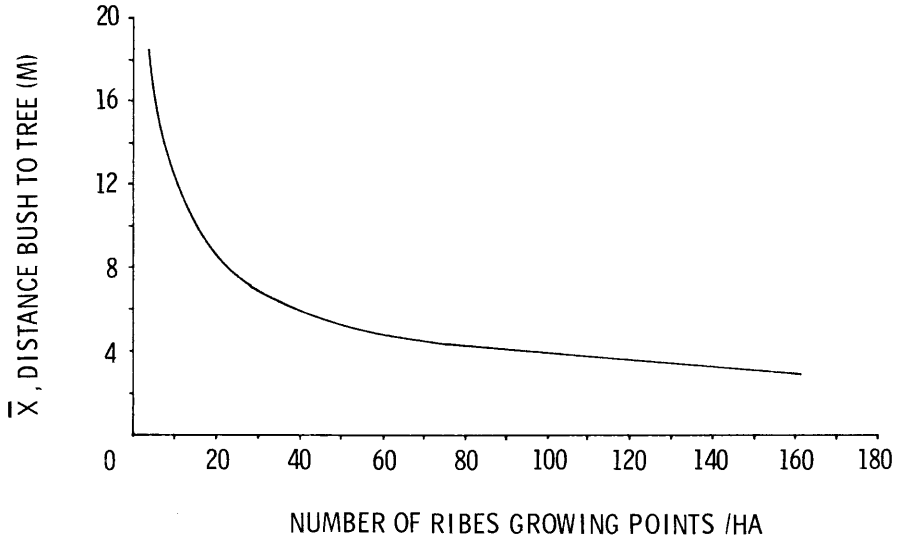

Figure 32.--Plot of average distance from pine trees to ribes growing points per hectare. Average distances determined graphically as explained in the text.

If the average distance from the target and the number of spores produced by the point source are known, how can this information be transformed into an expected spore load?

If one assumed that the ratio of cankers formed to spores trapped is independent of distance from spore source, then calculation of the percentage of total infections in each ring of Buchanan and Kimmey's (1938) experiment should reflect the percentage distribution of basidiospores in the rings. Such a calculation was made (fig. 33) and the resulting relationship was used to estimate basidiospore load as a function of average distance on the basis of concentric rings 3 m wide (fig. 34). In order to convert to absolute values, one must calculate the area within each ring. This area is found to be as follows:

$$A_n = A_1^2(2n-1)$$

where

A_n = area in the nth ring,

A_1 = area in the center ring,

n = number of the nth ring.

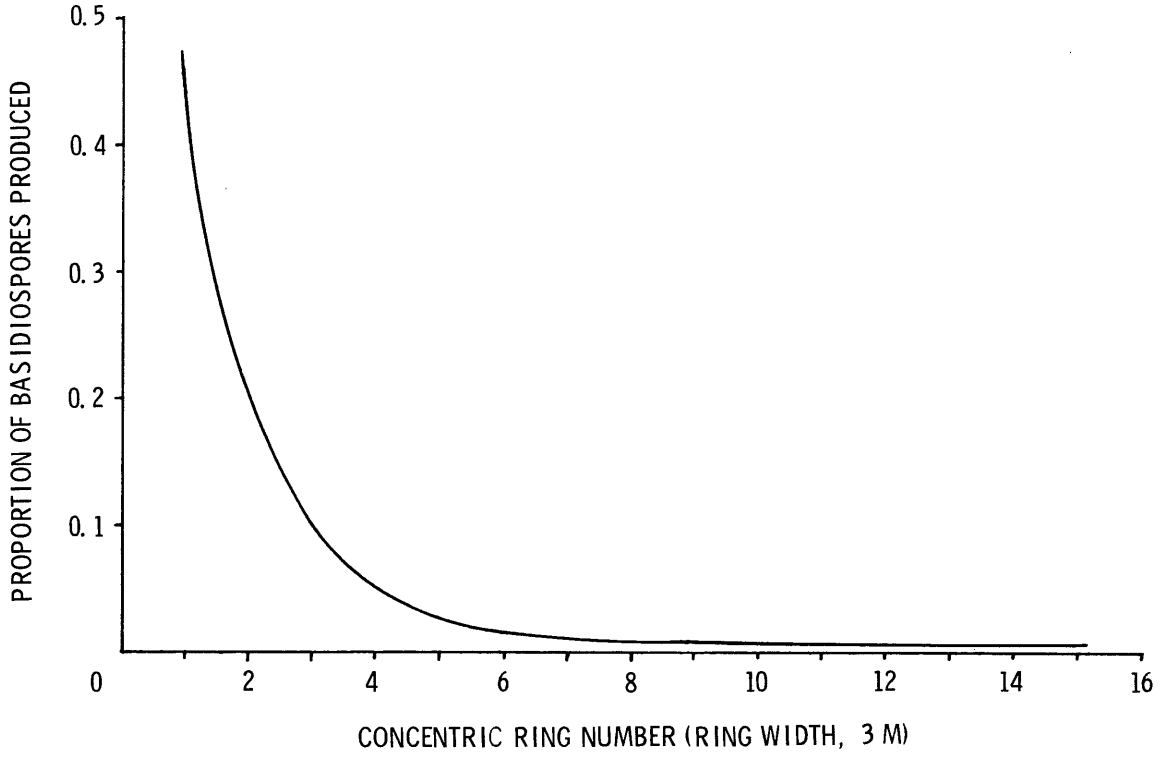

Figure 33.--Distribution of *Cronartium ribicola* basidiospore load from a point source into concentric rings 3 meters wide. Calculation based on count of cankers on *Pinus monticola* located in concentric rings around a point source (Buchanan and Kimmey 1938).

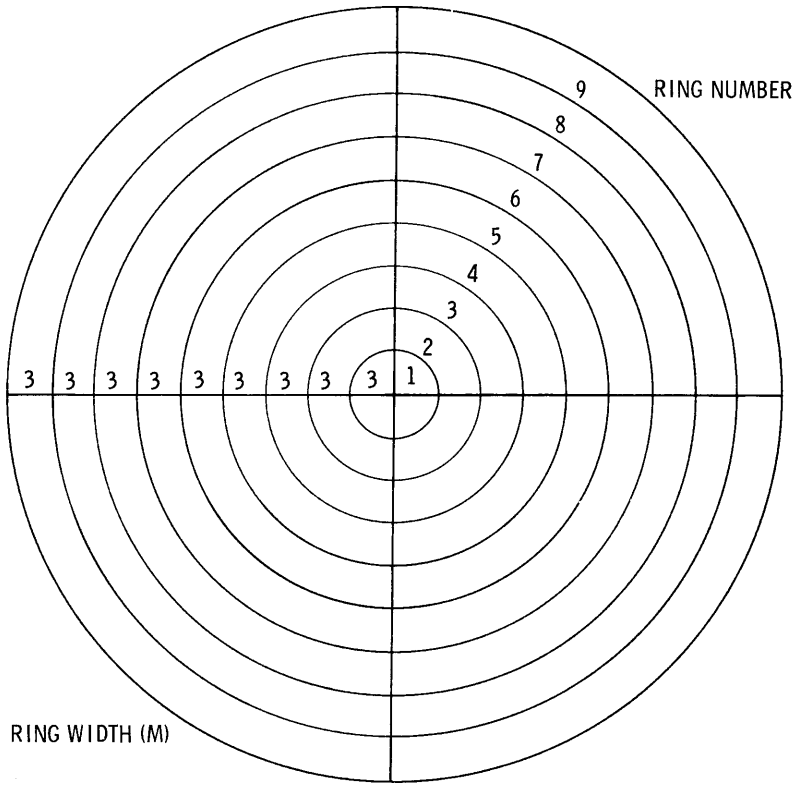

Figure 34.--Illustration of concentric rings used to calculate simulated *Cronartium ribicola* basidiospore loads on basis of average bush to tree distance and ring area.

We have simulated the quantity of basidiospores produced, calculated the area in a ring, determined the percent of the spores to be expected in a given ring, and can identify the ring by the average point source to tree distance. So, the basidiospore load expected from that point source can be computed. But, the background basidiospore load from other point sources in the vicinity must be considered. It has been estimated that 99.9 percent of the spores from a point source near the ground would land within 100 m of the source (Gregory 1952). This seems to be true for *C. ribicola* as indicated by Buchanan and Kimmey (1938) and Kimmey and Wagener (1961), if we assume that infections reflect basidiospore load. Thus, we calculated background as follows: The percentage of the basidiospores expected to fall within the boundary defined by the *n*th ring was subtracted from 1 to give the percentage of basidiospores beyond the average distance from source to tree. Background basidiospore load was a function of basidiospore load, average tree to source distance (ring number), and density of growing points. Basidiospore load expressed as Quantity of Basidiospores At Trees (QBAT) was calculated for the four *Ribes* species as follows:

$$F_{(89,93),(90,93),(91,93),(92,93)} =$$

$$\left(\frac{QBAB_i \cdot PBIRX}{282,743.34(2RX-1)} + \frac{QBAB_i \cdot GPF_i \cdot (1-PCT)}{100,000,000}\right) \cdot TARGET_i \cdot RD_i$$

$$= QBAT_i$$

where

$QBAT_i$ = basidiospore load resulting from *Ribes* sp. at average tree in spores per square centimeters,

$QBAB_i$ = Quantity of Basidiospores expected per square centimeter of leaf surface At *Ribes* sp. Bushes,

PBIRX = Proportion of $QBAB_i$ Basidiospores expected In Ring *X*,

$$= e^{-0.8RX} + 0.007, \quad (10)$$

RX = number of ring *x*,

282,743.34 = area in the center ring in square centimeters,

GPF_i = number of *Ribes* sp. growth points per hectare,

RD_i = bushes of *Ribes* sp. per hectare (from *Ribes* density submodel),

PCT = accumulated proportion of basidiospores expected in rings 1 through *x*,

$TARGET_i$ = *Ribes* sp. target = square centimeters leaf area (one side) per bush (from table 5),

100,000,000 = square centimeters in 1 hectare.

$$J_{(89,93)} = QBAT_1,$$

$$J_{(90,93)} = QBAT_2,$$

$$J_{(91,93)} = QBAT_3,$$

$$J_{(92,93)} = QBAT_4.$$

Then:

$$QBSAT = J_{(89,93)} + J_{(90,93)} + J_{(91,93)} + J_{(92,93)}$$

$$= \sum_{i=1}^{4} QBAT_i$$

PINE TARGET SUBMODEL

Branch Target

Branch needle generation.--An empirical function was derived that relates number of new needles to tree height (fig. 35). A bit of discussion of the derivation of this relationship is in order. The first step consisted of determining the total number of needles in crowns on trees of varying height. Buchanan (1936) measured the crown height and width and estimated the number of needles on 6,809 western white pines ranging in height from 0.03 to 9 m. He then developed an empirical formula that gives the number of needles as a function of crown height and width:

$$\text{Number of needles} = 17{,}680 \cdot \text{crown length} \cdot (2 \cdot \text{crown radius})^{1.16}$$

where

Crown length and radius are in meters.

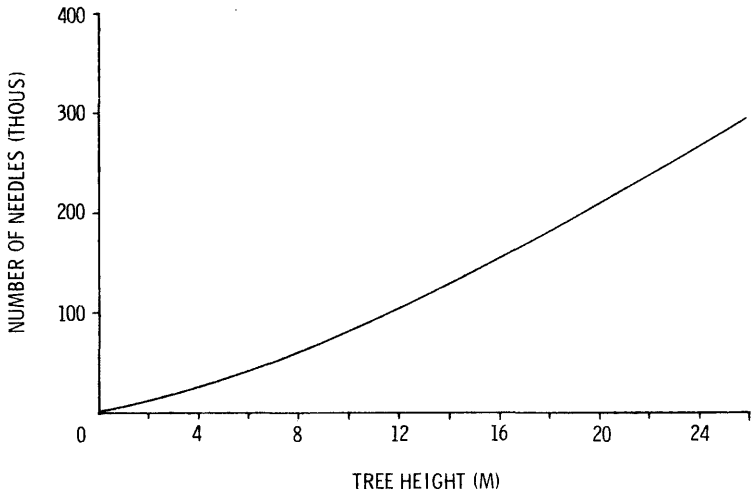

Figure 35.--Number of new *Pinus monticola* needles as a function of total height plotted from new needle column of table 19.

This formula was coupled with Buchanan's (1938) published crown width and length values for a group of trees ranging from 1.5 to 48 m in height to develop a curve of number of needles as a function of tree height. Since adequate data to form the lower end of the curve were not available, we collected, dissected, and counted the number of needles on 28 trees ranging from 0.1 to 2.71 m in height. The completed curve is shown in figure 36. This curve and the needle counts were used to develop a life table for number of needles as a function of tree height (table 19). The number of needles from the first year column was then plotted (fig. 35) to produce the curve of number of new needles as a function of tree height.

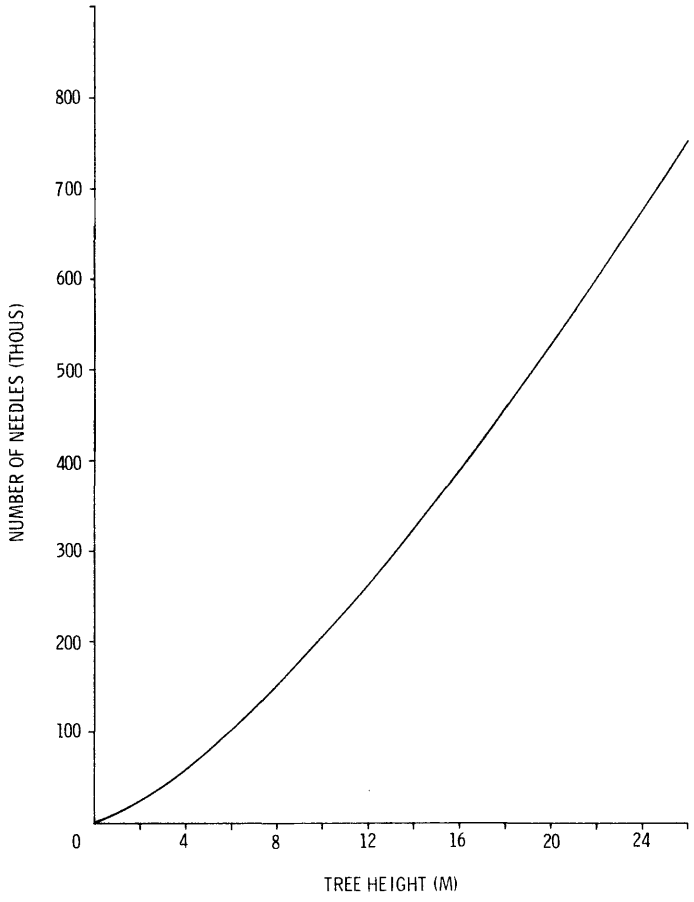

Figure 36.--Total number of branch needles in crown of *Pinus monticola* as a function of total height (calculated from Buchanan, 1936 and 1938).

Table 19.--*Life table of branch needle populations on a western white pine modeled after Buchanan's empirical formula and crown size data*

Tree age	Tree height[1]	Total branch needles[2]	New needles[3]	1-year-old needles[4]	2-year-old needles[5]
Years	*Meters*			*Number*	
2	0.2	85	60	25	0
3	.26	321	245	60	16
4	.38	1,024	740	245	39
5	.59	2,592	1,695	740	157
6	.99	5,252	3,085	1,695	475
7	1.20	8,628	4,455	3,085	1,088
8	1.50	15,175	8,739	4,455	1,981
9	2.00	22,473	10,874	8,739	2,860
10	2.50	30,476	13,992	10,874	5,610
11	3.00	39,087	18,114	13,992	6,981
12	3.40	46,370	19,273	18,114	8,983
13	3.90	55,920	25,018	19,273	11,629
14	4.30	63,892	26,501	25,018	12,373
15	4.80	74,244	31,681	26,501	16,062
16	5.30	84,997	36,302	31,681	17,014
17	5.90	98,396	41,755	36,302	20,339
18	6.40	109,951	44,890	41,755	23,306
19	7.00	124,258	52,561	44,890	26,807
20	7.60	139,020	57,640	52,561	28,819
21	8.20	154,213	62,829	57,640	33,744
22	8.80	169,818	69,984	62,829	37,005
23	9.40	185,817	75,497	69,984	40,336
24	10.10	204,958	84,531	75,497	44,930
25	10.70	221,755	88,755	84,531	48,469
26	11.40	241,791	98,767	88,755	54,269
27	12.00	259,327	103,579	98,767	56,981
28	12.70	280,193	113,206	103,579	63,408
29	13.40	301,483	121,779	113,206	66,498
30	14.10	323,184	128,727	121,779	72,678
31	14.80	345,281	138,372	128,727	78,182
32	15.50	367,763	146,748	138,372	82,643
33	16.20	390,619	155,036	146,748	88,835
34	16.90	413,838	164,590	155,036	94,212
35	17.70	440,807	176,684	164,590	99,533
36	18.40	464,774	182,423	176,684	105,667
37	19.10	489,076	183,222	182,423	113,431
38	19.80	513,705	203,367	193,222	117,116
39	20.50	538,653	211,237	203,367	124,049
40	21.30	567,549	225,750	211,237	130,562
41	22.00	593,161	231,797	225,750	135,614
42	22.70	619,071	242,342	231,797	144,932
43	23.40	645,275	254,119	242,432	148,814
44	24.10	671,767	262,064	254,119	155,584
45	24.90	702,389	277,181	262,064	163,144
46	25.60	729,479	284,053	277,181	168,245
47	26.30	756,842	294,839	284,053	177,950
48	27.00	784,471	307,270	294,839	182,362

[1]Height calculated with Brickell's (1970) site quality formula for ages 7 through 48; ages 2 through 6, actual height.

[2]Buchanan's empirical formula $1.36LW^{1.16}$ = thousands of needles (1936) and Buchanan's crown measurements (1938) were used to plot total needles, ages 7 through 48. Fig. 35 values were read from plot.

[3]Actual counts of new needles, ages 2 through 6 and calculated other ages new needles = total needles -1-year-old needles -2-year-old needles.

[4]Assume no needle mortality from current to 1-year-old class so previous year's current needles become current year's 1-year-old needles.

[5]Assume 35.8 mortality from 1-year-old class to 2-year-old class

These curves and the life table are very similar to those of Douglas-fir (Mitchell 1974). Thus,

$$ANNN = 3490 \cdot CTH^{1.365} \quad (11)$$

where

ANNN = number of new branch needles as a function of CTH (fig. 35).

A relationship that predicts Potential Infective Surface on branch needles was developed as follows: rows of stomata were counted (fall 1973) on a sample of 1972 and 1973 needles taken from 6-year-old nursery grown western white pine (author's unpublished data). In all, eight needles from each of 32 trees were examined. One-half the needles were of 1972 origin and one-half of 1973 origin. Number of rows varied from 4.17 to 7.1 from one year to the next within the same seedling and from 4.67 to 8.37 for one seedling to another within 1 year. The above findings only indicate some of the variation one might expect. The kind of variation indicated in this small sample could lead to doublings or halvings of target areas. In order to accommodate this variation, we computed the average number of rows and standard deviation on the 256 needles ($\bar{x} = 6.34$, $s = 0.89$). If we assume a normal distribution and accept a limit of ± 4 standard deviations, then the maximum number of stomatal rows expected is in the vicinity of 10 ($0.89 \times 4 + 6.34 = 9.8$).

Maximum needle length is assumed to be 10 cm. This assumption is based on an empirical relationship between needle length and tree height (fig. 37) obtained from table 20.

In the word model discussion of infective surface, maximum width of the infective strip in which each stomatal row is centered was identified as 0.01 cm (100μ). Thus, each needle has approximately 1 cm^2 maximum infective surface and

$$J_{(29,32)} = 3490\ CTH^{1.365}$$
$$= PISB.$$

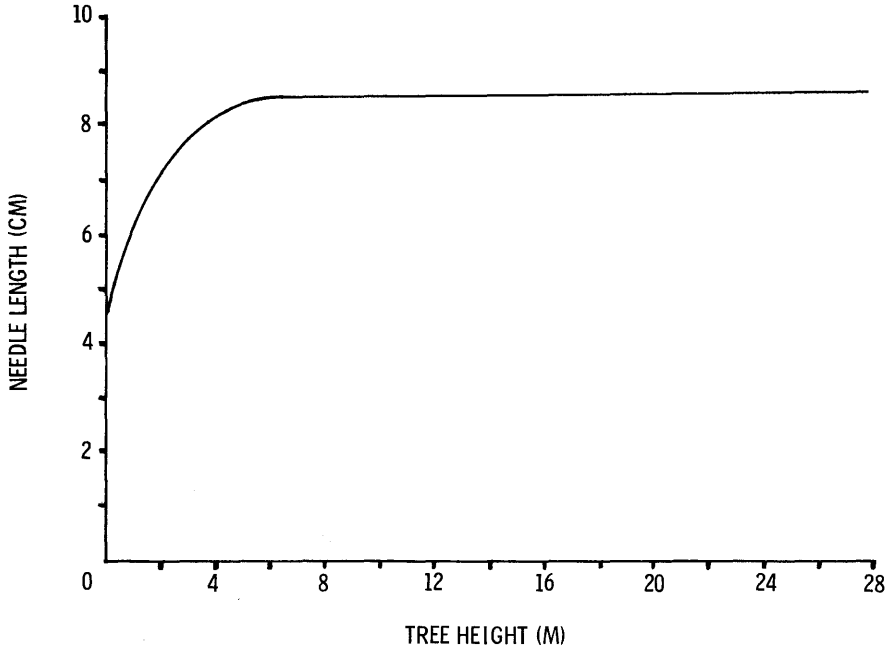

Figure 37.--Length of *Pinus monticola* branch needles as a function of tree height.

Stomatal row adjustment.--The computation of this flow is performed by dividing maximum number of rows, 10, by RSPN (Rows of Stomata Per Needle) to give the reduction factor RFACT. Then:

$$J_{(32,33)} = 0.1 \text{ PISB} \cdot \text{RSPN}$$
$$= \text{RAISB}$$

where

RAISB = Row Adjusted Infective Surface on Branch needles.

Needle length adjustment.--In order to accommodate some sources of variation for needle length, we have included an empirical equation (fig. 37 and table 11) that can account for tree size and a user-controlled factor QNEEDL to be set to mimic other sources of variation. When using the equation, the calculation is

$$\text{Branch needle length} = \frac{8.6}{1 + 0.9e^{-0.75\text{CTH}}} \qquad (12)$$

and

$$\text{QNEEDL} = \frac{\text{Branch needle length}}{10}$$

or we can set QNEEDL to provide the desired needle length. Thus, the flow is:

$$J_{(33,34)} = \text{RAISB} \cdot \text{QNEEDL}$$
$$= \text{QISB1}.$$

Aging infective surface.--Since QISB2 is not needed in the current year the equation is:

$$J_{(34,31)} = \text{QISB1}$$
$$= \text{QISB2}.$$

Aging infective surface.--Buchanan (1936) showed that 64.2 percent of the branch needles of a particular cohort are retained for their third growing season. So:

$$J_{(30,31)} = 0.642 \cdot \text{QISB2}.$$
$$= \text{QISB3}.$$

Needle death.--Buchanan (1936) showed that most branch needles die at the end of their third growing season; so, all needles in state variable 30 will be moved to state variable 10. Thus,

$$J_{(30,10)} = \text{QISB3}$$
$$+ \text{SINK}.$$

Stem Needle Target

Stem needle generation.--The stem-needle growth function computes the amount of new stem needle infective surface by the following equation:

$$J_{(29,25)} = 10 \cdot 12 \cdot 675(1-e^{-1.15CTH}) \cdot 0.01$$

where

10 = maximum number of stomatal rows,

12 = maximum needle length multiplier where the value is 12.0 instead of 10 because stem needles average 1.2 times branch needle length (table 20),

$675 \cdot (1-e^{-1.15CTH})$ = new direct stem-needle function (fig. 38), (13)

0.01 = infective strip width in centimeters.

Equation 13 resulted from counting the number of new stem needles on trees varying in height from 0.1 m to 2.71 m (same trees as discussed under branch needle generation). An equation was found that fit the empirical curve (fig. 38). This relationship was developed from a minimum of data, but like so many other empirical functions in this model, it could easily be made more representative, either by statistical fit or preferably by biological understanding. Finally, the above equation reduces to:

$$J_{(29,25)} = 810(1.0-e^{-1.15CTH})$$
$$= PISDS.$$

Stomatal row adjustment.--The derivation and use of RSPN was discussed under flow (32,33). Thus:

$$J_{(25,26)} = 0.1 \cdot PISDS \cdot RSPN$$
$$= RAISS$$

where

RAISS = Row Adjusted Infective Surface on direct-Stem needles.

Table 20.--*Average lengths of needles obtained from the stems and branches of western white pine trees of varying ages*

Tree age	Tree height[1]	Trees sampled	Length of stem needles[2] X	Length of stem needles[2] C.V.	Length of branch needles X	Length of branch needles C.V.	Branch/ stem[3]
Years	*Meters*	*No.*	*Millimeters*				
3	0.26	4	54 ± 9.5	0.18	50 ± 3.9	0.08	1.08
4	.38	4	61 ± 7.9	.13	55 ± 6.3	.11	1.11
5	.59	4	70 ±10.3	.15	56 ± 3.1	.06	1.25
6	.99	3	69 ± 5.3	.08	58 ± 4.4	.08	1.19
7	1.20	2	72 ±13.01	.181	59 ± 5.1	.09	1.22
8	1.50	1	71 --	--	62 --	--	1.15
9	2.00	1	87 --	--	66 --	--	1.32
10	2.50	1	89 --	--	72 --	--	1.24
50	27.45	18	-- --	--	89 ± 14.7	.17	--
Averages				0.14		0.08	1.20

[1]Heights calculated by Brickell's (1970) formula.
[2]Several hundred needles per tree were measured, but no statistical significance should be placed in these data. They are used for illustrative purposes.
[3]Ratio of length of branch needles to length of stem needles.

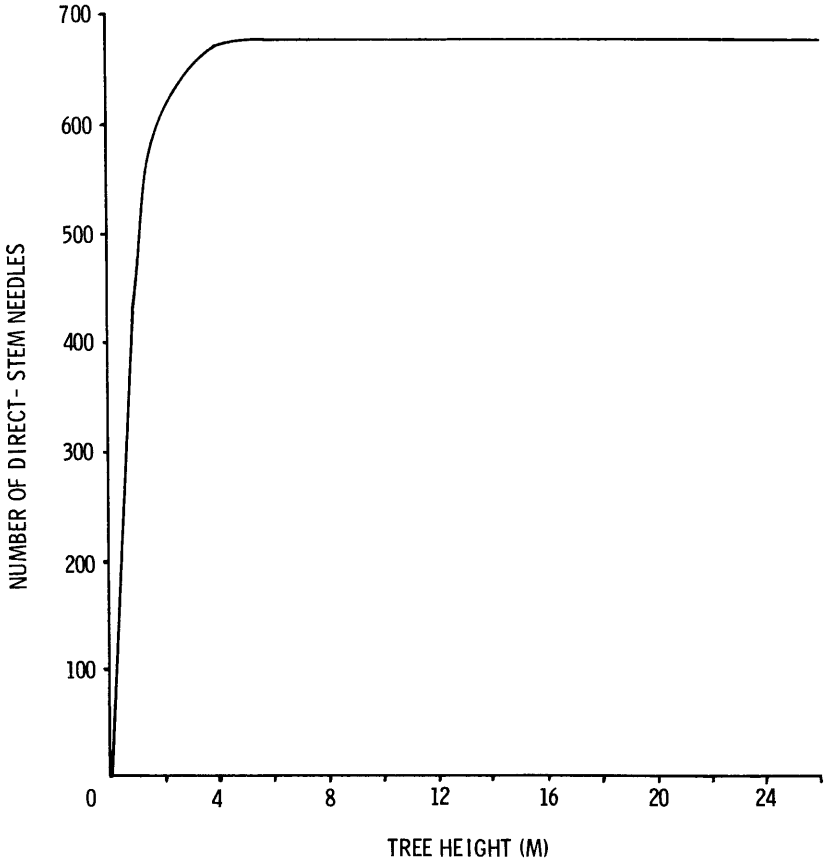

Figure 38.--Number of new *Pinus monticola* needles located directly on the stem as a function of tree height.

Needle length adjustment.--QSNEDL is obtained by dividing the needle length equation (eq. 12) by 12 instead of 10 because stem needles are longer than branch needles:

$$QSNEDL = \left(\frac{8.6}{1+0.9e^{-0.75CTH}}\right) /12 .$$

Thus,

$$J_{(26,27)} = RAISS \cdot QSNEDL$$
$$= QISS1.$$

Aging infective surface.--Since no first year stem needles die, the entire contents of state variable 27 flow to state variable 28.

$$J_{(27,28)} = QISS1$$
$$= QISS2.$$

Needle death.--The assumption was made that all the stem needles in their second year die. So:

$$J_{(28,10)} = QISS2$$
$$= SINK.$$

PINE INFECTION SUBMODEL

Basidiospore Infection

Basidiospore trapping.--Basidiospores of *C. ribicola* were cast onto primary needles of *P. strobus* inside a settling tower and the ratio of spores trapped to spores cast (spores per square millimeter) was determined (Hansen 1972). Four measurements reported were 0.01, 0.06, 0.08, and 0.18, $\bar{x} = 0.08$ and will be called "average trapping efficiency." Settling tower experiments similar to Hansen's should be done to get a large number of trapping efficiency ratios for needles from different species, different needle ages, different tree ages, and from trees showing different kinds of resistance because variation from this source could be an important contribution to variation of IY.

Thus, BSTIS (number of BasidioSpores Trapped on Infective Surface) was computed as follows:

$$J_{(93,94)} = QBSAT \cdot TEF,$$
$$= BSTIS,$$

where

TEF = Trapping Efficiency Factor of branch and stem needles (user controlled variable).

Basidiospore germination.--The mathematical relationship for describing this flow was constructed in much the same way as aeciospore germination was (flow 77,78). Equations 14 and 15 are based on figures 19 and 20, respectively. Thus:

$$BGL = 0.03(TIP)^2 - 0.95TIP + 9.52 \quad (14)$$

where

BGL = Basidiospore Germination Lag time in hours,

TIP = average Temperature of the Infection Period in °C,

and

$$BGP = 0.1(TIP)^2 - 3.17TIP + 27.12 \quad (15)$$

where

SGP = basidioSpore Germination Period in hours.

The germination is assumed to be normally distributed over time with a range equal to SGP and a starting point equal to BGL = 6.0, where

6 = time in hours required for teliospores to germinate and produce basidiospores.

Therefore:

GERMB = CNORMP(A, B, C)

where

A = DIP - (BGL + 6.0),

B = SGP/6.0,

C = SGP/2.0,

then:

$$J_{(94,95)} = BSTIS \cdot GERMB$$
$$= BSGER,$$

where

BSGER = number of trapped BasidioSpores expected to GERminate during a given infection period per square centimeter IS.

Basidiospore germ tube growth.--The number of BasidioSpores per square centimeter of leaf surface expected to produce germ tubes of Adequate Length for penetration (BSTAL) is calculated by:

$$PGERBP = CNORMP(BGTL,8.3,75.0)$$

$$J_{(95,96)} = PGERBP \cdot BSGER$$
$$= BSTAL$$

where

BGTL = BTGR•A = Basidiospore Germ Tube Length in microns,

BTGR = Basidiospore germ Tube Growth Rate

$$= 12.634(A8)^{1.8}e^{-(A8)^{2.8}} \qquad (16)$$

A = DIP-(BGL+6.0),

A8 = (TIP-0.2)16.8,

8.3 = range of penetration length = (100μ-50μ)/6 S.D.,

75.0 = germ tube length when 50 percent have penetrated.

Basidiospore infection establishment.--The number of species having germ tubes of adequate length for penetration are reduced by the basidiospore infection yield ratios (BIY) and a needle resistance factor QNLR. The flow is calculated:

$$J_{(96,97)} = BSTAL \cdot BIY \cdot QNLR,$$
$$= BSI,$$

where

BIY = spots/spore trapped on a square centimeter of infective surface of current year needles,

QNLR = factor to adjust for presence of reduced-needle-lesion-frequency resistance.

Basidiospore infections summed over infection periods.--This flow is computed by combining basidiospore infections per square centimeter of IS, target in IS per tree, and reducing the number of infections by the stem-needle orientation factor. Thus:

$$\sum_{1}^{P} J_{(6,7)} = \sum_{1}^{P} (BSI \cdot 0.5 \cdot QISS1)$$

$$= TNIS1$$

where

$\sum_{1}^{P}$ = summation of infections from each infection period to give a season total,

P = number of infection periods,

BSI = basidiospore infections per square centimeter of current year needles,

QISS1 = infective surface of current year stem needles, square centimeters per tree.

And since needle infections do not yield cankers for at least a year, the summed flow need not be changed.

Basidiospore infection summed over infection periods.--This flow is the same as the last one except that the needle orientation factor changes:

$$\sum_{1}^{P} J_{(6,12)} = \sum_{1}^{P} (BSI \cdot 0.25 \cdot QISB1),$$

$$= TNIB1$$

where

QISB1 = current year branch needle IS, square centimeters per tree.

Basidiospore infections summed over infection periods.--This is like the last except a new factor was added to account for the increased susceptibility of needles in their second season. This factor is SNAIF (Secondary Needle Age Infection Factor). So:

$$\sum_{1}^{P} J_{(6,19)} = \sum_{1}^{P} (BSI \cdot 0.25 \cdot SNAIF \cdot QISB2)$$

$$= TNIB2.$$

Needle Infection to Cankers

Canker appearance.--The fundamental relationship of this flow was depicted in figure 22. An empirical equation that describes canker appearance is:

$$\% \text{ cankered} = b^{-20(b^{-x})} \qquad (17)$$

where

b = parameter that is related to growth rate of the rust down the needle (see below),

x = years after inoculation with range of 1 to 4 years = YR.

The b parameter was related to host resistance through the assumption that a resistance mechanism can decrease growth rate of the fungus in the needles. If a b value of 24 gives a curve similar to the most susceptible families and the growth rate of the rust down the needle is 10 mm per month (Chapman[2]), then this point defines the susceptible interaction (fig. 39). By the same reasoning, if the curve for resistance families matches the empirical curve with b equal to 6 and if we assume that fungus growth rate was cut in half, then the straight line between the two points should provide the relationship between rust growth rate down the needle and the b parameter. An input variable RGRN (Rust Growth Rate in the Needle) is supplied to simulate resistance to the rust expressed as a reduction of rust growth in the needle. This variable allows us to simulate the rate of canker appearance following needle infection.

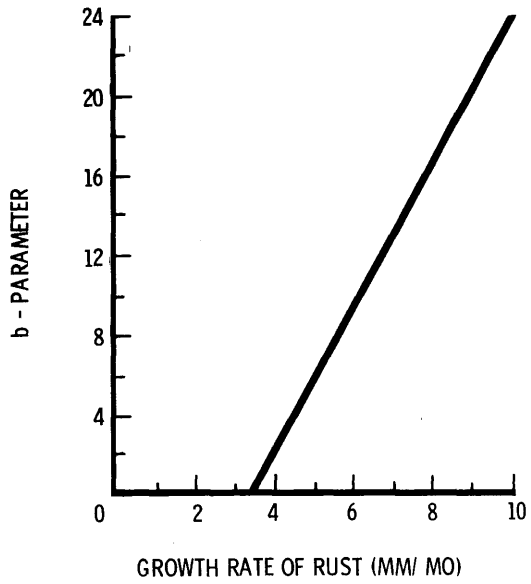

Figure 39.--Relationships between b parameter of equation 17 and growth rate of *Cronartium ribicola* down *Pinus monticola* needles.

If no resistance is present (RGRN = 10 mm/mo), then we can expect 60 percent of needle infections in X(11) to flow to X(14). But if RGRN = 5 mm/mo, then we would expect only 6 percent of the infections to flow. Thus:

$$J_{(7,11)} = TNIS1 \cdot b^{-20(b^{-1.5})},$$

$$= TCS1,$$

where

b = 3.6 RGRN - 12.0,

RGRN = rust growth rate in the needle, millimeters per month,

TCS1 = cankers appearing after 1 year from stem needles infected in their first year.

Since TCOS is a sum of all cankers appearing in a given year from stem-needle infections, its calculation will be deferred.

Needle infections aged.--The needle infections that did not develop to canker status are aged 1 year. Cankers are removed from the needle infections:

$$J_{(7,8)} = TNIS1-TCS1,$$

$$= TI2S1.$$

Canker appearance.--In this flow needle infections in their second year reach canker status and are summed with cankers appearing from $J_{(7,11)}$. Thus:

$$J_{(8,11)} = TI2S1 \cdot b^{-20(b^{-3.0})},$$

$$= TCS2,$$

where

$$b = 3.6 \cdot RGRN - 12.0,$$

TCS2 = cankers appearing after 2 years from stem needles infected in their first year.

Needle infections aged.

The flow is self-explanatory.

$$J_{(8,9)} = TI2S1-TCS2,$$

$$= TI3S1.$$

Canker appearance.--All the remaining infections from stem needles infected during their first growing season become cankers. All the cankers to appear from stem-needle infections in a given year can now be summed:

$$J_{(9,11)} = TI3S1,$$

$$= TCOS = TCS1 + TCS2 + TI3S1.$$

Canker appearance.--The same logic is applied to the calculation of number of incipient branch cankers as was used to calculate the number of new stem-needle cankers. Thus:

$$J_{(12,13)} = TNIB1 \cdot b^{-20(b^{-1.5})},$$

$$= CI1B1.$$

Needle infection aged.--Thus:

$$J_{(12,15)} = TNIB1 - CI1B1$$

$$= TI2B1.$$

Canker appearance.--This equation has been explained; thus:

$$J_{(15,16)} = TI2B1 \cdot b^{-20(b^{-3.0})}$$

$$= CI2B1$$

Needle infections aged.--So:

$$J_{(15,17)} = TI2B1 - CI2B1$$

$$= TI331.$$

Canker appearance.--So:

$$J_{(17,18)} = TI3B1$$

$$= CI3B1.$$

Lethal Canker Portion

Lethal canker generation.--If needles are assumed to be uniformly distributed throughout the crown, the expected number of lethal cankers can be derived as follows:

$$\frac{LC}{TC} = \frac{NLC}{TN}$$

where

LC = number of lethal cankers,

TC = number of cankers total,

NLC = number of needles in lethal cap,

TN = number of needles total.

Then:

$$\text{Proportion lethal} = \frac{NLC}{TN} \tag{18}$$

or:

$$NLC = TN \cdot (\text{proportion lethal}).$$

NLC was tabulated for a range of given tree heights (TH) and is presented in table 21.

The next problem was to find the length of the crown cap that is proportional to the lethal canker curve.

Since,

$$\text{Total needles} = 8{,}725\ (\text{tree height})^{1.365}$$

from figure 36, then:

$$\text{Tree height} = \left(\frac{\text{Total needles}}{8{,}725}\right)^{1/1.365}$$

and if the relationship between Tree Height (TH) and Total Needles (TN) holds for any length of TH and number of TN then:

$$LCCL = \left(\frac{NLC}{8{,}725}\right)^{1/1.365}$$

where

LCCL = length of lethal crown cap,

NLC = number of needles in lethal crown cap.

Lethal Crown Cap Length (LCCL) was computed and the result is given in table 21. The next step was to plot the crown cap lengths as a function of tree heights. The relationship was linear for total heights of 1 m and greater (fig. 40). Since trees under 1.5 m in height are labeled as seedlings where all cankers are lethal, only the linear portion of the curve is needed. Thus:

$$LCCL = 0.23 \cdot TH + 0.6 \tag{19}$$

when expressed as a function of tree height.

Table 21.--*Calculation of length of lethal-crown-cap in* Pinus monticola *under attack by* C. ribicola

Tree height	Total needles[1]	Proportion of cankers lethal[2]	Needles in lethal cap[3]	Lethal cap height[4]
Meters	*Number*		*Number*	*Meters*
0.5	3,387	1.00	3,387	0.5
.75	5,891	1.00	5,891	.75
1.00	8,725	.80	6,980	.85
1.25	11,832	.67	7,927	.93
1.50	15,175	.54	8,195	.96
2.00	22,474	.42	9,439	1.06
3.00	39,087	.31	12,117	1.29
4.00	57,887	.26	15,051	1.49
5.00	78,498	.24	18,840	1.76
6.00	100,680	.22	22,150	1.98
7.00	124,258	.21	26,094	2.23
8.00	149,102	.20	29,820	2.46
10.00	202,193	.19	38,417	2.96
12.00	259,327	.18	46,679	2.96
14.00	320,059	.17	54,410	3.82
16.00	384,051	.17	65,289	4.37

[1]Total number of needles = $8,725(\text{tree height})^{1.365}$.

[2]Proportion cankers lethal = $(0.65/\text{tree height at infection}^{1.25}) + 0.15$ (empirical curve figure 24).

[3]Number of needles in lethal cap = proportion of cankers lethal times total number needles.

[4]Lethal cap height = $(\text{number of needles in cap}/8,725)^{1/1.365}$.

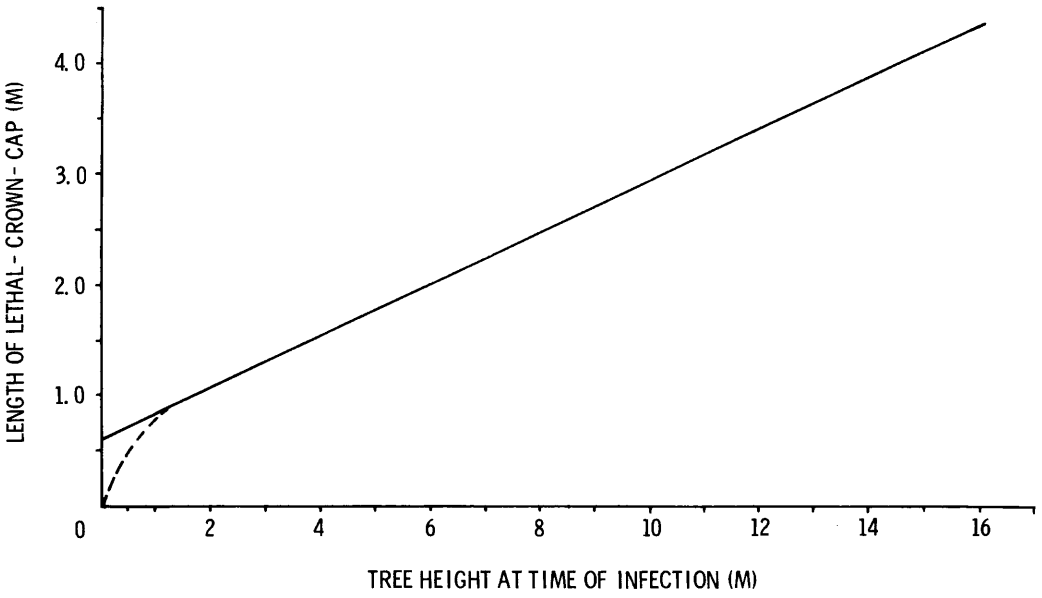

Figure 40.--Postulated relationship between length of lethal crown cap in *Pinus monticola* and tree height at time of infection by *Cronartium ribicola*.

Another question that we investigated was the influence of canker growth rate on the development of the disease within individual trees. Of specific interest was the effect of fungus growth rate on proportion of branch cankers that are lethal. If we assume that reduction of fungus encirclement rate (FER) would bring about a proportional reduction in distance a branch canker could traverse to become a bole canker (fig. 23), then there should be a similar influence on the slope of the crown-cap-height function. Then, the slope of the length-of-lethal-cap equation (0.23 in equation 19) can be stated as a function of FER and a proportionality constant (x):

$$\text{Slope} = x\text{FER}$$

and

$$x = \text{Slope}/\text{FER} = 0.24 \text{ yr/m}$$

where

FER = 0.958 m/yr,

Slope = 0.23.

Thus,

$$\text{LCCL} = (0.24\text{FER}) \cdot \text{PTH(I)} + 0.6 \qquad (20)$$

where

FER = fungus encirclement rate in meters per year,

PTH(I) = height of tree at time of infection,

I = index to height, which is number of years from needle infection to appearance of cankers.

Since proportion of lethal cankers is equal to number of needles in cap divided by number of needles total (equation 18) then:

$$\text{NLC} = (8{,}725(0.24 \cdot \text{FER}) \cdot \text{PTH(I)} + 0.6)^{1.365}$$

and

$$\text{TN} = 8{,}725(\text{PTH(I)})^{1.365}.$$

Then:

$$\text{Proportion of lethal cankers} = \frac{(8{,}725(0.24 \cdot \text{FER}) \cdot \text{PTH(I)} + 0.6)^{1.365}}{8{,}725(\text{PTH(I)})^{1.365}}$$

which leads to:

$$J_{(13,14)} = \text{CI1B1} \cdot \left(\frac{(0.24\ \text{FER})\ \text{PTH(I)} + 0.6}{\text{PTH(I)}}\right)^{1.365}$$

$$= \text{CL1B1},$$

where

PTH(I) = height of tree in meters at time of infection.

I = number of years from needle infection to canker appearance

= TIME-1 in this case.

Lethal canker generation.--These flows are analogous to flow (16→17).

$$J_{(16,14)} = CI2B1\left(\frac{0.25\ FER \cdot PTH(I) + 0.6}{PTH(I)}\right)^{1.365}$$
$$= CL2B1$$

where

I = TIME - 2.

Lethal canker generation.--

$$J_{(18,14)} = CI3B1\left(\frac{0.24 \cdot FER \cdot PTH(I) + 0.6}{PTH(I)}\right)^{1.365}$$
$$= CL3B1,$$

where

I = TIME - 3.

Canker appearance.--

$$J_{(19,20)} = TNIB2 \cdot b^{-20(b^{-1.5})}$$
$$= CI1B2.$$

Needle infections aged.--The needle infections that have not appeared as cankers are aged 1 year. The quantity is determined by subtraction:

$$J_{(19,21)} = TINB2 - CI1B2$$
$$= TI2B2.$$

Canker appearance.--Rationale has been discussed:

$$J_{(21,22)} = TI2B2 \cdot b^{-20(b^{3.0})}$$
$$= CI2B2.$$

Needle infections aged.--

$$J_{(21,23)} = TI2B2 - CI2B2$$
$$= TI3B2.$$

Canker appearance.--All remaining needle infections appear as cankers:

$$J_{(23,24)} = TI3B2$$
$$= CI3B2.$$

Lethal canker generation.--

$$J_{(20,14)} = CI1B2\left(\frac{0.24 \cdot FER \cdot PTH(I) + 0.6}{PTH(I)}\right)^{1.365}$$
$$= CL1B2$$

where

I = TIME - 1.

Lethal canker generation.--

$$J_{(22,14)} = CI2B2\left(\frac{0.24 \cdot FER \cdot PTH(I) + 0.6}{PTH(I)}\right)^{1.365}$$

$$= CL2B2$$

I = TIME - 2.

Lethal canker generation.--

$$J_{(24,14)} = CI3B2\left(\frac{0.24 \cdot FER \cdot PTH(I) + 0.6}{PTH(I)}\right)^{1.365}$$

$$= CL3B2$$

where

I = TIME - 3.

So, Total Lethal Branch Cankers (TLBC) to appear in a given year is:

TLBC = CL1B1 + CL2B1 + CL3B1 + CL1B2 + CL2B2 + CL3B2.

Total new cankers.--This flow provides the Average number of New Cankers Per Tree (ANCPT).

$$J_{(6,98)} = TCOS + CI1B1 + CI2B1 + CI3B1 + CI1B2 + CI2B2 + CI3B2$$

$$= ANCPT.$$

Canker accumulation: This flow Accumulates all Cankers Per Tree over all years (ACPT).

$$J_{(98,99)} = ACPT + ANCPT$$

$$= ACPT.$$

STAND INFECTION SUBMODEL

Seedlings

Seedling infection.--The equation controlling this flow is based on the regression given in figure 26.

Proportion Infected in Year Total cankers = PIYT

$$= \frac{1.0}{1.0 + \frac{1.228}{ANCPT}} \qquad (21)$$

where

ANCPT = Average number of New Cankers Per Tree in year Y.

CLNT will be set equal to STAND, which is the initial number of clean trees per hectare, and is a user-controlled variable. Thus:

$$J_{(35,43)} = CLNT \cdot PIYT$$

$$= CS1Y.$$

Spots-only resistance.--A user-controlled variable that fixes the level of spots-only resistance (SORL) controls this flow.

$$J_{(43,74)} = CS1Y \cdot SORL$$
$$= SORT,$$

where

SORT = number of trees expressing Spots Only ResisTance.

Infected seedlings age.--The spots-only-resistant trees are removed from X(43) by subtraction.

$$J_{(43,42)} = CS1Y - SORT$$
$$= CS2Y.$$

Stem-reaction resistance.--This flow is self-explanatory.

$$J_{(42,74)} = CS2Y \cdot SRRL$$
$$= SRRT$$

where

SRRT = number of trees expressing Stem-Reaction ResisTance.

Infected seedlings age.--The resistant trees are removed and the remaining trees aged 1 year.

$$J_{(42,48)} = CS2Y - SRRT$$
$$= CS3Y.$$

Infected seedlings age.--Dead seedlings are accumulated 3 years after cankers appear or 5 years after infection occurs. This state variable is used in the calculation of disease progress curves and is calculated:

$$J_{(48,50)} = CS3Y + CSDR$$
$$= CSDR.$$

Stem Needle Infection

Stem infections.--The proportion transferred is computed by the infection-probability function which has already been discussed (eq. 21). But, the variable TCOS is used in place of ANCPT:

$$\text{Proportion Infected in Year with Stem cankers} = \frac{1.0}{1.0 + \frac{1.228}{TCOS}} .$$

Then:

$$J_{(35,36)} = CLNT\left(\frac{1.0}{1.0 + \frac{1.228}{TCOS}}\right) .$$

Spots-only resistance.--The use of SORL has been explained.

$$J_{(36,74)} = SC1T \cdot SORL$$
$$= SSORT$$

where

SSORT = number of Stem-needle infected trees showing Spots-Only ResisTance.

Infected trees age.--The mechanics of this flow have been explained.

$$J_{(36,37)} = SC1T - SSORT$$
$$= SC2T.$$

Stem reaction resistance.--

$$J_{(37,74)} = SC2T \cdot SRRL$$
$$= SSRRT$$

where

SSRRT = number of Stem-needle infected trees showing Stem Reaction ResisTance.

Permanent inactivation.--Calculation of number of trees having all cankers either permanently or temporarily inactivated was treated as a probability problem. For example, assume the following:

Number of trees in X(37) = 10;
Level of permanent inactivation = 0.2;
Average number of cankers = 2.3.

In the instance of individual trees, the probability would be equal to the product of the individual probabilities. The probability of all cankers being permanently inactivated on a tree with two cankers would be 0.2 x 0.2 or 0.04. Although we know it not to be strictly accurate, we will assume that the same reasoning will apply to the average number of cankers per infected tree as follows: if the infected trees average 2.3 cankers per tree the probability of all the cankers on a tree permanently inactivating would be $0.2^{2.3}$ or 0.025. If X(37) contained 10 infected trees then 0.25 trees would flow to X(35). We have used the same logic in deriving the temporary inactivation function. Thus the proportion returned to X(35) is calculated:

$$CLNT = SCPIL^{SCPIT} \cdot SC2T$$

where

SCPIL = Stem Canker Permanent Inactivation Level,

SCPIT = average number of Stem Cankers Per Infected Tree from cankers that appear in current year (assume that cankers inactivate when they appear).

SCPIT is equal to the total number of stem needle cankers that appear during the current year divided by the number of stem-infected trees for the same year. The number of new stem infections is equal to TCOS (number per average tree) times the number of stems in the stand X(35), and the number of stem infections is equal to $X(35) \cdot (1.0(1.0+(1.228/TCOS)))$. Thus,

$$SCPIT = \frac{TCOS \cdot X(35)}{X(35) \cdot \left(\frac{1.0}{1.0 + 1.228/TCOS}\right)}$$

which reduces to:

$$SCPIT = TCOS + 1.228. \tag{22}$$

Then:

$$J_{(37,35)} = (SC2T - SSRRT) \cdot SCPIL^{SCPIT}$$
$$= TSCPI$$

where

TSCPI = number of Trees with Stem Cankers Permanently Inactive.

Temporary inactivation.--The derivation of the inactivation function has been discussed.

$$J_{(37,45)} = (SC2T - SSRRT - TSCPI)SCIL^{SCPIT}$$
$$= TSCTI$$

where

TSCTI = number of Trees with Stem Cankers Temporarily Inactivated.

Girdle storage.--The number of trees supporting at least one active stem canker that resulted from a direct stem infection that will be girdled by the rust.

$$J_{(37,38)} = SC2T - SSRRT - TSCPI - TSCTI$$
$$= SCGS.$$

Girdle process.--This flow is computed by subroutine GIRDLE (appendix IV), according to the following arguments and is the time required for the rust to complete the girdling process:

SCGT = flow out of GIRDLE (Stem Canker Girdled Trees),

SCGS = number of trees flowed in,

1 = flag for TGIRD1 equation (appendix IV),

TEM37B = number of trees moved into SCGS,

3 = index for PTH(INDX) determines canker location on bole,

0 = flag that indicates Branch Growth Period (BGP, see eq. 23) is not needed.

The number of Stem Canker Trees Dead (SCTD) in a given year is:

$$J_{(38,39)} = SCGT$$

$$SCTD = SCGT + SCGT.$$

Reactivation process.--Flow of trees that have had inactive stem cankers reactivated. The argument definitions for the GIRDLE function in this case are:

RSCIAS = flow out of the storage array = Reactivated Stem Cankers after InActivation Storage.

CIAS = identification of the storage array = Canker InActivation Storage,

3 = flag that indicates TGIRD = ICIAS (Time to GIRDle = Inactive Canker InActivation Storage period),

TEM37A = number of trees to be moved into the array CIAS,

0 = no INDX value because infection point not computed,

0 = flag that indicates BGP is not computed,

and

$$J_{(45,46)} = RSCIAS$$
$$= SCIGS.$$

Girdle process of reactivated cankers.--Flow of trees supporting reactivated stem cankers while girdling is completed. The arguments for subroutine GIRDLE in this case are:

SCITD = quantity of trees to flow from X(46) to X(47),

SCIGS = identification of the array used = Stem Canker Inactivation Girdle Storage,

1 = flag to identify the TGIRD formula used,

CIAS = quantity of trees flowed into array SCIGS to reside for TGIRD years,

INDX = flag used to identify PTH(INDX) used in computation of circumference that canker must encircle,

0 = flag indicating that BGP is not to be computed.

So:

$$J_{(46,47)} = SCIGS$$
$$= TDRDSC.$$

Branch Needle Infection

Branch infection.--Since we are still in the same time cycle, the amounts removed or added from CLNT must again be subtracted or added because the SIMCOMP compiler does not complete the flows until the end of the cycle. We compute:

$$J_{(35,44)} = (CLNT\text{-}SC1T + TSCPI)\frac{1.0}{1.0 + \frac{1.228}{TLBC}}$$

$$= BC1T$$

where

SCIT = flow X(35)→X(36)

TSCPI = flow X(37)→X(35)

TLBC = value of X(17).

Spots-only resistance.--To obtain this flow:

$$J_{(44,74)} = BCIT \cdot SORL$$

$$= BSORT$$

where

BSORT = number of trees with Branch canker Spots-Only Resistance.

Branch-infected trees aged 1 year.--

$$J_{(44,49)} = BS1T - BSORT$$

$$= BC2T.$$

Stem-reaction resistance.--

$$J_{(49,74)} = BC2T \cdot SRRL$$

$$= BSRRT$$

where

BSRRT = number of trees with Branch canker Stem Reaction ResisTance.

Permanent inactivation of branch cankers.--All variables and rationale have been discussed. Computation of number of lethal Branch Cankers Per Lethally infected Tree (BCPLT) uses equation 22 with the substitution of TLBC for TCOS and BCPIL is an externally supplied variable. So,

$$J_{(49,35)} = (BC2T - BSRRT)BCPIL^{BCPLT}$$

$$= TBCPI$$

where

TBCPI = number of Trees with Branch Cankers Permanently Inactivated

$$= (BS2T - BSRR - BSCPI)BCIL^{BCPLT}.$$

Temporary inactivation storage.--

$$J_{(49,51)} = (BC2T - BSRRT - TBCPI)BCIL^{BCPLT}$$
$$= TBCTI$$

where

TBCTI = number of Trees with Branch Cankers Temporarily Inactivated.

Girdle storage.--This flow computes the number of trees with active branch cankers that will await completion of the girdling process.

$$J_{(49,60)} = BC2T - BSRRT - TBCPI - TBCTI$$
$$= BCSG$$

where

TSBCG = number of Trees to be stored in Branch canker Girdle.

Girdle process.--The equation for this flow was developed from the word model and empirical equations based on Buchanan's (1938) data (fig. 41,42). The derivation is:

Years to reach bole =

$$\frac{0.5 \cdot 0.66(0.24 \cdot FER \cdot PTH(I) + 0.6) \cdot 0.35\sqrt{PTH(I)}}{0.5FER(0.44PTH(I) + 0.3)}$$

where

0.5 = division of branch length by one-half,

0.66 = division of lethal-crown-cap height by two-thirds,

(0.24•FER•PTH(I)+0.6) = height of lethal-crown-cap (from eq. 20),

$0.35\sqrt{PTH(I)}$ = crown radius at base (figure 41),

0.5 FER = fungus growth rate down the branch given as growth rate of the fungus around the bole, (FER)•0.5,

(0.44PTH(I)+0.3) = total height of the crown (figure 42).

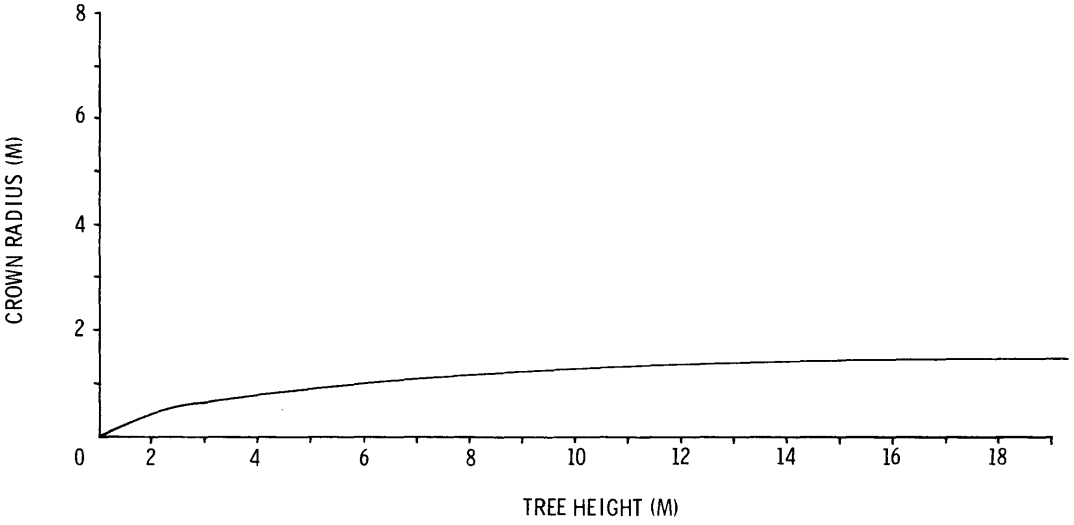

Figure 41.--Plot of *Pinus monticola* crown radius on total height (data from Buchanan, 1938).

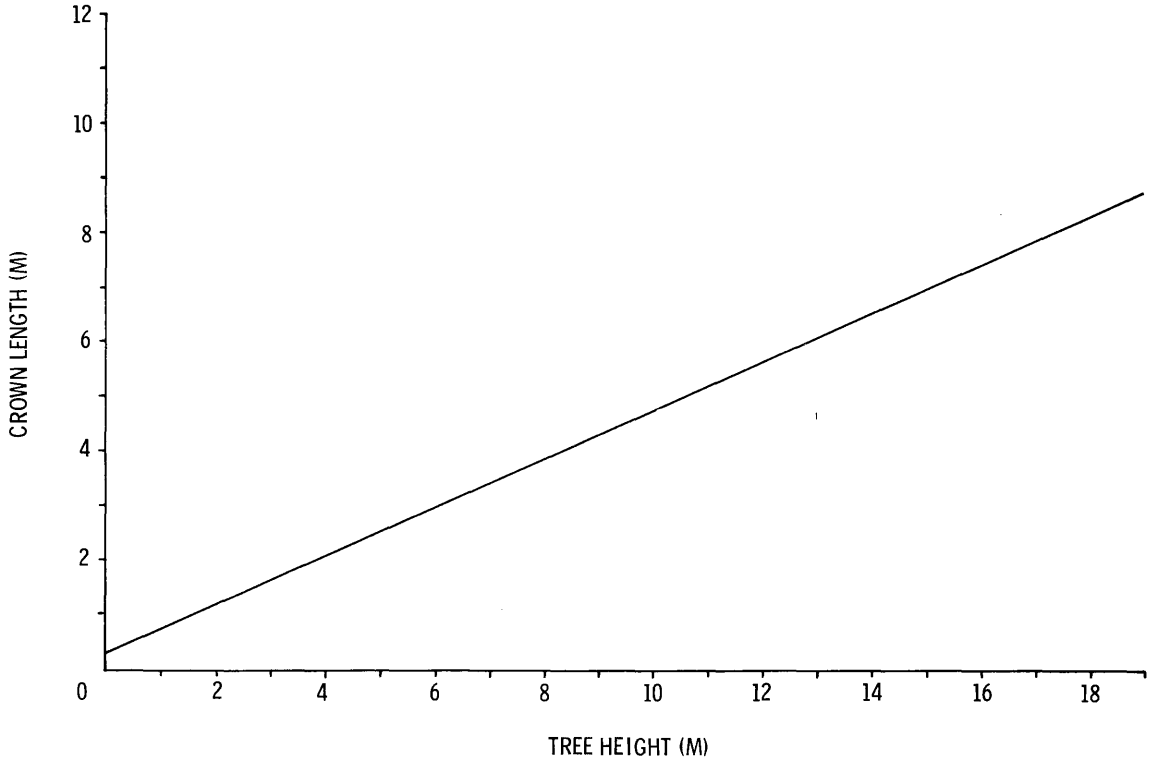

Figure 42.--Plot of *Pinus monticola* crown height on total height (data from Buchanan, 1938).

The above expression reduces to:

$$\text{Years to reach bole} = \frac{\sqrt{PTH(I)}(0.03 \cdot FER \cdot PTH(I) + 0.069)}{FER(0.22PTH(I) + 0.15)} + 2$$

$$= INDX = BGP. \quad (23)$$

INDX gives the period required for growth of the rust down the branch. This value is the period from appearance of an incipient canker until this canker reaches the stem. The 2 is added because it took the canker 2 years to reach state variable X(49). INDX is used in two places. First, it is used to compute the expected distance from the top of the tree at time of infection to the point where the canker is simulated to enter the bole. The development of this idea was treated earlier. Also, in the case of the current flow, the additional 2 years are needed so BGP is set equal to INDX. Second, INDX is used in the computation of circumference to arrive at a girdle period, in which case the additional 2 years are not needed; so 2 was subtracted from the constant, 5, in TGIRD1 and the constant becomes 3 in TGIRD2. The arguments for TGIRD2 are CTH, PTH(INDX), CLF, FER, TCGR, and BGP. All have been discussed and defined. Thus,

GIRDLE(BCTD,BCGS,2,TSBCG,INDX,BGP)

computes storage period, where:

BCTD = quantity of trees flowed out,

BCGS = array identity,

2 = flags TGIRD2,

SBCG = quantity of trees flowed in (trees Stored for Branch Canker Girdle),

INDX = time from appearance of incipient canker to stem entry for height calculations,

BGP = period for growth down branch,

and

$$J_{(60,61)} = \text{BCTD} = \text{DRBC}.$$

Reactivation process.--The derivation of GIRDLE has been discussed.

RBCIAS = quantity of trees flowed out of the array,

BCIAS = branch canker inactivation storage the array identity,

3 = flag that TGIRD (storage period) is equal to ICIAS,

TBCTI = number of trees flowed into array BCIAS (number of Trees with Branch Cankers Temporarily Inactivated),

0 = flag that INDX is not used,

0 = flag that BGP is not used,

and

$$J_{(51,55)} = \text{RBCIAS} = \text{BCISG}.$$

Girdle process.--The time required for reactivated branch cankers to girdle the bole is given by subroutine GIRDLE and the following arguments:

BCITD = number of trees flowed out of the array,

BCIGS = branch canker girdle and branch-growth period storage array,

2 = flag that TGIRD2 is the equation used,

TICR = number of trees flowed into the array BCIGS (number of trees with inactive cankers reactivated),

INDX = flag used to identify PTH(INDX) used in computation of circumference that canker must encircle,

BGP = length of canker growth period down the branch in years,

and

$$J_{(55,56)} = \text{BCITD} = \text{DRRBC}.$$

APPENDIX II

Function Height

One of the principal forcing variables for the blister rust model is tree height. The following paragraphs explain the construction of a model that produces height increment as a function of stand age and site index.

HTI is a function of stand age (TIME), an internal or external variable, and site index (SITE), an external variable. The value of HTI is used to update average Current-Tree Height (CTH), a computed variable. Successive annual estimates of CTH will be retained for up to 20 years in an array (PTH(I)), which is indexed by the number of years from current simulated time.

The interaction between *C. ribicola, P. monticola,* and *Ribes* spp. is related to stand height through its influence on light penetration and other variables. Also, the quantity and quality of susceptible pine host target area is assumed to be directly linked to CTH and values of past average stand heights are used to estimate average bole circumference at particular points of infection. These estimates are combined with estimates of fungal growth rate to project the length of time required for the rust to girdle the bole. The computation of *Ribes* density, used for predicting the quantity of inoculum available, is derived from an index of tree crown height and number of living trees in the stand (TLT).

Function "height" predicts HTI through a two-component model:

1. An equation to predict the expected value of the increment.

2. A mechanism designed to draw a random value of HTI from a population (assumed to be normally distributed) described by the expected value and an estimate of the variance about the expected value.

These components were derived as follows: Brickell (1970) used a Richard's function as a model for a western white pine site index equation:

$$S = b_1 H(1-b_2 e^{-b_3 A})^{-b_4}$$

where

e = base of the natural logarithm,

S = site index (feet at 50 years b.h. age),

H = average height of dominant and codominant trees,

A = age of the oldest dominant tree in the even-aged stand,

(b_1, b_2, b_3, b_4) = estimated parameters.

This equation was solved for H,

$$H = (S/b_1)(1-b_2 e^{-b_3 A})^{b_4}$$

and then differentiated with respect to age to obtain an expression for instantaneous rate of increment in the average height of dominant and codominant members of the stand (h):

$$h = dH/dA = b_1' \cdot b_2 \cdot b_3 \cdot b_4 \cdot S \cdot (1-b_2 e^{-b_3 A})^{(b_4-1)} \cdot e^{-b_3 A} \qquad (24)$$

where

$$b_1' = 1/b_1.$$

Figure 43, derived by substituting Brickell's (1970) parameter estimates, shows that equation 1 has sufficient flexibility to mimic the expected pattern of change in tree height with respect to time. In order to derive parameter estimates appropriate to our model needs and modeling assumptions, we required observations of annual increment from a sample of trees, drawn without respect to crown class, from a wide range of site indices. Appropriate sources of data were records of two other studies.

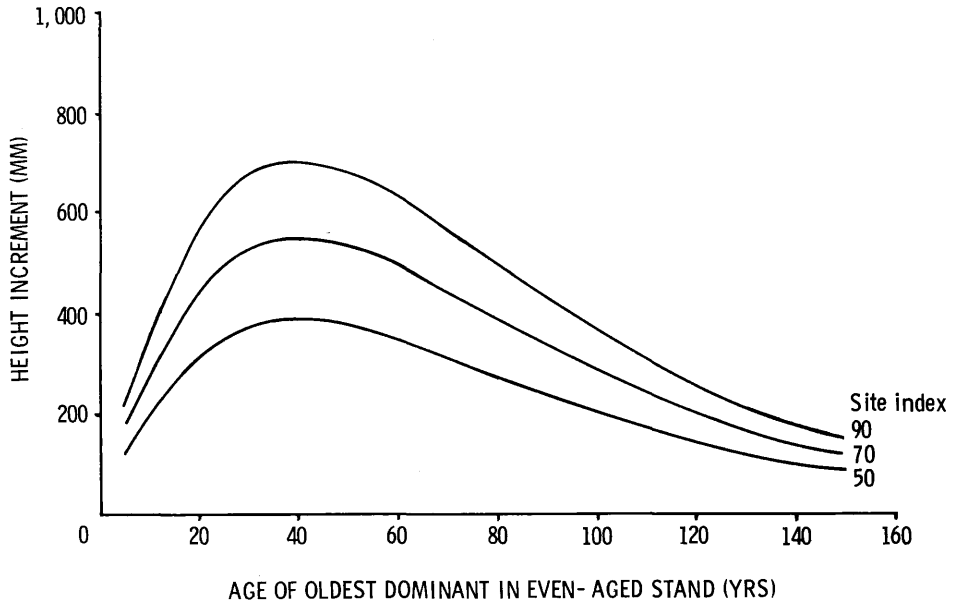

Figure 43.--Expected annual increment in the average height of dominant and codominant members of a western white pine stand as a function of age and site index (adapted from Brickell, 1970).

The first of these was a set of 124 estimates of annual increment resulting from measuring internode lengths on 28 young white pine that were growing on an excellent site (estimated site index 112). These trees were dissected and all branch and stem internodes were measured and needles per internode counted to supply more data on needle distribution and number for the pine target simulation. The trees were collected near Elk River, Idaho, and ranged in age from 3 to 9 years.

The second set of data was information recorded on trees selected for progeny testing as part of the blister rust resistance breeding program (Bingham and others 1971). Data included height, age, and site index for all candidate trees. In addition, 29 of the candidate trees, distributed among five site index classes, were photographed in 1952 and 1953. The bole axis and film plane were nearly parallel and the view of the bole and crown from the photo point was unobstructed. These

photographs were mounted on an Addo-X increment-core measuring device. Total height and all internode lengths that could be accurately associated with a tree age were measured. Appropriate scale factors translated these measurements so that an additional 629 observations of annual increment were developed. The distribution of observations among site indexes and age classes is shown in table 22.

Table 22.--*Distribution of western white pine height increment data among age and site classes*

Age class	Site index					
	53	63	75	104	112	Total
	Number of increment measurements					
0-5				1	109	110
6-10			8	17	22	47
11-15		5	14	46	19	84
16-20	4	15	15	60	25	119
21-25	7	15	22	59	20	123
26-30	15	15	22	45	6	103
31-35	15	15	20	25		75
36-40	15	4	17	1		37
41-45	15		15			30
46-50	12		7			19
51-55	2		4			6
Total	85	69	144	254	201	753

The distribution shows paucity of data at young ages in the low site classes and older ages in the high site classes. At ages where annual height increment is near maximum (20 to 40 years), all classes, nevertheless, are fairly well represented.

Parameters, estimated from these data using Marquardt's (1966) nonlinear least squares algorithm, are as follows:

$$b_1 = 0.653617$$
$$b_2 = 1.024494$$
$$b_3 = 0.024202$$
$$b_4 = 2.071822$$

These parameters were substituted into equation (24) and the expression was simplified to the form given in equation (25).

$$h = 0.033577 \cdot S \cdot (1-1.02449 \cdot e^{-0.024202 \cdot A})^{1.07182} \cdot e^{-0.024202 \cdot A} \qquad (25)$$

where

h = average annual height increment on a stand basis (meters) = computed variable HTI,

S = estimated site index (feet at 50 years b.h. age) = external variable SITE,

A = average stand age = computed variable TIME.

Equation (25) is used to compute the expected value of the annual increment in average stand height.

The theory describing the estimation of the variance about the regression surface for nonlinear models is not well developed. Marquardt's algorithm, however, minimizes an objective function, which has been transformed by a Taylor series expansion to an expression which is linear with respect to the estimated parameters. Assuming that parameter estimates are stable, the confidence bands about the regression surface can be approximated in accordance with linear theory. This extension of linear theory was deemed adequate to meet our modeling needs. Figure 44 illustrates the relationship between annual increment in average stand height and stand age for site index 75, and displays the 95 percent confidence bands computed from equation (26). Equation (26) was derived from the output of the fitting procedure and incorporated into the simulation program.

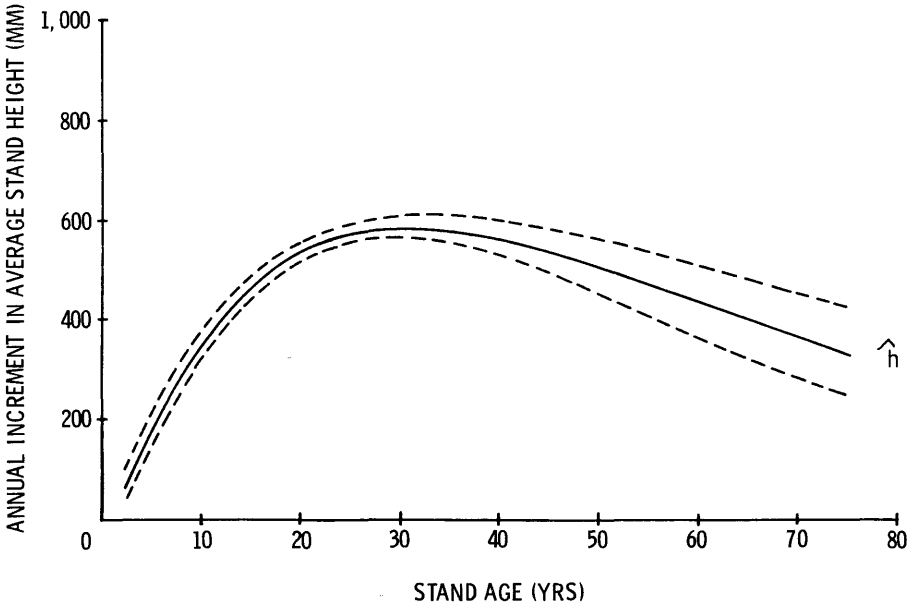

Figure 44.--Expected annual increment in average stand height ($\hat{h}$) versus stand age for site index 75 western white pine. Bands surrounding $\hat{h}$ represent approximate 95 percent confidence bands.

$$s^2 = \{ \sum_{i=1}^{4} \sum_{j=1}^{4} ptp_{ij} \cdot (P_i - \bar{p}_i) \cdot (P_j - \bar{p}_j) \} \cdot PHT \qquad (26)$$

where

ptp_{ij} = the elements of the inverse moment matrix resulting from the fitting procedure,

P_i, P_j = the partial derivatives of equation (24) with respect to parameters i and j, evaluated at the appropriate values of S and A.

$$\left(P_1 = \frac{\partial(\text{eq. } 1)}{\partial b_1} \,\middle|\, \{S, A, \hat{b}_1, \hat{b}_2, \hat{b}_3, \hat{b}_4\}\right)$$

$\bar{p}_i, \bar{p}_j$ = the average values of the partial derivatives of equation (24) with respect to parameters i and j resulting from the fitting procedure,

PHT = the mean squared residual.

Prediction of HTI is a three-step procedure:

1. Equation (25) is evaluated to determine expected value,

2. Equation (26) is evaluated to estimate the variance about the expected value,

3. A number is drawn from the normal distribution described by the estimated variance and the expected value.

Function "height" yields total height of an average tree in the stand at an age equal to TIME.

APPENDIX III

Subroutine Spores

A method was needed that would accept input information about the nature of infection periods and *Ribes* species and calculate the "expected" germination percentage of teliospores. The following model was constructed to make this calculation.

If the rate of basidiospore cast, or its integral, cumulative basidiospore cast, can be expressed as a function of telial column size parameters, then the number of basidiospores produced in an infection period should be estimable from teliospore numbers, telial column size parameters, and the duration of the infection period.

Bega (1959) conducted an experiment wherein individual telial columns were placed in ideal environments and allowed to germinate to exhaustion. He reported cumulative basidiospore cast by 1-hour time intervals for four telial columns of varying lengths and diameters. To our knowledge, these data are the only published quantitative information on the relationship between telial column size and basidiospore production for *C. ribicola*.

We converted these data to show cumulative basidiospore production as a proportion of total production for each telial column (fig. 45). These data show a 5- to 8-hour delay between the onset of suitable environment and the beginning of basidiospore cast and an inflection at 13 to 17 hours. Following this inflection, cumulative basidiospore cast generally increases at a decreasing rate until the column is exhausted. Bega (1959) concluded that the magnitude of the decreasing rate appears to be related to column size.

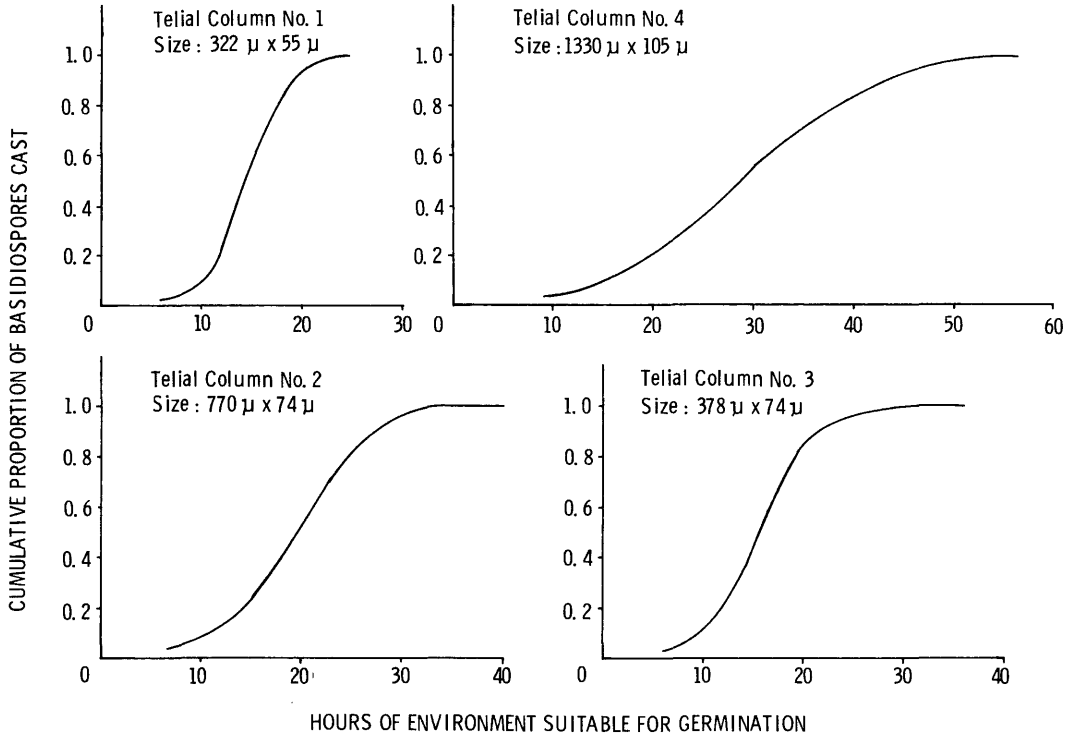

Figure 45.--Cumulative percent of *Cronartium ribicola* basidiospores cast from telial column of various lengths and diameters (calculated from Bega, 1959).

We next graphed the data to show the proportional hourly rate of basidiospore cast (fig. 46). Several patterns were observed:

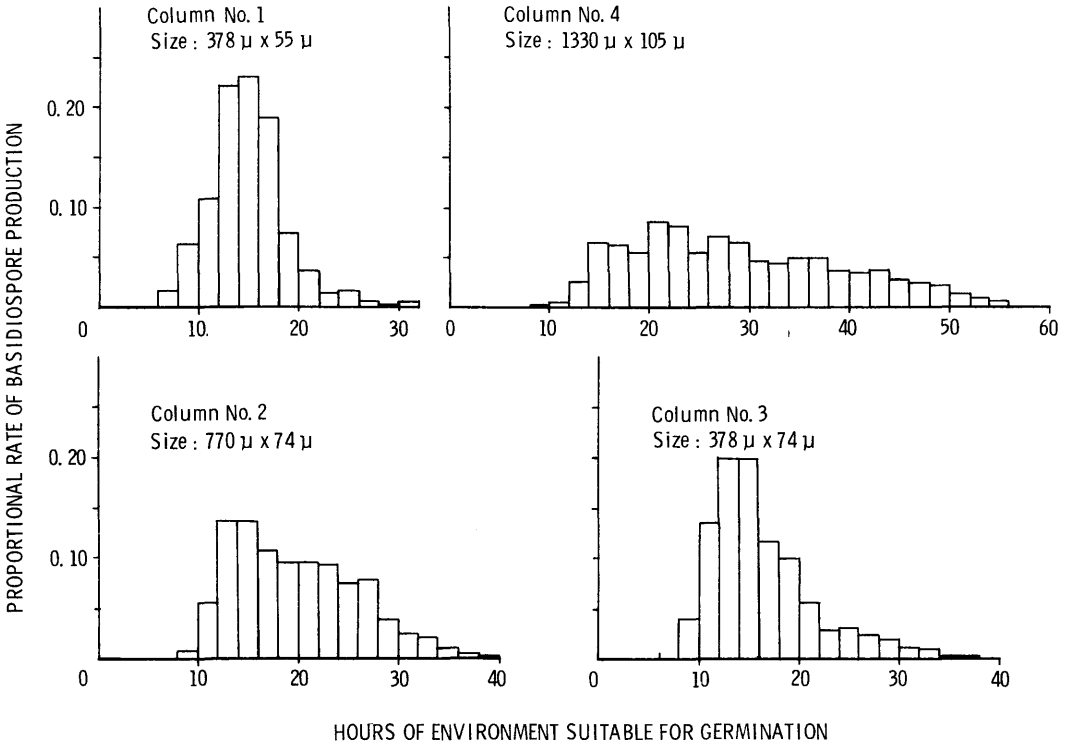

Figure 46.--Proportional rate of basidiospore production observed from four *Cronartium ribicola* telial columns of various lengths and diameters (calculation based on data from Bega 1959).

1. Each rate curve was positively skewed with a maximum in the vicinity of 14 to 20 hours.

2. The height of the maximum was inversely related to column diameter.

3. Each maximum was succeeded by a series of local maxima, which were spaced at 4- to 8-hour intervals and decreased in magnitude as time of exposure to germination conditions increased.

4. The length of time required to exhaust a column was directly related to column diameter.

These patterns strongly suggest that the rate of basidiospore cast is related to the arrangement of teliospores within a column.

We examined several sections of telial columns to see if there was some apparent geometric arrangement of teliospores that could be expressed as a simple model. In longitudinal section, teliospores are arranged as chains of bulging cylinders with diameters slightly larger in the middle than at each end. Adjacent chains are offset so that the center bulge of a teliospore in one chain closely conforms to the restricted area at the joining of two teliospores in the adjacent chains (see Colley 1918). Spore arrangements observed in horizontal sections reflected this offset as teliospore diameters appeared to be quite variable. The uniformity of spore size exhibited in vertical sections, however, suggests that this variation is

☆ U.S. GOVERNMENT PRINTING OFFICE: 1980—777-028/59 Region No. 8

an artifact of the vertical arrangement. It would seem reasonable to consider the individual teliospore as a cylinder with a diameter equal to the average of the teliospore diameters observed in a column cross section.

We further observed that teliospores, when examined in a cross section, were arrayed in rings about a single center spore or a center cluster of four spores. These patterns can be translated into simple geometric models (fig. 47) for which the number of spores in a ring (N_i) can be approximated from the proximity of the ring to the center of the column (for the center cluster, i=1). For columns with a single center spore,

$$N_i = \begin{cases} 1, \text{ if } i=1 \\ 6 \cdot (i-1) \text{ if } i>1, \end{cases}$$

and for columns with a center cluster of four spores,

$$N_i = 6i-2 \quad .$$

The structure of the innermost ring can be determined from the "diameter" of the telial column when measured in units of average teliospore diameter. An even column diameter implies a center cluster of four spores; and an odd column diameter implies a single center spore.

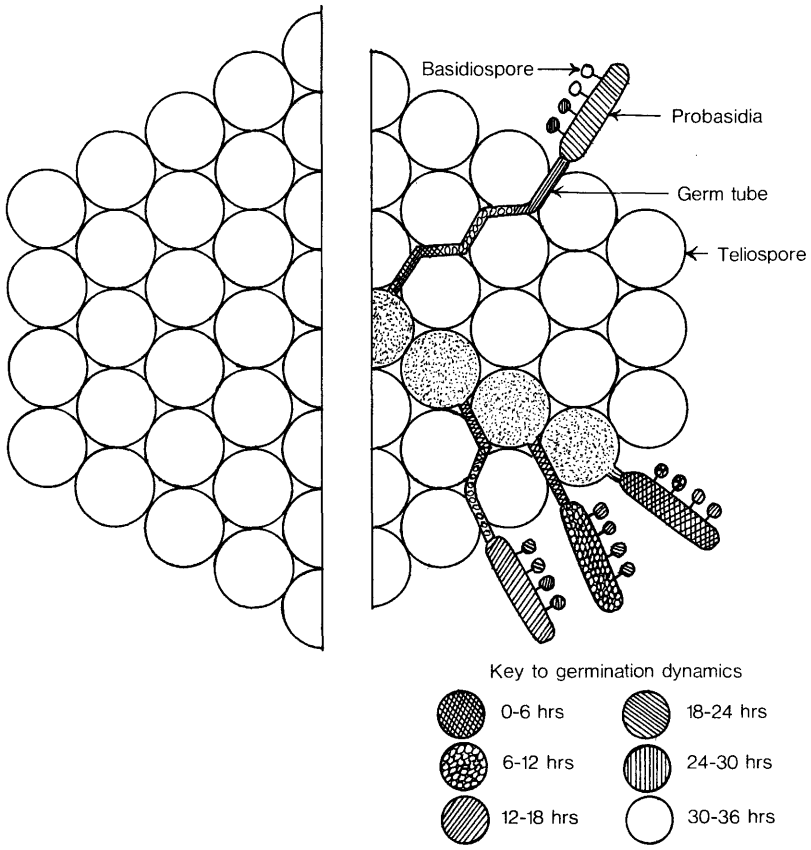

Figure 47.--Geometric model of the arrangement of teliospores within a *Cronartium ribicola* telial column. The section at the left shows the arrangement of spores if the inner-most ring is composed of a single spore. The timing of basidiospore production relative to the start of the infection period is illustrated by the shaded teliospores. Both sections represent columns composed of four rings and would theoretically completely germinate in 36 hours.

This simple geometric model of column structure is well suited to interpretation of the proportional hourly basidiospore cast rate data. Colley (1918) observed that teliospores appear to germinate in order of proximity to the exterior of the column. Assuming that teliospore viability is relatively constant throughout a column, the maximum rate of basidiospore cast should then correspond to the germination of the outer ring, resulting in the observed positive skew in the production rate curves. If we further assume that basidiospore cast from a specific ring is normally distributed over a fixed time interval, then the sequential germination of successively inward rings should result in a pattern of regularly spaced local maxima, decreasing in magnitude as time of exposure to germination conditions increases. Since these rate curves never approach zero between local maxima, an overlap between the germination periods of adjacent rings would seem likely.

Finally, if the length of time required to exhaust a ring is fixed, columns with more rings, that is, greater diameters, will necessarily require more time to completely exhaust. Columns with relatively large diameters, however, will have proportionately fewer spores in the outside ring. Therefore, the greater the diameter of the column, the smaller the magnitude of the maximum in the proportional cast rate curve.

We used this interpretation as the framework for a model to describe the rate of basidiospore cast. We assume a 6-hour delay between the start of an infection period and the beginning of basidiospore cast. We further assume that the cast from an individual ring will be normally distributed over a 12-hour period with a standard deviation of 2 hours. Overlap between the germination periods of adjacent rings is approximated as 6 hours. These time parameters were estimated from the pattern of occurrence of maxima in the cast rate curves for Bega's (1959) columns. Simulations based on the size characteristics of these columns show a close correspondence to observed cast rates (fig. 48). We wish to emphasize that the model nevertheless is based on a rather loose, but plausible, interpretation of an extremely small sample and is quite tentative.

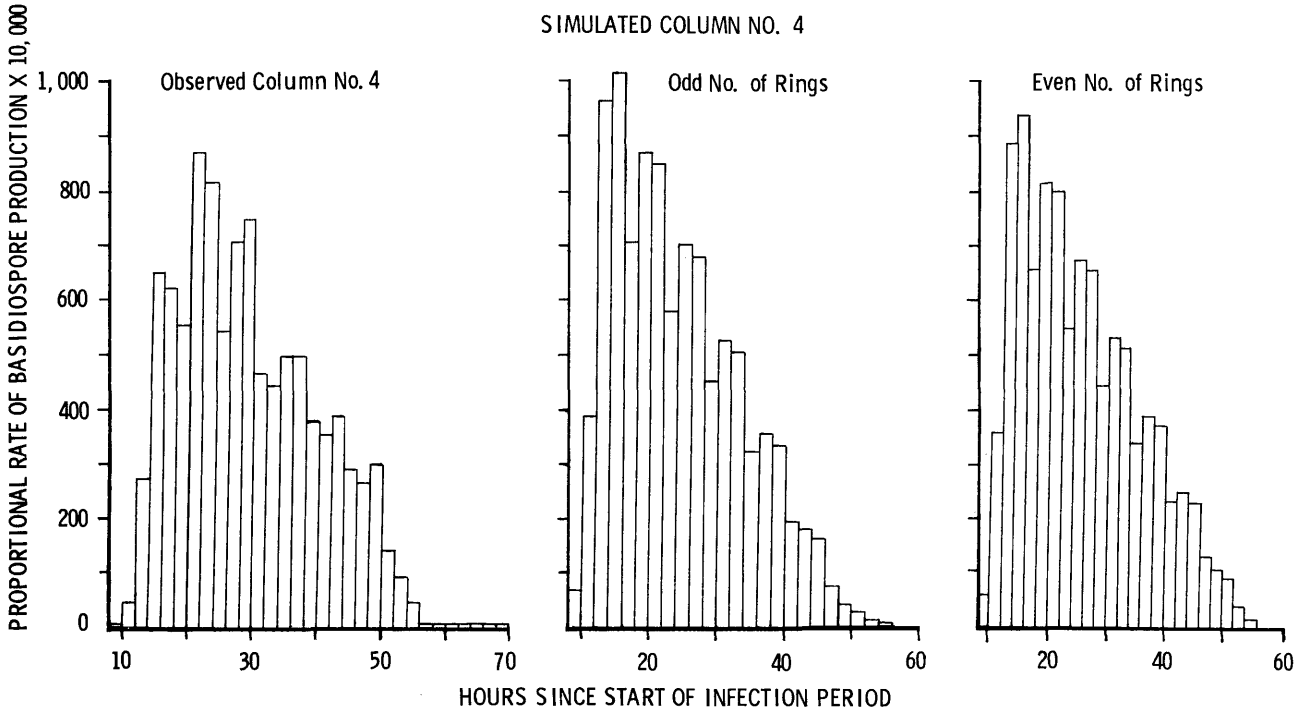

Figure 48.--Comparison of observed and simulated proportional rates of basidiospore production from a *Cronartium ribicola* telial column 1330μ long and 105μ in diameter (observed data from Bega, 1959).

The information required to drive this model of teliospore germination is Telial Column diameter (Width) (TCW), average TelioSpore Diameter (TSD), and the expected Duration of the Infection Period (DIP). Using the above described time parameters, these arguments are employed to compute the proportion of total potential basidiospores that will be cast (PCAST). The distribution of cast rate for an individual ring is incorporated as an array (CNORMZ) with elements corresponding to the integrals of the standardized normal density function evaluated for $1/2\sigma$ increments:

$$\text{CNORMZ(1)} = \frac{1}{\sqrt{2\pi}} \int_{-\infty}^{-2.5} e^{-x^2/2}\, dx = 0.0062$$

$$\vdots$$

$$\text{CNORMZ(11)} = \frac{1}{\sqrt{2\pi}} \int_{-\infty}^{+2.5} e^{-x^2/2}\, dx = 0.9938 \quad .$$

CNORMZ is then indexed by the number of hours that a particular ring has been casting basidiospores. The sequence of model calculations begins with the estimation of cross-sectional dimensions of the telial column: telial column diameter,

```
NTSD = TCW(ISP)/TSD + 0.5,
```

and the number of spore rings in the column,

```
NR = NTSD/2.0 + 0.51.
```

Next, the infection period duration is adjusted to reflect the 6-hour lag,

```
DIP = D - 6.0,
```

and the length of time required to completely exhaust the column is estimated,

```
ETIME = 6.0*(NR + 1.0).
```

If DIP is greater than ETIME, all available teliospores are assumed to germinate and PCAST is returned to the calling program with a value of 1.0. Otherwise, the proportion of total basidiospores cast must be computed from the estimated column dimensions.

To facilitate estimation of the proportion of available basidiospores cast when the column does not exhaust, the proportion of teliospores in each ring RATIO(I) must be computed. For convenience of summation, RATIO is indexed from the outside of the column in, corresponding to the theoretical order of germination. The value of RATIO for a particular ring can be derived from the number of rings in the column and the number of teliospores in a Cross SECTion of the column (CSECT). For columns with a single center spore,

```
CSECT = 3.0*NR*(NR-1.0)+1.0
```

and

$$\text{RATIO(I)} = \begin{cases} (6.0*(J-1.0))/\text{CSECT} & \text{for I<NR} \\ 1.0/\text{CSECT} & \text{for I=NR} \end{cases}$$

where

```
J = NR - I + 1.
```

For columns with a center cluster of four spores,

```
CSECT = 4.0 * NR + 3.0 * NR * (NR-1.0)
```

and

```
RATIO(I) = ((6.0*J) - 2.0)/CSECT.
```

Next, the Number of Complete Rings Germinating is computed:

```
NCRG = (DIP - 6.0)/6.0+0.05
```

and PCAST is set equal to the sum of the first NCRG values for RATIO(I).

With the assumed time parameters, one or two rings may not completely germinate. The value of PCAST must be adjusted to include the proportions of basidiospores cast from these partially germinated rings. The first of these partially germinated rings will have an index:

```
I = NCRG+1.
```

The proportion of available basidiospores cast by the Ith ring is determined by the appropriate reference to the array CNORMZ:

```
INDX = DIP - 6.0*NCRG,
```

and PCAST is adjusted accordingly:

```
PCAST = PCAST + RATIO(I) * CNORMZ(INDX).
```

Finally, INDX is decremented by 6, I is incremented by 1, and the adjustment to PCAST is repeated to reflect the contribution to basidiospore cast from the (NCRG+2) ring.

APPENDIX IV

Subroutine Girdle

A way was needed to hold some infections at a steady state while the simulator cycled tree growth and infections on other trees. We accomplished the holding action by feeding simulated infected trees into an array at a specified point and then advancing the array 1 year at a time. These "infected" trees would then come "out" of the array at the desired time to be flowed to the next state variable. The following derivation mainly concerns the method of calculating the time a given kind of "infected" tree will remain in storage. The first derivation pertains to the storage time required for girdling of the stem by a canker that reaches the stem through a stem-needle. Thus:

$$TGIRD1(A,B,C,D) = ((0.042 \cdot (A-B) \cdot (A-1.14))/(A-1.40))/(C-D)+5$$

where

A = CTH,

B = PTH(INDX) = PTH(3),

C = FER,

D = TCGR = tree circumference growth rate,

5 = additional time in years it takes after girdling for death to occur.

CTH is read from function HEIGHT. INDX = 3 in this case because the infection would be on wood 3 years old if it reached the bole in 2 years from an infection on a needle infected in its first year. Since second-year stem needles are assumed to drop immediately after infection, only first-year needles can have infection and most infection from these needles should reach the bole in 2 years, the value of 3 was selected. This number is used to calculate the circumference of the bole so that girdle time can be calculated. The infection is considered to be a point on the bole when the infection is 2 years old. We know this is not completely accurate but we have no data with which to model otherwise.

The second general formulation pertains to cankers that formed on branches. So:

$$TGIRD2(A,B,C,D,E,F) =$$

$$((0.042 \cdot (A-B+C) \cdot A-1.14))/A-1.40))/D-E) +3 +F$$

where

A = CTH

B = PTH(INDX)

C = CLF

D = FER

E = TCGR

F = BGP

The circumference is determined by the following scheme for both stem-needle and branch-needle cankers, where

1. Bole is a perfect cone.

2. D.b.h. is measured at 1.4 m,

3. $\text{D.b.h.} = \frac{\text{CTH} - 1.14}{75.59}$ (Deitschman, Glenn H. unpublished), (27)

4. Circumference = $2\pi r$.

5. Solve for similar right triangles (fig. 49).

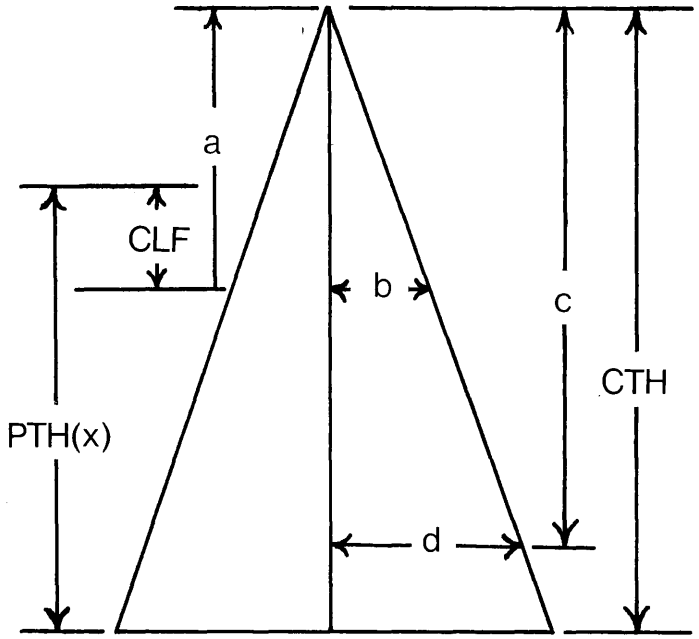

Figure 49.--Family of right triangles solved to simulate circumference of a *Pinus monticola* stem at the point of entry of a *Cronartium ribicola* bole canker.

$$\frac{a}{b} = \frac{c}{d} \qquad b = \frac{ad}{c}$$

where

a = CTH-PTH+CLF,

b = radius in meters at point of rust entry,

c = CTH - 1.4,

$d = \frac{\text{CHT} - 1.14}{2 * 75.59}$ = radius at b.h.

6. CLF = Crown length factor.

CLF is defined as the average distance from top of tree at time of infection to point where branch canker and stem needle canker will enter the bole and is a function of the height at time of infection and growth rate of the rust. We will continue the discussion of CLF, but please keep in mind that this value is used to compute TGIRD2, not TGIRD1. This point, defined as the distance down the bole from the tip of the crown, is determined as follows. The basic target we are concerned with is the lethal crown cap as will be discussed. This is the portion of the crown where

the stem needles are located and is where the branches are short enough that branch cankers can reach the bole. Equation (20) provides the length of the lethal crown cap as a function of tree height and fungus growth rate. We will assume, based on a subjective evaluation of the distribution of needles within the cap, that the most likely point of bole penetration is two-thirds of the way down the bole in the lethal crown cap. Thus,

$$CLF = 0.66((0.24*FER)*PTH(x) + 0.6)$$

and

$$\text{Circumference at point of entry} = \frac{2\ \pi\ (CTH-PTH(x)+CLF)\ \left(\frac{CTH-1.14}{151.2}\right)}{CTH-1.40}$$

which reduces to:

$$\text{Circumference at point of entry} = \frac{0.042(CTH-PTH(x)+CLF)(CTH-1.14)}{CTH-1.40}$$

where the variables have been previously named. The equation in the case of stem-needle infections is as above minus CLF. The net fungus encirclement rate determines the girdling period. Thus,

$$\text{Years to girdle} = \frac{\text{Circumference of bole at entry point}}{\text{Tree circumference growth rate - Fungus encirclement rate}}$$

and the equation is:

$$TGIRD1 = \frac{\frac{(0.042(CTH-PTH)(I))(CTH-1.14)}{CTH-1.40}}{FER-(0.000325*SITE-0.00125)}$$

where

I = INDX which was previously discussed,

SITE = index of site quality,

FER = fungus encirclement rate, an external variable,

0.00325*SITE-0.00125 = TCGR = Tree Circumference Growth Rate.

The equation for TCGR was derived from a regression of tree height on diameter (Deitschman, Glenn H., unpublished, this Station). Since the rate of diameter growth is about the same at different heights in a tree (Chapman and Meyer 1949), we assumed that the rate of increase in circumference at breast height was equal to the rate of increase anywhere else on the bole. That the rate of circumference increases as a function of SITE was derived by multiplying d.b.h. at 50 years as determined by equation (27) by π and dividing the result by 50 years for SITE = 50, 70, and 90. When plotted, the result conformed to the linear equation:

$$TCGR = 0.00325*SITE-0.00125$$

where

TCGR = tree circumference growth rate in meters per year,

SITE = height in feet at 50 years of age.

In the case of flow (38→39), the length of time that the tree remains in X(38) is set by the computation of TGIRD1, which in this flow, is the time required to complete the girdling process. But, infected western white pine live an average of

5 additional years after girdling before death occurs (Hungerford, R. D., unpublished, this Station). Thus, trees are retained in X(38) for girdle time + 5 years. This "storage" function is accomplished by indexing the number of trees flowing from X(37), labeled (TEM37B), into an array at point TGIRD1. Each element of the array is then stepped up 1 year each cycle. At the end of TGIRD1 years, the number of trees in the top slot is advanced to X(39) or the trees "die."

McDonald, G. I., R. J. Hoff, and W. R. Wykoff.
1981. Computer simulation of white pine blister rust epidemics. I. Model formulation. USDA For. Serv. Res. Pap. INT-258, 136 p. Intermt. For. and Range Exp. Stn., Ogden, Utah 84401.

A simulation of white pine blister rust is described in both word and mathematical models. The objective of this first generation simulation was to organize and analyze the available epidemiological knowledge to produce a foundation for integrated management of this destructive rust of 5-needle pines. Verification procedures and additional research needs are also discussed.

KEYWORDS: Computer simulation of epidemics, integrated pest management, *Cronartium ribicola*, *Pinus monticola*, deployment of resistance

McDonald, G. I., R. J. Hoff, and W. R. Wykoff.
1981. Computer simulation of white pine blister rust epidemics. I. Model formulation. USDA For. Serv. Res. Pap. INT-258, 136 p. Intermt. For. and Range Exp. Stn., Ogden, Utah 84401.

A simulation of white pine blister rust is described in both word and mathematical models. The objective of this first generation simulation was to organize and analyze the available epidemiological knowledge to produce a foundation for integrated management of this destructive rust of 5-needle pines. Verification procedures and additional research needs are also discussed.

KEYWORDS: Computer simulation of epidemics, integrated pest management, *Cronartium ribicola*, *Pinus monticola*, deployment of resistance

The Intermountain Station, headquartered in Ogden, Utah, is one of eight regional experiment stations charged with providing scientific knowledge to help resource managers meet human needs and protect forest and range ecosystems.

The Intermountain Station includes the States of Montana, Idaho, Utah, Nevada, and western Wyoming. About 231 million acres, or 85 percent, of the land area in the Station territory are classified as forest and rangeland. These lands include grasslands, deserts, shrublands, alpine areas, and well-stocked forests. They supply fiber for forest industries; minerals for energy and industrial development; and water for domestic and industrial consumption. They also provide recreation opportunities for millions of visitors each year.

Field programs and research work units of the Station are maintained in:

Boise, Idaho

Bozeman, Montana (in cooperation with Montana State University)

Logan, Utah (in cooperation with Utah State University)

Missoula, Montana (in cooperation with the University of Montana)

Moscow, Idaho (in cooperation with the University of Idaho)

Provo, Utah (in cooperation with Brigham Young University)

Reno, Nevada (in cooperation with the University of Nevada)